DESIGN OF ARBITRARILY SHAPED INERTIAL AND THREE DIMENSIONAL PENTAMODE ACOUSTIC CLOAKS

by

Qi Li

B.S., Dalian University of Technology, 2010

M.S., Dalian University of Technology, 2013

Submitted to the Graduate Faculty of

Swanson School of Engineering in partial fulfillment

of the requirements for the degree of

Doctor of Philosophy

University of Pittsburgh

2018

UNIVERSITY OF PITTSBURGH

SWANSON SCHOOL OF ENGINEERING

This dissertation was presented

by

Qi Li

It was defended on

July 11, 2018

and approved by

William W. Clark, PhD, Professor, Department of Mechanical Engineering & Materials Science

Albert C. To, PhD, Associate Professor, Department of Mechanical Engineering & Materials Science

Hong Koo Kim, PhD, Professor, Department of Electrical and Computer Engineering

Dissertation Director: Jeffrey S. Vipperman, PhD, Professor & Vice Chair of Department of Mechanical Engineering & Materials Science

DESIGN OF ARBITRARILY SHAPED INERTIAL AND THREE DIMENSIONAL PENTAMODE ACOUSTIC CLOAKS

Qi Li, PhD

University of Pittsburgh, 2018

Acoustic cloaks are devices that can make a space acoustically invisible. Acoustic cloaks can be designed using transformation acoustics. The properties of these cloaks are, by necessity, anisotropic. Inertial acoustic cloaks have anisotropic density and isotropic bulk modulus, while pentamode cloaks have isotropic density and anisotropic stiffness.

The ultimate goal of this work is to build cloaks of arbitrary 2D and 3D shape that are composed of homogenous materials. Five different design methods are presented which contribute toward this goal. The first contribution of the work is a method of designing 2D inertial acoustic cloaks having arbitrary shapes, based on transformation acoustics to map along radial directions. The derived properties are complicated. By dividing the cloak into small sections, the transverse anisotropy is removed, but the radial anisotropy remains. The properties within each section are inhomogeneous, but could theoretically be realized using layered media.

The second and third contributions of the work are two methods of designing 2D arbitrarily shaped cloaks such that homogeneous material properties occur. One method

accomplishes homogeneity by simply dividing the cloaks into triangular patterns. Each triangle in physical space is mapped to a corresponding triangle in virtual space, resulting in homogeneous properties. The second method is through the use of multiple transforms. Arc sections are divided into two triangles. The first triangle undergoes a single transform, while the second undergoes two. The fourth contribution of the work is extending these methods to three dimensions. Here, 3D arbitrarily shaped cloaks can be composed of homogeneous tetrahedral parts.

The fifth contribution of the work is the introduction of a new pentamode material that is amenable to designing 3D cloaks. Pentamode materials have special structures such that only compressional waves are supported. Hexagonal cells with double-cone structures (DCS) are designed and analyzed, which can approximate the shape of a layered spherical pentamode structure. From the dispersion relations, it is observed that there are bandgaps where all shear modes disappear. The effect of the unit cell geometry on the acoustic properties is studied. Unit cells for a 3D pentamode acoustic cloak are explored.

TABLE OF CONTENTS

NOMENCLATURE ..... **VII**

ACKNOWLEDGMENTS ..... **IX**

1.0 INTRODUCTION **1**

1.0.1 Overview of cloaking **1**

1.0.2 Objectives of this work **3**

1.1 LITERATURE REVIEW ON ACOUSTIC CLOAKS **5**

1.1.1 Inertial cloaks **6**

1.1.2 Pentamode cloaks **8**

1.1.3 Other type of acoustic cloaks **10**

1.2 CONTRIBUTIONS OF THIS WORK **11**

1.3 OUTLINE OF THE DISSERTATION **13**

2.0 BRIEF REVIEW OF FUNDAMENTALS **14**

2.1 INERTIAL ACOUSTIC CLOAKS **14**

2.1.1 Derivation of inertial acoustic cloaks with transformation acoustics **14**

2.1.2 Transformation type **17**

2.1.3 Transformation relations **21**

2.1.4 Layered structures **25**

2.2 PENTAMODE ACOUSTIC CLOAKS **28**

2.2.1 Pentamode materials **28**

2.2.2 Pentamode cloaks 29

3.0 ARBITRARILY SHAPED ACOUSTIC CLOAKS DESIGNED BY MAPPING ALONG RADIAL DIRECTIONS 32

3.1 DERIVATION OF THE PROPERTIES OF ARBITRARILY SHAPED ACOUSTIC CLOAKS 32

3.2 BUILDING THE CLOAKS WITH LAYERED STRUCTURES 35

3.3 ANALYSIS OF THE ELLIPTICAL CLOAK 41

4.0 TWO DIMENSIONAL ARBITRARILY SHAPED ACOUSTIC CLOAKS DERIVED WITH TWO-STEP TRANSFORMATION 47

4.1 DERIVATION OF THE HOMOGENEOUS PROPERTIES WITH A TWO-STEP TRANSFORMATION 47

4.2 ANALYSIS OF THE CLOAKING PERFORMANCE 55

4.3 ANALYSIS OF THE FACTORS THAT AFFECT THE MATERIAL PROPERTIES 57

4.4 FABRICATION FEASIBILITY OF THE CLOAK 61

5.0 TWO DIMENSIONAL ACOUSTIC CLOAKS WITH ARBITRARY HOMOGENEOUS PATTERNS 65

5.1 DERIVATION OF THE PROPERTIES 65

5.2 SIMULATION AND ANALYSIS OF AN APPROXIMATELY CIRCULAR CLOAK WITH THREE-PART SECTIONS 68

5.3 SIMULATION OF A RECTANGULAR CLOAK WITH FIVE-PART SECTIONS 74

6.0 THREE DIMENSIONAL ARBITRARILY SHAPED ACOUSTIC CLOAKS COMPOSED OF HOMOGENEOUS PARTS 78

6.1 DERIVATION OF THE PROPERTIES OF THE CLOAKS WITH A THREE-STEP TRANSFORMATION 79

6.2 DERIVATION OF THE HOMOGENEOUS PROPERTIES WITH A GENERAL TRANSFORMATION 86

6.3 NUMERICAL SIMULATION OF TWO POLYHEDRAL CLOAKS COMPOSED OF HOMOGENEOUS PARTS 88

6.4 GEOMETRICAL FACTORS THAT AFFECT THE PROPERTIES 93

7.0 THREE-DIMENSIONAL PENTAMODE ACOUSTIC CLOAKS COMPOSED OF HEXAGONAL UNIT CELLS 97

7.1 DIVISION OF A SPHERICAL SURFACE 97

7.2 HAXAGONAL PENTAMODE UNIT CELL 99

7.3 DISPERSION RELATIONS OF THE HEXAGONAL UNIT CELL WITH VARYING GEOMETRIES 107

7.4 VARIATION OF THE PROPERTIES ON THE GEOMETRIC PARAMETERS OF THE DOUBLE-CONE STRUCTURE 112

7.5 WAYS TO INTRODUCE ANISOTROPY INTO HEXAGONAL CELLS116

7.6 DESIGN OF PRIMITIVE CELLS FOR SPHERICAL PENTAMODE CLOAKS 125

8.0 CONCLUSION AND FUTURE WORK 128

BIBLIOGRAPHY 133

LIST OF TABLES

Table 4.1 Required properties of one section for a realizable cloak..... 61

Table 4.2 The required velocities of the approximately circular cloak 64

Table 7.1 Dimensions and properties of the primitive cell in each layer 126

LIST OF FIGURES

Figure 1.1 Reprint showing virtual space (left) that is transformed to physical space (right)..... 2

Figure 2.1 Transformation from the virtual space (Ω) to the physical space (ω)..... 15

Figure 2.2 Virtual space and physical space with the interior boundary corresponding to a point (a) virtual space (b) physical space..... 18

Figure 2.3 Virtual space and physical space with the interior boundary corresponding to an area (a) virtual space (b) physical space..... 19

Figure 2.4 Virtual space and physical space with the interior boundary corresponding to a line (a) virtual space (b) physical space..... 20

Figure 2.5 Virtual space and physical space with the interior boundary corresponding to a short line (a) virtual space (b) physical space..... 20

Figure 2.6 Mapping relations from an annular virtual space to an annular physical space..... 22

Figure 2.7 Simulation of a cloak with a linear transformation..... 23

Figure 2.8 Simulation of a cloak with a fractional polynomial transformation..... 24

Figure 2.9 Simulation of a cloak with square root type transformation..... 25

Figure 2.10 Layered structures of two materials arranged alternatively..... 26

Figure 2.11 Simulation results of a plane wave with amplitude of 1 Pa through a space with the layered cloak..... 27

Figure 2.12 Face-centered-cubic primitive cell with double-cone structures and its Brillouin zone (a) primitive cell (b) Brillouin zone..... 29

Figure 2.13 Dispersion relations of the face-centered-cubic primitive cell..... 30

Figure 3.1 An acoustic cloak with arbitrary interior and exterior boundaries..... 33

Figure 3.2 Simulation of a plane wave with amplitude of 1 Pa through the field with an arbitrarily shaped acoustic cloak with exact required properties 34

Figure 3.3 Configuration and division of a square cloak: (a) configuration (b) division 35

Figure 3.4 Layered structures of the square cloak in the first quadrant 37

Figure 3.5 Simulation of a plane wave with amplitude of 1 Pa in two directions (a) without cloak in direction 1 (b) with square cloak in direction 1 (c) without cloak in direction 2 (d) with square cloak in direction 2 38

Figure 3.6 Configuration and division of the elliptical cloak: (a) configuration (b) division ... 39

Figure 3.7 Layered structures of the elliptical cloak in the first quadrant 39

Figure 3.8 Simulation of a plane wave with an amplitude of 1 Pa in three directions (a) without cloak (b) with elliptical cloak in direction 1 (c) with elliptical cloak in direction 2 (d) with elliptical cloak in direction 3 40

Figure 3.9 Normalized amplitude of the scattered waves without and with the elliptical cloak at $r=5\lambda_b$ for incident waves from three directions (as in Figure 3.8) 42

Figure 3.10 Reduced total RCS of the elliptical cloak for three angles of incidence (as in Figure 3.8) 43

Figure 3.11 The effect of the elliptical cloak at different frequencies (a) r_0/λ_b =0.5 (b) r_0/λ_b =1 (c) r_0/λ_b =1.5 44

Figure 3.12 Densities of the layered materials along radial directions for all sections 45

Figure 3.13 Bulk moduli of the layered materials along radial directions 46

Figure 4.1 An arbitrarily shaped acoustic cloak with a section as an example 48

Figure 4.2 Schematics of the two-step transformation of a section from virtual space to physical space (a) virtual space (b) intermediate space (c) physical space 49

Figure 4.3 A hexagonal cloak composed of homogeneous parts built with layered structures . 52

Figure 4.4 Simulation of a plane wave with amplitude of 1 Pa through a space with an object (a) without cloak in direction 1 (b) with the hexagonal cloak in direction 1(c) without cloak in direction 2 (d) with hexagonal cloak in direction 2 53

Figure 4.5 A non-regular cloak built with layered structures 54

Figure 4.6 Simulation of a plane wave with amplitude of 1 Pa for a space with an object (a) without cloak, direction 1 (b) with the irregular cloak, direction 1 (c) without cloak, direction 2 (d) with the irregular cloak, direction 2 55

Figure 4.7 Normalized amplitudes of the scattered waves without and with the irregular cloak at $r=5\lambda_b$ for incident waves in two directions 56

Figure 4.8 Reduced total RCS of the irregular cloak for various normalized frequencies for two angles of incidence (as in Figure 4.6) 57

Figure 4.9 One section of a regular polygonal cloak for two-step transformation 58

Figure 4.10 Variation of material properties with |OA/|OB| at $\theta=\pi/10$ and |OF|/|OA|=1 59

Figure 4.11 Variation of material properties with θ at |OA|=|OF|=0.1 59

Figure 4.12 Variation of material properties with |OF|/|OA| at |OA|=0.2 and (a) $\theta=\pi/9$ (b) $\theta=\pi/36$ 60

Figure 4.13 An approximately circular cloak with layered structures 62

Figure 4.14 Simulation of a plane wave with amplitude of 1Pa through a space with an object (a) without cloak (b) with the approximately circular cloak 63

Figure 4.15 Reduced total RCS of the circular cloak built with two-part sections 63

Figure 5.1 Mapping relations from the virtual space (Ω) to the physical space (ω) in triangular patterns 66

Figure 5.2 Transformation from a triangular area to another 66

Figure 5.3 Transformation of a section with three triangles from virtual space to physical space 69

Figure 5.4 Variation of principal densities of each part with parameters α and β 70

Figure 5.5 Variation of bulk modulus of each part with parameters α and β 70

Figure 5.6 Variation of velocities of sound of each part with parameters α and β 71

Figure 5.7 A circular cloak composed of three-part sections built with layered structures 72

Figure 5.8 Simulation of a plane wave with amplitude of 1Pa propagating through a space with the circular cloak with triangular pattern (a) without cloak (b) with the cloak 73

Figure 5.9 Normalized amplitude of the scattered waves without and with the circular cloak at $r=5\lambda_b$ 73

Figure 5.10 Reduced total RCS of the circular cloak 74

Figure 5.11 Mapping of a section with five parts from virtual space to physical space 75

Figure 5.12 A rectangular cloak with triangular pattern built with layered structures 76

Figure 5.13 Simulation of a plane wave with amplitude of 1Pa propagating through a space with the rectangular cloak (a) without cloak (b) with cloak 76

Figure 5.14 Reduced total RCS of the square cloak 77

Figure 6.1 Cubic cloak by mapping along radial directions 78

Figure 6.2 A section from a 3D acoustic cloak with arbitrary shapes 80

Figure 6.3 Schematic diagram of the three-step mapping (a) first step (b) second step (c) third step 81

Figure 6.4 Transformation from one tetrahedron in virtual space to another in physical space 87

Figure 6.5 Transformation of corresponding tetrahedra from the virtual space to the physical space 89

Figure 6.6 An octahedral cloak model 90

Figure 6.7 Simulation of a space with an obstacle (a) without cloak (b) with the octahedral cloak 91

Figure 6.8 A polyhedral cloak model with 32 faces 91

Figure 6.9 Simulation of a space with an obstacle (a) without cloak (b) with the polyhedral cloak 92

Figure 6.10 Reduced total RCS of the polyhedral cloak 92

Figure 6.11 A simplified section from a regular polygonal cloak 93

Figure 6.12 Effects of θ on the principal velocities when η=0.05 for (a) Part 1 (b) Part 2 (c) Part 3. 94

Figure 6.13 Effects of η on the principal velocities when θ=10° for (a) Part 1 (b) Part 2 (c) Part 3 95

Figure 7.1 A polyhedron with hexagonal surfaces and square faces 98

Figure 7.2 Primitive cell of a hexagonal unit cell composed of double-cone structures 99

Figure 7.3 Double-cone structure used in designing the pentamode materials 100

Figure 7.4 Brillouin zone of the hexagonal unit cell 101

Figure 7.5 Primitive cell composed of double-cone structures when $h=h_c$ (D=0.07l, d=0.01l) 102

Figure 7.6 Dispersion relations along ΓM direction of the Brillouin zone of the primitive cell 102

Figure 7.7 The five modes along the ΓM direction (x) at relatively low frequencies 103

Figure 7.8 Dispersion relations along ΓA direction for the primitive cell..... 104

Figure 7.9 The five modes along the ΓA direction (z) at relatively low frequencies 105

Figure 7.10 Dispersion relations of the primitive cell when $k=k_c$ (D=0.07l, d=0.01l)..... 106

Figure 7.11 Primitive cell composed of double-cone structure when h=4.16h_c (D=0.07l, d=0.01l)..... 107

Figure 7.12 Dispersion relations of the primitive cell when h=4.16h_c (D=0.07l, d=0.01l) 108

Figure 7.13 Primitive cell composed of double-cone structure when h=0.372h_c (D=0.07l, d=0.01l)..... 109

Figure 7.14 Dispersion relations of the primitive cell when h=0.372h_c (D=0.07l, d=0.01l) ... 109

Figure 7.15 Primitive cell composed of double-cone structure when h=0 (D=0.07l, d=0.01l)110

Figure 7.16 Dispersion relations of the primitive cell when h=0 (D=0.07l, d=0.01l) 111

Figure 7.17 Dispersion relations of the primitive cell when D=0.2l (h=h_c, d=0.01l)..... 111

Figure 7.18 Dispersion relations of the primitive cell when d=0.02l (h=h_c, D=0.07l)..... 112

Figure 7.19 Dispersion branches along x and z directions when h=h_c (D=0.07l, d=0.01l)..... 113

Figure 7.20 Velocities with θ in xy plane when h=h_c (D=0.07l, d=0.01l) 114

Figure 7.21 Velocities with ϕ in xz plane when h=h_c (D=0.07l, d=0.01l) 114

Figure 7.22 The effect of the thin-end radius of the double-cone structure on the properties (h=h_c, D=0.07l) 115

Figure 7.23 The effect of the middle radius of the double-cone structure on the properties (h=h_c, d=0.01l) 116

Figure 7.24 Dispersion branches along x and z directions when h=4.16h_c (D=0.07l, d=0.01l)117

Figure 7.25 The velocities along the direction of θ when h=4.16h_c (D=0.07l, d=0.01l) 118

Figure 7.26 The velocities along the direction of ϕ when h=4.16h_c (D=0.07l, d=0.01l) 118

Figure 7.27 Dispersion branches in x and z directions h=0.372h_c (D=0.07l, d=0.01l) 119

Figure 7.28 The velocities along the direction of θ when h=0.372h_c (D=0.07l, d=0.01l) 120

Figure 7.29 The velocities along the direction of ϕ when h=0.372h_c (D=0.07l, d=0.01l) 120

Figure 7.30 The variation of compressional velocities with h (D=0.07l, d=0.01l) 121

Figure 7.31 The primitive cell with different double-cones 122

Figure 7.32 The variation of compressional velocities with d_2 (d_1= 0.1l, D=0.5l, h=h_c) 123

Figure 7.33 The variation of compressional velocities with d_2 (d_1= 0.1l, D=0.5l, h=0.543h_c) 123

Figure 7.34 The variation of compressional velocities with D_2 (d_1=d_2= 0.04l, D_1=0.5l, h=h_c)124

Figure 7.35 Compressional wave velocities of the layered pentamode cloak 127

NOMENCLATURE

(r, θ, φ)	Polar coordinates in the physical space
(R, Θ, Φ)	Polar coordinates in the virtual space
(x, y, z)	Cartesian coordinates in the physical space
(X, Y, Z)	Cartesian coordinates in the virtual space
$\boldsymbol{J}$	Jacobian matrix in the transformation
ρ_b	Density of the background medium
κ_b	Bulk modulus of the background medium
λ_b	Wavelength of the waves travelling in the background medium
c_b	Sound speed in the background medium
$\overline{\overline{\boldsymbol{\rho}}}$	Density tensor of the cloaks
$\overline{\overline{\boldsymbol{\rho}_\Lambda}}$	Density tensor of the cloaks in principal directions
ρ_r	Density element of a circular or spherical cloak in the radial direction
ρ_t	Density element of a circular or spherical cloak in the transverse direction
c_r	Sound speed of a circular or spherical cloak in the radial direction
c_t	Sound speed of a circular or spherical cloak in the transverse direction

$\rho_{\|\|}$	The smaller density element in the diagonalized density tensor
$\rho_{\perp}$	The larger density element in the diagonalized density tensor
$c_{\|\|}$	Sound speed in the principal direction of $\rho_{\|\|}$
$c_{\perp}$	Sound speed in the principal direction of $\rho_{\perp}$
ρ_{α} , ρ_{β} , ρ_{γ}	Density elements in the principal directions of a 3D tetrahedral part
κ	Bulk modulus of the cloaks
ρ_1, ρ_2	Densities of layered materials
κ_1, κ_2	Bulk moduli of layered materials
$c_{\|\|}^{C}$	Compressional wave velocity of pentamode materials in the horizontal direction
$c_{\|\|}^{S}$	Shear wave velocity of pentamode materials in the horizontal direction
$c_{\perp}^{C}$	Compressional wave velocity of pentamode materials in the vertical direction
$c_{\perp}^{S}$	Shear wave velocity of pentamode materials in the vertical direction

ACKNOWLEDGMENTS

Over the past five years, I have received support and encouragement from a great number of individuals. First, I would like to thank my advisor, Dr. Jeffrey S. Vipperman, sincerely for his guidance and supervision. During these years, he gave me valuable suggestions and help in my research and the writing of my dissertation. I also want to thank Dr. William Clark, Dr. Albert To, Dr. Hong Koo Kim. I am fortunate to have them as my dissertation committee members. They gave valuable suggestions to make my dissertation clear and complete.

I am grateful to all of those with whom I have had the pleasure to work during these years. I am also grateful to my family and friends for their help and support. At last, I wish to thank my loving and supportive wife, Jun Zou. The moment she agreed to marry me is the most exciting time in my life.

1.0 INTRODUCTION

1.0.1 Overview of cloaking

Invisibility cloaks have often appeared in science-fiction writings or movies as magic devices. They can make a person or an object invisible. With the advancement of metamaterials, it is possible to design and fabricate cloaks. Metamaterials are artificial materials whose properties can be gained from their structures, using the inclusion of small inhomogeneities or resonant structures to enact effective macroscopic behavior.

Invisibility cloaks were first demonstrated for electromagnetic waves. Acoustic cloaks are similar devices, but work in acoustic field. When an acoustic wave, travelling in a medium, strikes an obstacle, there will be reflections in front of the obstacle and shadows behind it. Active SONAR systems are designed by submitting acoustic waves and detecting the reflections. Acoustic cloaks can be used to reduce or eliminate the effect of the obstacle, rendering SONAR less effective, if not ineffective.

There are many methods in designing acoustic cloaks, especially for those that only work in a single direction. A broadly used method in designing metamaterial devices including acoustic cloaks is through coordinate transformation. The properties of the devices can be derived by transforming a virtual space to the physical space. The virtual space is usually set with the properties of the background medium. A wave in virtual space travels through the

uniform medium unimpeded. The transformation permits the required material properties to be derived for the physical space, in order to bend and/or stretch the acoustic waves around the desired cloaked space. Any shaped object can then be "hidden" inside the cloaked space, as illustrated in Figure 1.1. Since the transformation is not unique, the properties of the devices can be tailored intentionally.

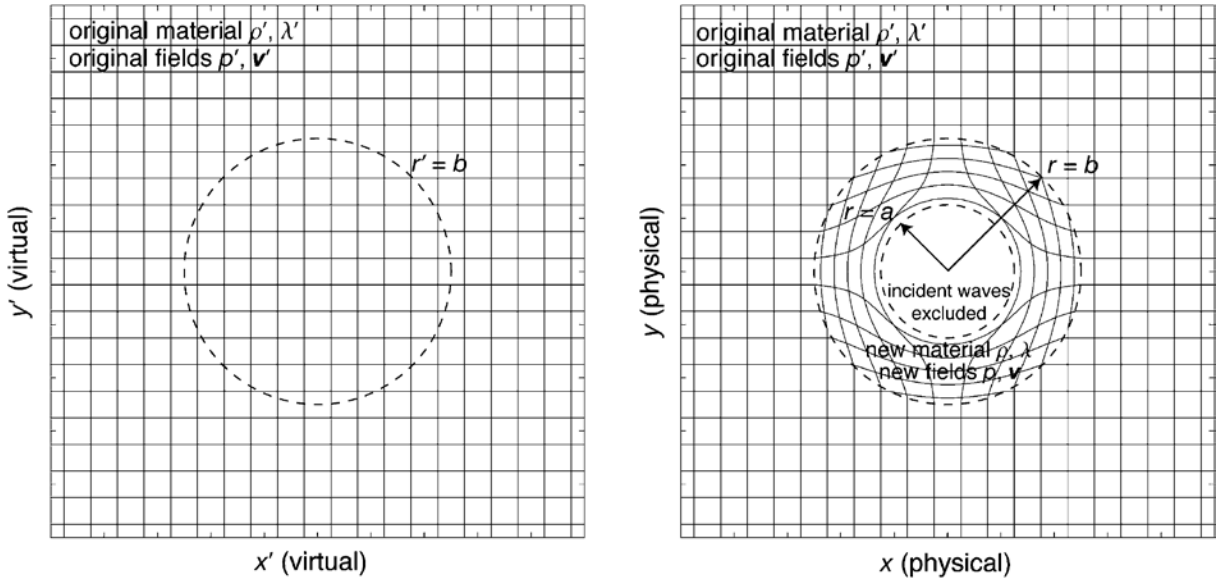

Figure 1.1 Reprint showing virtual space (left) that is transformed to physical space (right). The transform "stretches" the very center point of the circle on the left ($r = 0$) to form the opening in the physical space ($r < a$), that can be used to conceal an object. (Craster & Guenneau, 2012)

The cloaks devised with coordinate transformation have specifically designed properties. The properties of the acoustic cloaks are usually anisotropic (having a physical property that has a different value when measured in different directions) and inhomogeneous (having different values when measured at different positions). An acoustic cloak usually covers a space and guides the acoustic waves to pass around it without going through it. There are no reflections in front of the cloak and when the waves exit the cloak, it is as if the object were not there. From

outside of the cloak, ideally no disturbance is created by the cloak and its cloaked space. The space is acoustically “invisible”.

The acoustic cloaks designed with coordinate transformation can be omnidirectional, that is, working for sound waves from any direction. For this case, the transformation must be conducted in all directions. These cloaks are not designed for a specific frequency. They are also broadband, that is, they can work within a wide range of frequencies. They can be used to build sound proof houses, advanced concert halls or stealth warships.

In theory, acoustic cloaks can be designed with acoustic metamaterials. However, the material properties of the acoustic cloaks at some region are so extreme (i.e. infinite) that they cannot be built with materials in nature. Therefore, more contributions are needed for acoustic cloaks to be realized.

1.0.2 Objectives of this work

The ultimate goal of this cloaking work is to develop arbitrarily shaped, omnidirectional, broadband cloaks from metamaterials with properties and structures that are easy to fabricate. Specifically, this work has focused on designing 2D and 3D broadband cloaks with arbitrary shapes and 3D spherical pentamode acoustic cloaks. Five different methods will be presented to achieve part or all these goals.

The first method of designing 2D inertial acoustic cloaks having arbitrary shapes is based on using transformation acoustics to map along radial directions. Since the interior and exterior boundaries can be complicated, the properties can also be complicated. By dividing the cloak into small sections, the transverse anisotropy is removed, but the radial anisotropy remains.

The properties within each section are inhomogeneous, but could theoretically be realized using layered media. (Li & Vipperman, 2014)

The second and third methods concern designing 2D arbitrarily shaped inertial cloaks such that homogeneous material properties occur. One method accomplishes homogeneity by simply dividing 2D arbitrarily shaped acoustic cloaks into triangular patterns. Each triangle in physical space is then mapped to a corresponding triangle in virtual space, resulting in homogeneous properties. Each part can be built with an alternating layered structure comprised of only two materials. The second method of accomplishing 2D arbitrarily shaped cloaks with homogeneous materials is through the use of multiple transforms. Arc sections are first divided into two triangles, which are stretched along the two directions of the edges. The first triangle undergoes a single transform, while the second undergoes two. (Li & Vipperman, 2017) The fourth method is extending these methods to three dimensions. Here, rather than dividing a 2D arc section into two triangles, a 3D tetrahedral arc section is divided into three tetrahedra, each undergoing one, two, or three transformations. (Li & Vipperman, 2018) Also, a tetrahedron in virtual space can be directly mapped to another in physical space, leading to homogeneous properties.

The fifth method is the introduction of a new pentamode material that is amenable to designing 3D cloaks. Pentamode materials have special structures such that only compressional waves are supported. They have fluid-like properties in that no shear waves can exist, sometimes leading them to be called “meta-fluids.” Most of the work to date has focused on “crystalline” pentamode materials composed of DCS arranged to form face-centered-cubic (FCC) unit cells. The dispersion relationships show that there is a band of frequencies where all shear modes disappear. One limitation of FCC materials is that they cannot be arranged in a spherical shape.

Here, a hexagonal unit cell is proposed that can approximate the shape of a layered spherical pentamode structure. Hexagonal cells with DCS are designed and analyzed. From the dispersion relations, it is observed that there are also bandgaps where all shear modes disappear. The effect of the unit cell geometry on the acoustic properties is studied. The required anisotropic properties for cloaking can be realized by adjusting multiple geometric parameters within the structure. Unit cells for a 3D pentamode acoustic cloak are explored.

1.1 LITERATURE REVIEW ON ACOUSTIC CLOAKS

Acoustic metamaterials are engineered artificial materials whose properties depend on their structures which can be altered at will. With acoustic metamaterials, effective properties that cannot be found in nature can be realized, such as negative density (Huang, Sun, & Huang, 2009) or bulk modulus (Fang, et al., 2006) or both (Li & Chan, 2004) (Graci´a-Salgado, Torrent, & S´anchez-Dehesa, 2012). As a result, very interesting devices can be designed with metamaterials.

Transformation acoustics is a common technique to derive the properties of special devices. (Craster & Guenneau, 2012) With transformation acoustics, the physical space is mapped to a virtual space. The properties of devices are derived through the transformation of coordinates from a free field virtual space to a physical space that contains the devices. The method works by compressing, expanding, or stretching the waves through material anisotropy of the metamaterial. As a result, interesting new devices can be devised, such as acoustic cloaks, wave benders, and acoustic super- and hyper-lenses. (Craster & Guenneau, 2012) (Chen & Chan, 2010)

For acoustic cloaks designed with transformation acoustics, either the density or the stiffness or both can be anisotropic. The cloaks with anisotropic density and isotropic bulk modulus are called “inertial cloaks”, while the cloaks with anisotropic stiffness are called “pentamode cloaks”. (Norris, 2008) Broadband and omnidirectional cloaks can be created with either type. Other methods of designing acoustic cloaks are also reviewed below.

1.1.1 Inertial cloaks

Inertial acoustic cloaks possess anisotropic density and isotropic bulk modulus. Shortly after the electromagnetic (EM) cloaks were demonstrated (Pendry, Schurig, & Smith, 2006), a 2D acoustic cloak (Cummer & Schurig, 2007) was presented by comparing 2D acoustic equations with 2D Maxwell equations. In the next year, 3D acoustic cloaks were derived with transformation acoustics. (Chen & Chan, 2007) (Cummer S. A., et al., 2008)

Since the required materials are inhomogeneous and anisotropic, they cannot be found in nature. However, two-dimensional arrays of rigid cylinders in a fluid or a gas define, in the limit of large wavelengths (wavelength must be much larger than the cylinder diameter), a class of acoustic metamaterials whose effective mass densities are anisotropic. (Torrent & Sánchez-Dehesa, 2007) Multilayered structures of homogeneous materials were also used to design acoustic cloaks. (Torrent & Sánchez-Dehesa, 2008) (Cheng, Yang, Xu, & Liu, 2008) (Cheng & Liu, 2009) Pendry & Li (2008) discussed a structure with anisotropic properties and its application to build ground cloaks. Popa & Cummer (2009) designed and characterized a broadband acoustic composite metamaterial made of periodic arrangements of highly subwavelength unit cells in a fluid. Similar structures were later experimentally tested.

(Zigoneanu, Popa, Starr, & Cummer, 2011) A multilayered acoustic metamaterial consisting of more than two different layers was also studied. (Zhu, Huang, & Hu, 2012)

The properties of a perfect cloak that maps the cloaked space to a point in virtual space are singular at the interior boundaries. A ‘reduced cloak’ was proposed in electromagnetics whereby density elements and bulk modulus are multiplied by a factor, leading to properties that are physically realizable. (Cummer, Popa, Schurig, Smith, & Pendry, 2006) The method was later extended to acoustic cloaks. (Chen, Yang, Luo, & Ma, 2008)

The transformation of the cloaked space to a small, finite area is another way to improve material properties. (Chen, et al., 2007) A larger area leads to better material properties, but also provides a larger residual scattering cross-section. It was shown for EM cloaks that selected transformation relations can have a significant impact on the material properties. (Cummer, Liu, & Cui, 2009) (Rajput & Srivastava, 2014) The transformations used in deriving the cloak properties were analyzed for achieving attainable material properties. (Urzhumov, Ghezzo, Hunt, & Smith, 2010)

Compared with omnidirectional cloaks, unidirectional cloaks are much easier to realize. The “carpet cloak” was first designed for electromagnetics. (Li & Pendry, 2008) An acoustic “ground cloak” which covers a cloaked space against a reflecting plane was designed and fabricated. (Kan, et al., 2015) A unidirectional cloak with homogeneous parts was proposed by Zhu, et al. (Zhu, Ding, & Zhao, 2010). The cloak can be divided in half to form a ground cloak. 2D ground cloaks were studied in air and water. (Popa & Cummer, 2011)(Popa, Zigoneanu, & Cummer, 2011) (Xiong, Chen, Wang, & Zhu, 2015) (Bi, Jia, Lu, Ji, & Yang, 2017) (Bi, Jia, Sun, Yang, Zhao, & Yang, 2018) An omnidirectional 3D ground cloak in air was designed and tested by extending the 2D theory to 3D. (Zigoneanu, Popa, & Cummer, 2014) This kind of cloak in a

two-layered background of water and NaCl aqueous solution is designed with steel and porous materials. (Zhu, et al., 2015)

Omnidirectional cloaks can also be composed of homogeneous parts. A 2D diamond EM cloak was proposed with a two-step coordinate transformation. (Li, Guan, Sun, Wang, & Zhang, 2009) Similarly, a 3D EM diamond cloak was designed with a three-step coordinate transformation. (Wang, et al., 2010) These cloaks were introduced to acoustics. (Li, Huang, Yang, Lan, & Sun, 2012) A triangular acoustic cloak with homogeneous parts was also proposed. (Zhu, et al., 2016)

EM cloaks with arbitrary shapes were studied extensively. (Wu, Zhang, Meng, & Li, 2008) (Zhang, Luo, Chen, & Wu, 2008) (Li & Li, 2008) (Jiang, et al., 2008) (Nicolet, Zolla, & Guenneau, 2008) (Chen, Fu, & Yuan, 2009) Acoustic cloaks with arbitrary shapes were also explored. Numerical methods were used to derive their properties. (Hu, Zhou, & Hu, 2009) (Yang, Huang, Cai, Xie, & Yang, 2013) (Wang X. , et al., 2010)

1.1.2 Pentamode cloaks

Besides inertial cloaks, pentamode cloaks can be created. The first pentamode structure was proposed by Milton & Cherkaev (1995), who studied a two-phase composite comprised of a combination of a sufficiently compliant isotropic phase and a sufficiently rigid isotropic phase. Pentamode structures can only support a single stress - compressional. Since the shear waves disappear, pentamode materials were studied for their potential for building cloaks. (Milton, Briane, & Willis, 2006) Norris (2008) generalized acoustic cloaks and proposed the use of pentamode materials. Conceptually perfect pentamode metamaterials would flow away like a fluid, but practical pentamode metamaterials comprised of flexible structures have been

fabricated. (Kadic, Bückmann, Stenger, Thiel, & Wegener, 2012) As with inertial cloaks, the transformation from the physical space to virtual space affects the properties of the cloaks. Special transformations for pentamode acoustic cloaking were studied, producing cloaks with special properties, for example, constant density. (Gokhale, Cipolla, & Norris, 2012)

Phonon band structures of 3D pentamode metamaterials with a FCC unit cell composed of double-cone structures (DCS) were calculated. (Martin, Kadic, Schittny, Bückmann, & Wegener, 2012) Bandgaps were observed where only compressional modes occurred within specific frequency ranges. It was shown that the mechanical and acoustical properties of the structure were affected by the geometries of the unit cell and the DCSs. With the variation of its structure, highly anisotropic properties were derived. (Kadic M., Bückmann, Schittny, & Wegener, 2013) A modified pentamode structure was proposed whose mass density and bulk modulus can be tailored independently, potentially facilitating design. (Kadic M., Bückmann, Schittny, Gumbsch, & Wegener, 2014) Besides symmetric elements, pentamode materials with asymmetric DCSs were also studied. (Cai, Wang, Li, Xu, & Tian, 2015)

The 2D equivalent of a pentamode material is the “bimode material.” Because of their similarities to pentamode materials in 3D, they are sometimes also referred to as pentamode materials. At the same time that pentamode materials were proposed, 2D bimode materials with honeycomb structures were also proposed. (Milton & Cherkaev, 1995) Highly anisotropic properties were derived from the honeycomb structures. (Layman, Naify, Martin, Calvo, & Orris, 2013) A 2D latticed pentamode cloak in water was designed. (Chen, Liu, & Hu, 2015)

The feasibility of constructing acoustic cloaks using layered pentamode-type fluids has been reported. (Scandrett, Boisvert, & Howarth, 2010) In later reports, the layers were

optimized for broadband performance. (Scandrett, Boisvert, & Howarth, 2011)(Boisvert, Scandrett, & Howarth, 2016)

1.1.3 Other type of acoustic cloaks

Besides the abovementioned cloaks, there are other types of acoustic cloaks. Different methods can be used to derive acoustic cloaking.

Unidirectional cloaks are easier to design and realize than omnidirectional cloaks. For example, a 2D acoustic cloak was designed based on the cancellation from cylinders around the obstacle. (García-Chocano, et al., 2011) The positions of the cylinders were optimized. The model was extended to 3D with axisymmetric structure. (Sanchis, et al., 2013) Another one-directional acoustic cloak was designed with copper chambers, including one pressure absorber and one pressure projector connected by an isolated energy channel. Acoustic waves propagate through the channels and leave the inner region cloaked. (Zhao, Chen, Li, & Qiu, 2015) A broadband unidirectional acoustic cloak with two flat acoustic lenses based on phase gradient meta-surfaces was also designed. (Wang, Wan, Chen, Song, & Wang, 2016) Finally, unidirectional cloaks can also be designed with parity-time symmetric media. (Zhu, Ramezani, Shi, Zhu, & Zhang, 2014) (Sounas, Fleury, & Alù, 2015)

2D cloaks work in any direction within the plane of the cloak. A 2D cylindrical cloak in water with a lumped anisotropic transmission line composed of cavities and tubes was designed and tested. (Zhang, Xia, & Fang, 2011) An omnidirectional 2D acoustic cloak with axisymmetric cylindrical lattices was designed by optimizing their positions to reduce the effect of the obstacle. (Jo, Jeong, Kwon, Park, & Oh, 2015)

A cloak works by bending acoustic waves around the cloaked region of space. As a result, little or no energy enters the cloaked space and likewise little or no energy can leave. The bending of waves can be used to create rather unconventional and creative cloaks. For example, “external cloaks” have been developed in EM field which can cancel the effect of an object at a distance away from the cloaking shell consisting of complementary materials with double-negative properties (negative effective permittivity and permeability). (Lai, Chen, Zhang, & Chan, 2009). The device with a complementary layer in acoustics was also studied. (Shen, et al., 2012) It was called an ‘anti-cloak’. The acoustic field can be detected inside the anti-cloak while the outside field remains undisturbed. This could, for example, permit a submarine to listen while not being detected. An acoustic cloaking shell consisting of complementary media with single-negative parameters (either negative effective density or bulk modulus) was proposed. (Zhu, Liang, Kan, Zou, & Cheng, 2011) (Xu, et al., 2012)

1.2 CONTRIBUTIONS OF THIS WORK

The ultimate goal of this work is to build cloaks of arbitrary 2D and 3D shape that are composed of homogenous materials, which are easier to realize. Five different design methods are presented which contribute toward this goal.

The first contribution of this work is a method of designing two-dimensional, inertial acoustic cloaks (presented in Chapter 3.0) having arbitrary shapes, based on using transformation acoustics to map along radial directions. Since the interior and exterior boundaries can be complicated, the properties can also be complicated. By dividing the cloak into small sections, the transverse anisotropy is removed, but the radial anisotropy remains. The properties within

each section are inhomogeneous, but could theoretically be realized using layered media. However, each layer would be of a different material, the properties of which would become quite extreme, particularly at the interior boundaries.

The second and third contributions of this work are two methods of designing 2D arbitrarily shaped cloaks such that homogeneous material properties occur. One method accomplishes homogeneity by simply dividing 2D arbitrarily shaped acoustic cloaks into triangular patterns (Chapter 5.0). Each triangle in physical space is then mapped to a corresponding triangle in virtual space, resulting in homogeneous properties. Each part can be built with an alternating layered structure comprised of only two materials. The second method of accomplishing 2D arbitrarily shaped cloaks with homogeneous materials is through the use of multiple transforms (Chapter 4.0). Arc sections are first divided into two triangles, which are stretched along the two directions of the edges. The first triangle undergoes a single transform, while the second undergoes two. The fourth contribution of this work is presented in Chapter 6.0, and is an extension of these methods to three dimensions. Here, rather than dividing a 2D arc section into two triangles, a 3D tetrahedral arc section is divided into three tetrahedra, each undergoing one, two, or three transformations. The transformation can also be conducted by a direct mapping from a tetrahedron to another. Depending upon the degree of the symmetry, the cloak can usually be constructed using a handful of homogeneous parts.

The fifth contribution of the work is the introduction of a new pentamode material that is amenable to designing 3D cloaks, which is presented in Chapter 7.0. Pentamode materials have special structures such that only compressional waves are supported. They have fluid-like properties in that no shear waves can exist, sometimes leading them to be called “meta-fluids.” Most of the work to date has focused on “crystalline” pentamode materials composed of DCSs

arranged to form face-centered-cubic (FCC) unit cells. The dispersion relationships show that there is a band of frequencies where all shear modes disappear. One limitation of FCC materials is that they cannot be arranged into a spherical shape for 3D cloaking. Here, a hexagonal unit cell is proposed that can approximate the shape of a layered spherical pentamode structure. Hexagonal cells with DCSs are designed and analyzed. From the dispersion relations, it is observed that there are also bandgaps where all shear modes disappear. The effect of the unit cell geometry on the acoustic properties is studied. The required anisotropic properties for cloaking can be realized by adjusting multiple geometric parameters within the structure. Unit cells for a 3D pentamode acoustic cloak are explored.

1.3 OUTLINE OF THE DISSERTATION

The dissertation begins with a brief review of theoretical fundamentals of inertial and pentamode acoustic cloaks in Chapter 2.0. In Chapter 3.0, 2D inertial acoustic cloaks with arbitrary shapes that are designed by mapping along radial directions are presented. Chapter 4.0 contains the 2D arbitrarily shaped inertial acoustic cloaks that are divided into triangular parts with homogeneous properties using a two-step transformation method. Arbitrarily shaped inertial acoustic cloaks that have been divided into arbitrary triangular patterns are presented in Chapter 5.0. 3D acoustic cloaks composed of homogeneous tetrahedral parts are studied in Chapter 6.0. In Chapter 7.0, the pentamode material with a hexagonal unit cell is discussed. Finally, conclusions and future work are presented in Chapter 8.0.

2.0 BRIEF REVIEW OF FUNDAMENTALS

Both inertial and pentamode acoustic cloaks are studied in this dissertation. The fundamentals used for designing inertial and pentamode acoustic cloaks are reviewed.

2.1 INERTIAL ACOUSTIC CLOAKS

Inertial acoustic cloaks have anisotropic density and isotropic bulk modulus. Transformation acoustics is used to derive the properties of inertial acoustic cloaks in the following subsections.

2.1.1 Derivation of inertial acoustic cloaks with transformation acoustics

Suppose there is a cloak placed in a medium with homogeneous, isotropic and constant properties, the acoustic equations in the background medium are

$$\begin{aligned} \nabla p &= \rho_b \frac{\partial \boldsymbol{v}}{\partial t} \\ \frac{\partial p}{\partial t} &= \kappa_b \nabla \cdot \boldsymbol{v} \end{aligned} \tag{2.1}$$

where ρ_b and κ_b are the density and bulk modulus of the medium, p is pressure, and $\boldsymbol{v}$ is velocity.

The properties of the cloaks can be derived with transformation acoustics. (Craster & Guenneau, 2012) (Chen & Chan, 2007) The transformation from the virtual space to the

physical space is defined by a pointwise deformation T, as shown in Figure 2.1. The original background medium is considered the "virtual space". The acoustic equations in the virtual space are denoted with a subscript "X."

$$\nabla_X p_X = \rho_b \frac{\partial \boldsymbol{v}_X}{\partial t}$$
$$\frac{\partial p_X}{\partial t} = \kappa_b \nabla \cdot \boldsymbol{v}_X \tag{2.2}$$

Suppose the variables are harmonic with a radian frequency of ω, then combining the two equations together and eliminating velocities gives

$$\nabla_X \cdot \left[\rho_b^{-1} \nabla_X p_X\right] + \frac{\omega^2}{\kappa_b} p_X = 0 \tag{2.3}$$

Coordinate transformation is taken by mapping the points in the virtual space (Ω, Figure 2.1) to the physical space occupied by the cloak, (ω, Figure 2.1). In effect, we're opening a hole in physical space, in which an object can be concealed.

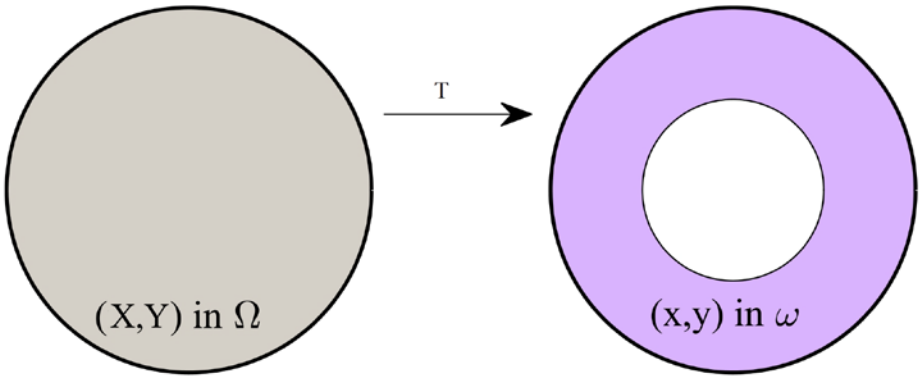

Figure 2.1 Transformation from the virtual space (Ω) to the physical space (ω)

The Jacobian matrix of the transformation is used to determine the cloak material properties. Selection of a coordinate system is at the discretion of the user, and will impact the

degree of difficulty in deriving the properties. In a Cartesian coordinate system, the 3D Jacobian matrix is defined as

$$\boldsymbol{J} = \begin{bmatrix} \dfrac{\partial x}{\partial X} & \dfrac{\partial y}{\partial Y} & \dfrac{\partial z}{\partial Z} \\ \dfrac{\partial y}{\partial X} & \dfrac{\partial y}{\partial Y} & \dfrac{\partial y}{\partial Z} \\ \dfrac{\partial z}{\partial X} & \dfrac{\partial z}{\partial Y} & \dfrac{\partial z}{\partial Z} \end{bmatrix} \tag{2.4}$$

where (x, y, z) are in physical space, and (X, Y, Z) are in virtual space. In a cylindrical coordinate system,

$$\boldsymbol{J} = \begin{bmatrix} \dfrac{\partial r}{\partial R} & \dfrac{\partial r}{R\partial \Theta} & \dfrac{\partial r}{\partial Z} \\ \dfrac{r\partial \theta}{\partial R} & \dfrac{r\partial \theta}{R\partial \Theta} & \dfrac{r\partial \theta}{\partial Z} \\ \dfrac{\partial z}{\partial R} & \dfrac{\partial z}{R\partial \Theta} & \dfrac{\partial z}{\partial Z} \end{bmatrix} \tag{2.5}$$

where (r, θ, z) are in physical space, and (R, Θ, Z) are in virtual space. Finally, for spherical coordinates,

$$\boldsymbol{J} = \begin{bmatrix} \dfrac{\partial r}{\partial R} & \dfrac{\partial r}{R\partial \Theta} & \dfrac{\partial r}{R\partial \Phi} \\ \dfrac{r\partial \theta}{\partial R} & \dfrac{r\partial \theta}{R\partial \Theta} & \dfrac{r\partial \theta}{R\partial \Phi} \\ \dfrac{r\partial \phi}{\partial R} & \dfrac{r\partial \phi}{R\partial \Theta} & \dfrac{r\partial \phi}{R\partial \Phi} \end{bmatrix} \tag{2.6}$$

where (r, θ, ϕ) are polar coordinates in physical space, and (R, Θ, Φ) are in virtual space.

The relationship of the gradient operators between the two spaces is governed by $\boldsymbol{J}$ as

$$\nabla_X = \boldsymbol{J}^T \nabla \, . \tag{2.7}$$

The relationship between the velocities in the two spaces is given by

$$\boldsymbol{v} = \frac{\boldsymbol{J}}{\det(\boldsymbol{J})} \boldsymbol{v}_X \, . \tag{2.8}$$

Suppose the density is a tensor in the physical space, then the acoustic equations in the physical space are given by

$$\nabla p = i\omega \overline{\overline{\boldsymbol{\rho}}}\, \boldsymbol{v}\,, \qquad i\omega p = \kappa \nabla \cdot \boldsymbol{v}\,. \tag{2.9}$$

Substituting Equations (2.7) and (2.8) into Equations (2.9), we get

$$\det(\boldsymbol{J})\left(\boldsymbol{J}^T \overline{\overline{\boldsymbol{\rho}}}\, \boldsymbol{J}\right)^{-1} \nabla_X p = i\omega \boldsymbol{v}_X \text{ ,and} \qquad i\omega p = \frac{\kappa}{\det(\boldsymbol{J})} \nabla_X \cdot \boldsymbol{v}_X\,. \tag{2.10}$$

Combining the two equations together and eliminating velocities, we get

$$\nabla_X \cdot \left[\det(\boldsymbol{J})\left(\boldsymbol{J}^T \overline{\overline{\boldsymbol{\rho}}}\, \boldsymbol{J}\right)^{-1} \nabla_X p \right] + \frac{\omega^2}{\kappa / \det(\boldsymbol{J})}\, p = 0\,. \tag{2.11}$$

By comparing Equation (2.3) with (2.11), p equals p_X when

$$\det(\boldsymbol{J})\left(\boldsymbol{J}^T \overline{\overline{\boldsymbol{\rho}}}\, \boldsymbol{J}\right)^{-1} = \rho_b{}^{-1}\text{, and} \qquad \kappa / \det(\boldsymbol{J}) = \kappa_b\,. \tag{2.12}$$

The required density tensor and bulk modulus of the cloaks are thus given by

$$\overline{\overline{\boldsymbol{\rho}}} = \rho_b \det(\boldsymbol{J})\left(\boldsymbol{J}^T\right)^{-1} \boldsymbol{J}^{-1}, \qquad \kappa = \kappa_b \det(\boldsymbol{J})\,. \tag{2.13}$$

2.1.2 Transformation type

In transformation acoustics, the virtual space is mapped to the physical space. The virtual space is usually the background media. What the interior boundary of the cloak maps to in the virtual

space, defines the size of the residual scattering cross section. As discussed earlier, for a 2D acoustic cloak, this could be a point, a line, or a smaller area in virtual space. The cloaked area is a larger hollow space in which an object can be concealed, and to which the point, line, or smaller area in the virtual space is mapped.

In a perfect cloak, the interior boundary is mapped from a point in the virtual space. An annular area in physical space is mapped from a circular one in virtual space with the interior boundary of the cloak corresponding to a point, as shown in Figure 2.2. The points in the cloak are mapped from the virtual space one to one except the interior boundary. The outer boundary of the cloak is coincident with the mapped boundary in the virtual space. One can see how the physical space has been distorted, which can bend or stretch acoustic waves around the hole formed in physical space (Figure 2.2b). The distortion is created by introducing material anisotropy.

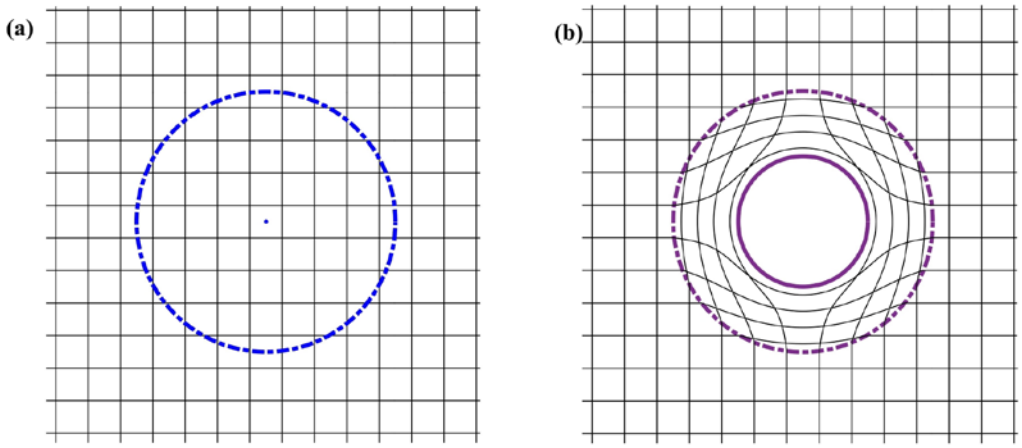

Figure 2.2 Virtual space and physical space with the interior boundary corresponding to a point (a) virtual space (b) physical space

The properties of a “perfect” cloak at the interior boundary are singular. To avoid singularity, an “approximate cloak” can be formed by mapping the cloaked region of the cloak from a small area, as shown in Figure 2.3.

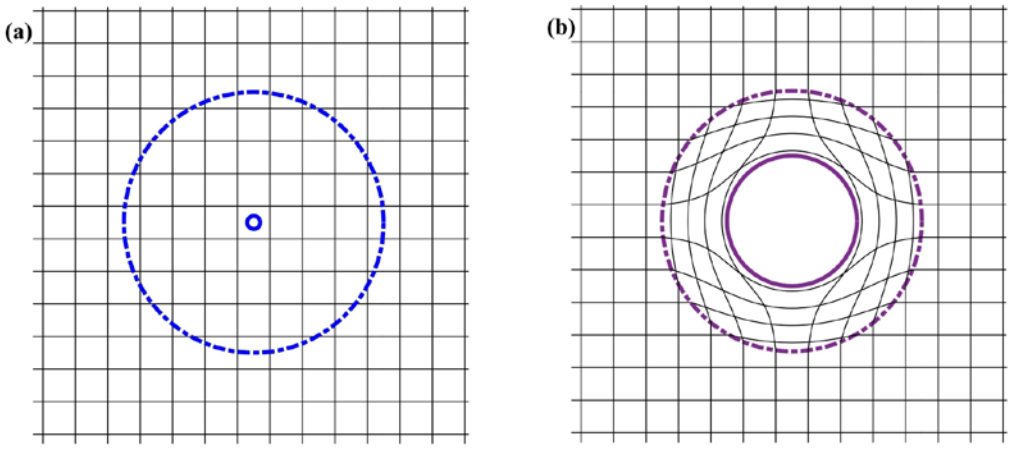

Figure 2.3 Virtual space and physical space with the interior boundary corresponding to an area (a) virtual space (b) physical space

The interior boundary of the cloak can also be mapped from a line, as shown in Figure 2.4. A line in virtual space is stretched upward and downward to form a diamond space in physical space. Because the cloaked area is mapped from a line, the cloak only works in the direction parallel to the line (1D cloak). If the line is stretched only “upward”, a “ground cloak” is formed, which can conceal an object in a space against a reflecting plane. The line can be divided into more segments. For example, a trapezoidal ground cloak can be formed.

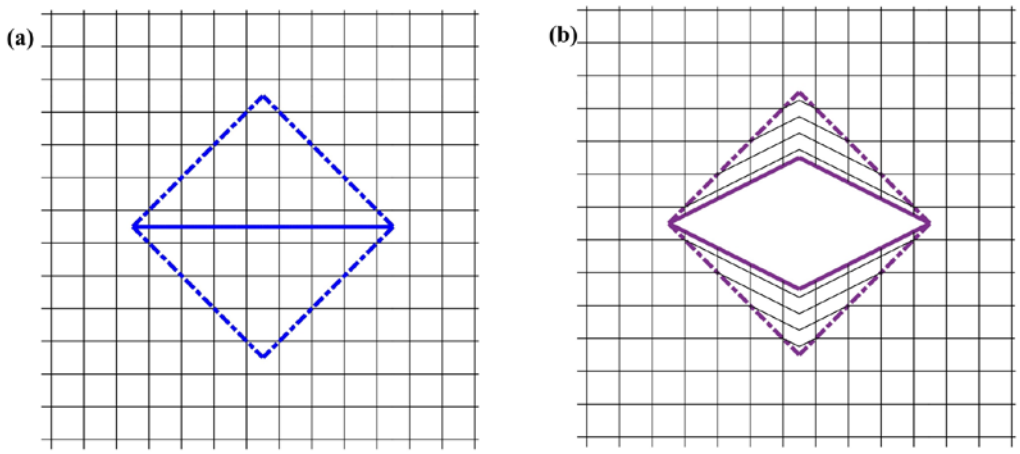

Figure 2.4 Virtual space and physical space with the interior boundary corresponding to a line (a) virtual space (b) physical space

The interior boundary of the cloak can also be mapped from a short "line", as shown in Figure 2.5. Starting with a short line, it is first stretched in the parallel direction to create a longer line, and then stretched in the perpendicular direction as in Figure 2.4. The difference is that because the resulting space on the left is small, the "approximate" cloak works in all directions.

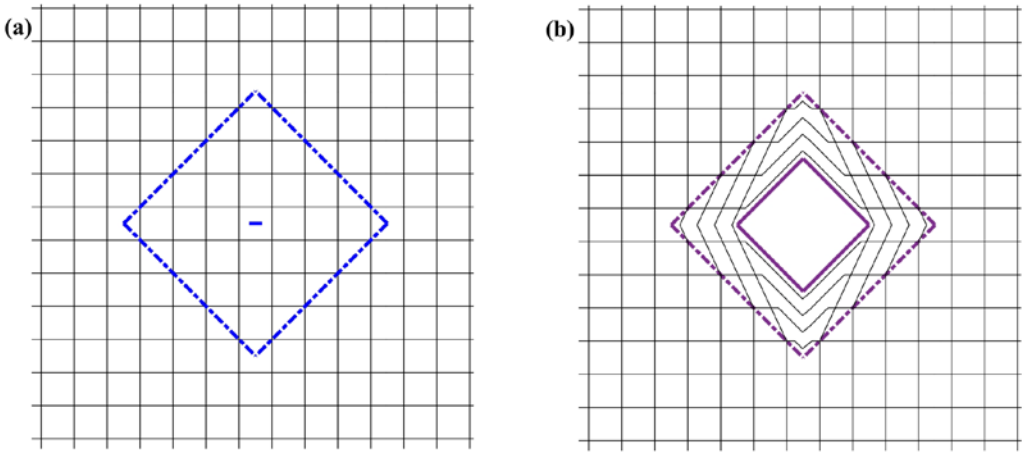

Figure 2.5 Virtual space and physical space with the interior boundary corresponding to a short line (a) virtual space (b) physical space

For 3D cloaks, the cloaked space is a volume, which can similarly be mapped from a point, a line, an area, or a smaller volume. The perfect 3D cloaks are those that the cloaked space is mapped from a point or a line. A 3D ground cloak is the one whose cloaked space is mapped from an area. The cloaks whose cloaked space is mapped from an area or a small volume are called “approximate cloaks”. They have high frequency limits when the wavelength of sound approaches the dimensions of the residual area. “Perfect cloaks,” mapped from a point require extreme (infinite) material properties at the inner boundary. However, designing approximate cloaks addresses the issues with these singularities.

2.1.3 Transformation relations

Transformation from virtual space to physical space (or from physical space to virtual space) is not unique. Different transformations from the physical space to the virtual space lead to different properties.

Annular cloaks that are mapped along radial directions are the basic models. The required properties of the cloaks (Norris, 2008) are

$$\begin{aligned} \frac{\rho_r}{\rho_b} &= f'\left(\frac{r}{f}\right)^{d-1}, \\ \frac{\rho_t}{\rho_b} &= \frac{1}{f'}\left(\frac{r}{f}\right)^{d-3}, \\ \frac{\kappa}{\kappa_b} &= \frac{1}{f'}\left(\frac{r}{f}\right)^{d-1}. \end{aligned} \tag{2.14}$$

where d= (2 or 3) is the dimension of the cloak, and $f(r)$ is the transformation function from the physical space to the virtual space, f’ is the derivative of f with respect to r. The transformations and thus material properties are not unique.

For an annular cloak with inner radius of 1 and outer radius of 2 mapped to another annulus with inner radius of 0.05 and outer radius of 2 in virtual space, some possible transformations from the physical space to the virtual space are shown in Figure 2.6. Some of these will be explored in more detail next.

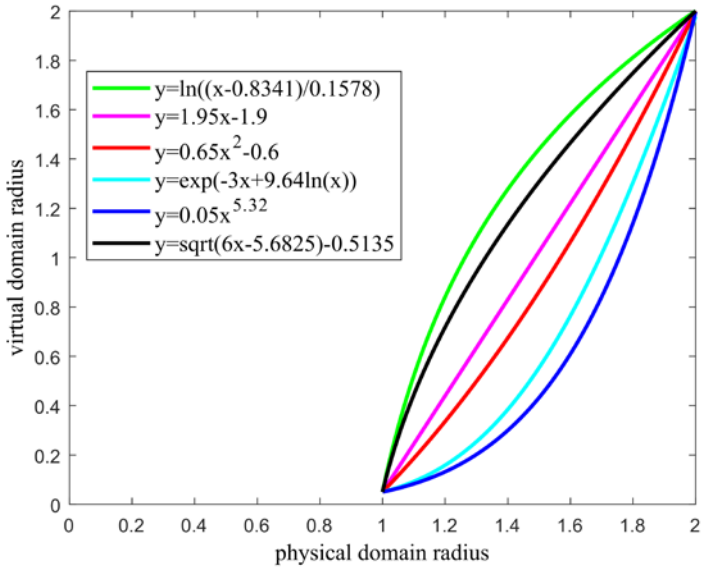

Figure 2.6 Mapping relations from an annular virtual space to an annular physical space

The simplest model is a linear transformation, which is given by

$$R = 1.95r - 1.9\,. \tag{2.15}$$

The resulting properties are

$$\begin{aligned} \frac{\rho_r}{\rho_b} &= \frac{1.95r}{1.95r-1.9}, \\ \frac{\rho_t}{\rho_b} &= \frac{1.95r-1.9}{1.95r}, \\ \frac{\kappa}{\kappa_b} &= \frac{1}{1.95}\frac{r}{1.95r-1.9}\,. \end{aligned} \tag{2.16}$$

A simulation of a cloak designed using this transformation is shown in Figure 2.7. The cloak works well and the waves are linearly compressed within the cloak.

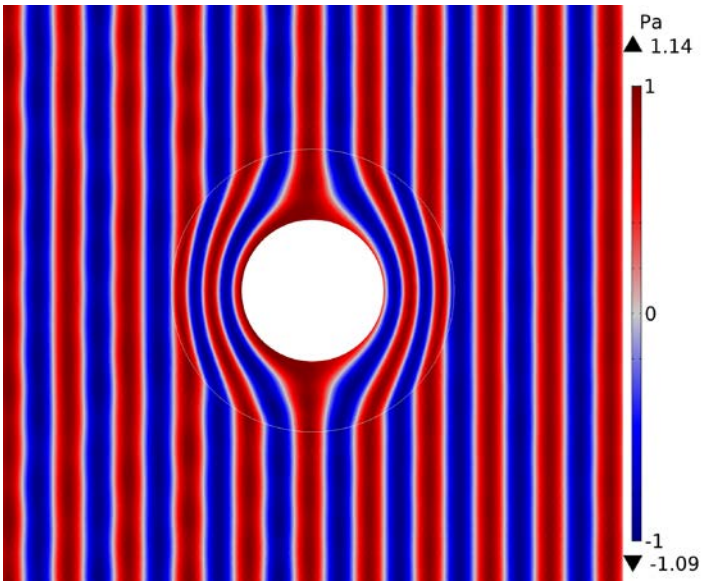

Figure 2.7 Simulation of a cloak with a linear transformation

Special transformation leads to special properties. Another transformations is given by

$$R = 0.05r^{5.32}. \tag{2.17}$$

The material properties become

$$\begin{aligned} \frac{\rho_r}{\rho_b} &= 5.32, \\ \frac{\rho_t}{\rho_b} &= \frac{1}{5.32}, \\ \frac{\kappa}{\kappa_b} &= \frac{400}{5.32r^{8.64}}. \end{aligned} \tag{2.18}$$

An advantage of this transformation is that ρ_r and ρ_t are constant for the whole domain, whereas densities in Equations (2.16) exhibit radial dependence. The simulation of this cloak is shown in

Figure 2.8, and is again observed to work well. As can be observed in the figure, the waves are compressed more near the outer radius of the cloak than the inner.

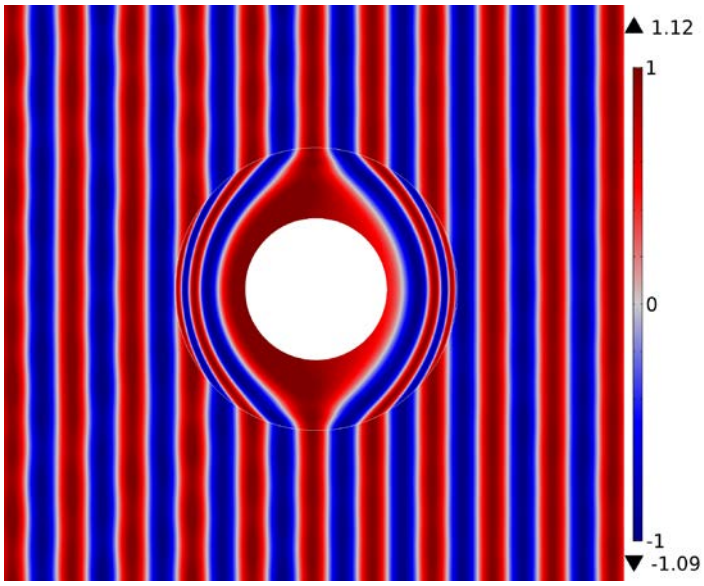

Figure 2.8 Simulation of a cloak with a fractional polynomial transformation

Another possible transformation is given by

$$R = \ln\left(\frac{r\text{-}0.8341}{0.1578}\right). \tag{2.19}$$

The properties are

$$\begin{aligned}
\frac{\rho_r}{\rho_b} &= \frac{r}{r\text{-}0.8341}\frac{1}{\ln\left(\frac{r\text{-}0.8341}{0.1578}\right)}, \\
\frac{\rho_t}{\rho_b} &= \frac{r-0.8341}{r}\ln\left(\frac{r\text{-}0.8341}{0.1578}\right), \\
\frac{\kappa}{\kappa_b} &= \frac{r(r-0.8341)}{\ln\left(\frac{r\text{-}0.8341}{0.1578}\right)}.
\end{aligned} \tag{2.20}$$

The simulation with the cloak is shown in Figure 2.9. The cloak also works and it is seen that waves are compressed more around the inner radius of the cloak.

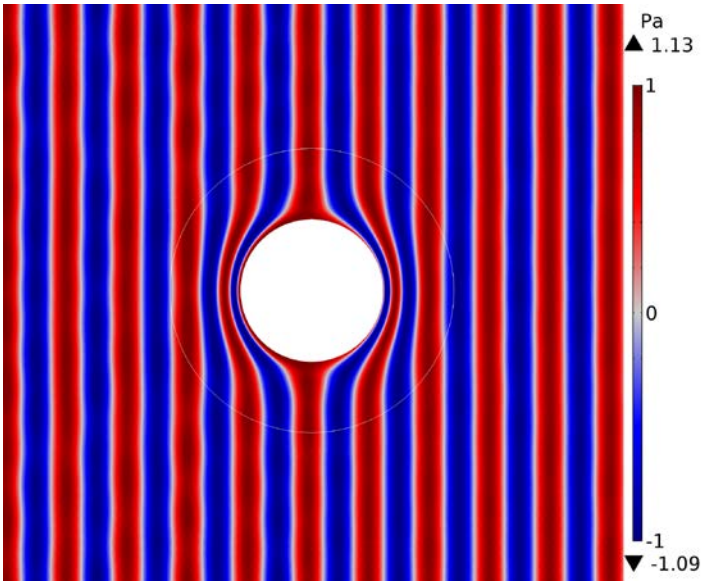

Figure 2.9 Simulation of a cloak with square root type transformation

2.1.4 Layered structures

The properties of inertial acoustic cloaks are anisotropic. One way to derive anisotropic density is to use layered structures. When the thickness of each layer is much smaller than the wavelength, the alternating layered structure can be described as an effective anisotropic medium. With two homogeneous and isotropic layers 1 (mass density ρ_1 bulk modulus κ_1) and 2 (mass density ρ_2, bulk modulus κ_2) arranged alternatively, as shown in Figure 2.10, the effective densities and bulk modulus (Cheng, Yang, Xu, & Liu, 2008) (Torrent & Sánchez-Dehesa, 2008) are given by

$$\rho_{\perp} = \frac{\rho_1 + \eta\rho_2}{1+\eta}, \qquad \frac{1}{\rho_{||}} = \frac{1}{1+\eta}\left(\frac{1}{\rho_1} + \frac{\eta}{\rho_2}\right), \tag{2.21}$$

$$\frac{1}{\kappa} = \frac{1}{1+\eta}\left(\frac{1}{\kappa_1} + \frac{\eta}{\kappa_2}\right),$$

where η is the thickness ratio of layer 2 over layer 1.

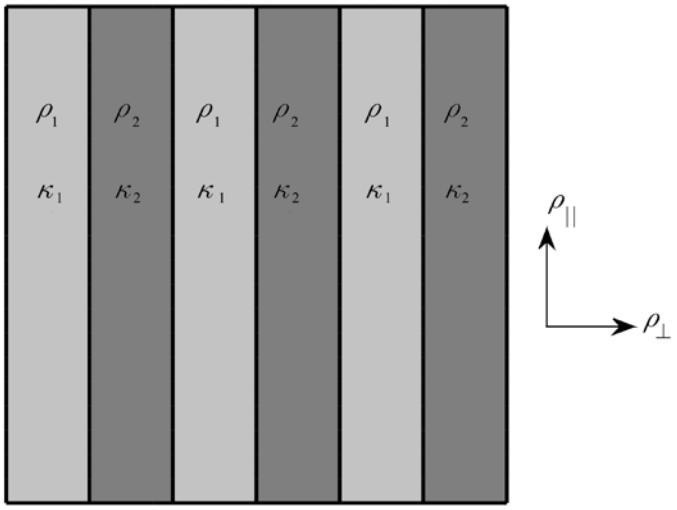

Figure 2.10 Layered structures of two materials arranged alternatively

For a perfect circular cloak with inner radius of *a* and outer radius of *b*, the linear transformation from physical space to virtual space is

$$R = \frac{b}{b-a}(r-a). \tag{2.22}$$

where *R* is the radius in virtual space, and *r* is the radius in physical space.

The properties of the cloaks derived with Equations (2.14) are

$$\begin{aligned} \frac{\rho_r}{\rho_b} &= \frac{r}{r-a}, \\ \frac{\rho_t}{\rho_b} &= \frac{r-a}{r}, \\ \frac{\kappa}{\kappa_b} &= \left(\frac{b-a}{b}\right)^2 \frac{r}{r-a}. \end{aligned} \tag{2.23}$$

By solving the Equations (2.21) and (2.23), the required properties of the layer 1 and layer 2 are

$$\frac{\rho_1}{\rho_b}, \frac{\rho_2}{\rho_b} = \frac{r}{r-a} \pm \sqrt{\left(\frac{r}{r-a}\right)^2 - 1}, \qquad \frac{\kappa_1}{\kappa_b} = \frac{\kappa_2}{\kappa_b} = \left(\frac{b-a}{b}\right)^2 \frac{r}{r-a}. \tag{2.24}$$

The simulation of a plane wave with amplitude of 1 Pa propagating through a space with the layered cloak is simulated with COMSOL Multiphysics, as shown in Figure 2.11. The cloak was built with concentric layered structures with the properties given by Equations (2.24) and good cloaking behavior can still be observed. Although the cloak is broadband, the layers introduce a low-frequency limit in the design, where the wavelength should be much larger than the layer thickness.

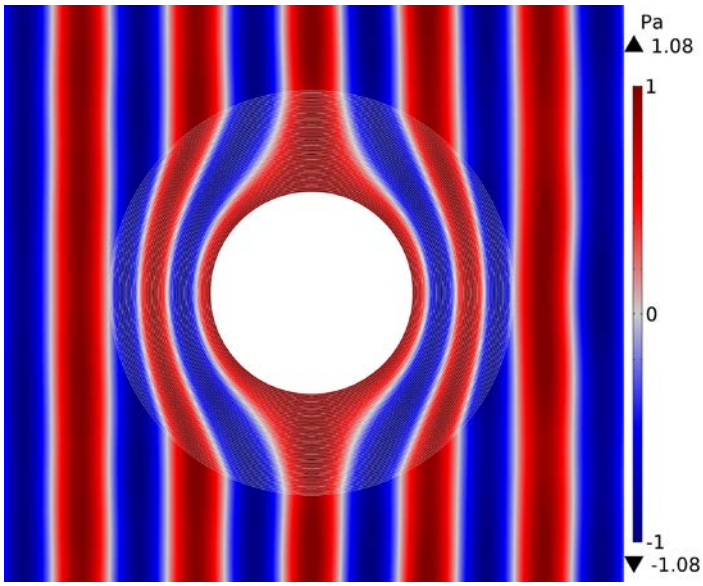

Figure 2.11 Simulation results of a plane wave with amplitude of 1 Pa through a space with the layered cloak

2.2 PENTAMODE ACOUSTIC CLOAKS

Besides inertial acoustic cloaks, pentamode materials can also be used to design acoustic cloaks. Pure pentamode acoustic cloaks have isotropic density and anisotropic stiffness. (Norris, 2008)

2.2.1 Pentamode materials

2D bimode materials and 3D pentamode (PM) materials have special properties. They can only withstand compressional stresses. All the shear modes disappear.

Double-cone structures (DCSs) are usually used to design pentamode materials. The thin ends of the double-cone structures are not zero to maintain the strength and stability of the structure. The finite ends prevent perfect PM behavior by introducing some shear modes. However, these tend to be orders of magnitude smaller. The pentamode materials used in previous works were face-centered cubic (FCC) pentamode structure. The primitive cell and its first Brillouin zone are shown in Figure 2.12. In Figure 2.12a, four double-cone structures are indicated in purple. The thin ends join to form the vertices of the lattice. In Figure 2.12b, the irreducible zone is shown inside of the Brillouin zone. The wave properties of the unit cell can be derived from the irreducible zone (Martin, Kadic, Schittny, Bückmann, & Wegener, 2012).

Dispersion relations describe the properties of a wave travelling through a medium. They relate wavenumbers to frequencies. The dispersion relations of the primitive cell were computed using COMSOL Multiphysics finite element software. The structure is simulated in vacuo. The side length of the unit cell is l. The diameter of the thick-end is $0.08l$, and the thin-end is $0.015l$. The properties of the materials for the DCSs are: E=3GPa, ρ=1100 kg/m3 and Poisson's ratio=0.3. The dispersion relations of the irreducible zone are shown in Figure 2.13.

There is a bandgap, indicated in gray, where shear waves disappear and only compressional waves exist. This indicates the locus of values for the side length of the unit cell, *l*, approximately 0.7-3.7 l/λ, where λ is the wavelength of acoustic waves in air.

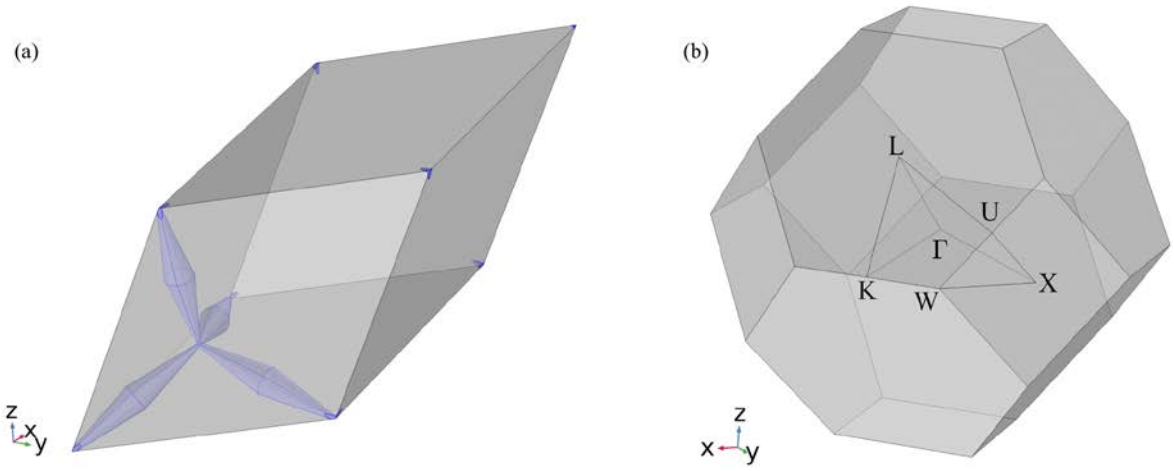

Figure 2.12 Face-centered-cubic primitive cell with double-cone structures and its Brillouin zone (a) primitive cell (b) Brillouin zone

The geometries of the unit cell affect the effective properties of the material. For example, anisotropy can be introduced by moving the connection point away from the center of the tetrahedron formed where the four ends of the double-cone structures connect. The anisotropy can be exploited to realize acoustic cloaking.

2.2.2 Pentamode cloaks

Pentamode acoustic cloaks were first proposed by Norris (2008). For a cylindrical or spherical cloak, the density is given by

$$\frac{\rho}{\rho_b} = f'\left(\frac{f}{r}\right)^{d-1}, \tag{2.25}$$

where, *d*= (2 or 3) is the dimension of the cloak, and *f(r)* is the transformation function from the physical space to the virtual space, *f'* is the derivative of *f* with respect to *r*.

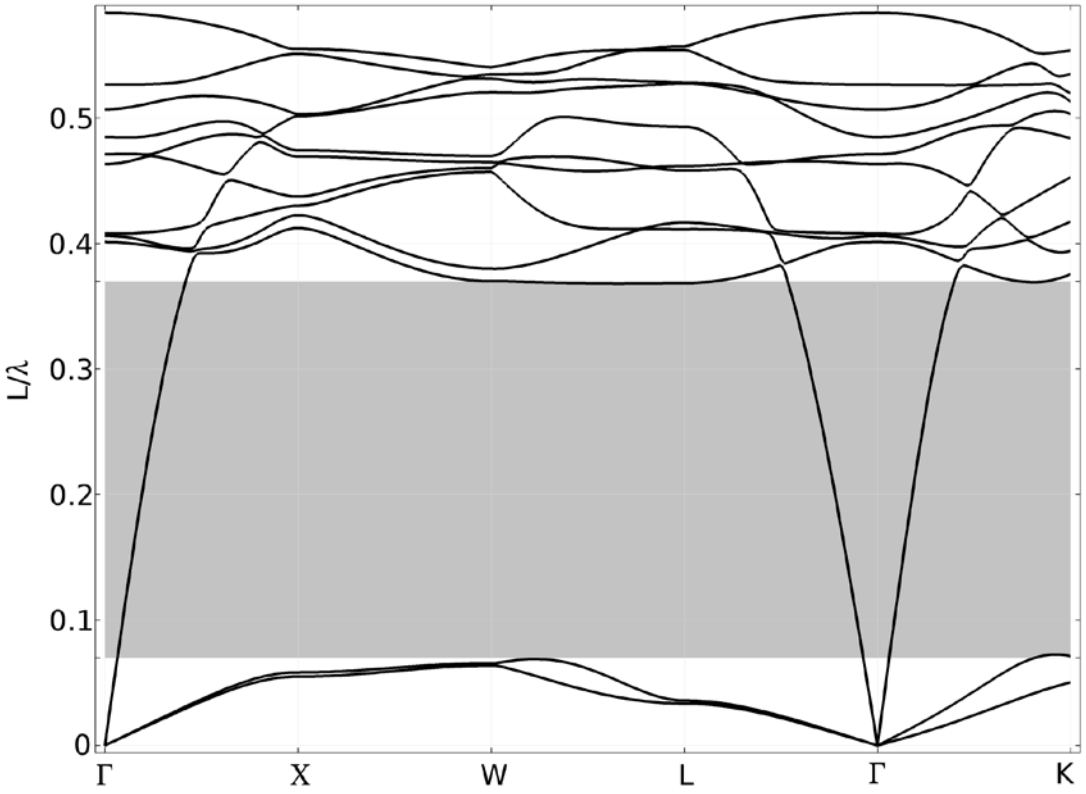

Figure 2.13 Dispersion relations of the face-centered-cubic primitive cell

The stiffness matrix is calculated from

$$\boldsymbol{C} = \left(\sqrt{K_r} I_r + \sqrt{K_t} I_t\right) \otimes \left(\sqrt{K_r} I_r + \sqrt{K_t} I_t\right), \tag{2.26}$$

where, $\otimes$ is the tensor product operator, and

$$K_r = \frac{1}{f'}\left(\frac{f}{r}\right)^{d-1}, \quad K_t = f'\left(\frac{f}{r}\right)^{d-3},$$

With the transformation function, the properties of the pentamode cloaks can be derived. However, that begs the question of how to build it.

3.0 ARBITRARILY SHAPED ACOUSTIC CLOAKS DESIGNED BY MAPPING ALONG RADIAL DIRECTIONS

One of the contributions of this work is a proposed way to design arbitrarily shaped, 2D acoustic cloaks with inhomogeneous and anisotropic properties. Their properties are derived with transformation acoustics and layered structures are used to realize the cloaks. Numerical simulations are conducted for two different shapes and their material properties are examined.

3.1 DERIVATION OF THE PROPERTIES OF ARBITRARILY SHAPED ACOUSTIC CLOAKS

The most studied 2D cloak is in circular shape and it is easiest to derive its properties in polar coordinate system. However, in general, an acoustic cloak can have any shape. The properties of the cloaks with arbitrary shapes are more complicated, and thus it is more difficult to design the cloaks.

An acoustic cloak with arbitrary interior and exterior boundaries is shown in Figure 3.1. A mapping relation from virtual space to physical space along radial directions in polar coordinate system is given by

$$\begin{cases} r = R_{in} + \dfrac{R_{ex} - R_{in}}{R_{ex}} R \\ \theta = \Theta \end{cases} \tag{3.1}$$

where, $R_{in}(\theta)$ is the function of the interior boundary of the cloak, and $R_{ex}(\theta)$ is the function of the exterior boundary of the cloak. The cloaked space is mapped to a point.

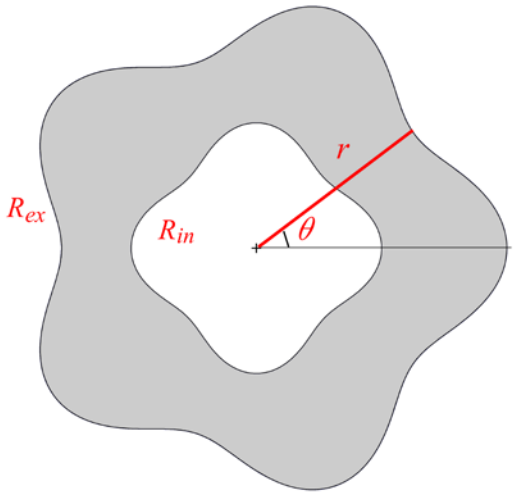

Figure 3.1 An acoustic cloak with arbitrary interior and exterior boundaries

Expressions for the density tensor and bulk modulus of the cloak derived from Equations (2.13) are

$$\frac{\overline{\overline{\boldsymbol{\rho}}}}{\rho_b} = \begin{bmatrix} \dfrac{r}{r - R_{in}} & -\dfrac{1 - \dfrac{R_{in}}{R_{ex}} \dfrac{dR_{in}}{d\theta} - \dfrac{d}{d\theta}\left(\dfrac{R_{in}}{R_{ex}}\right)}{r - R_{in}} \\ 1 - \dfrac{R_{in}}{R_{ex}} & \\ sym & \dfrac{r - R_{in}}{r}\left(1 + \dfrac{\left(1 - \dfrac{R_{in}}{R_{ex}} \dfrac{dR_{in}}{d\theta} - \dfrac{d}{d\theta}\left(\dfrac{R_{in}}{R_{ex}}\right)\right)^2}{\left(1 - \dfrac{R_{in}}{R_{ex}}\right)^2}\right) \end{bmatrix} \tag{3.2}$$

$$\frac{\kappa}{\kappa_b} = \left(1 - \frac{R_{in}}{R_{ex}}\right)^2 \frac{r}{r - R_{in}} \tag{3.3}$$

The density of the cloak is anisotropic, which is expressed by a second-order tensor. It also has off-diagonal elements. The density tensor and the bulk modulus of the cloak are both functions of r and θ. Thus, the properties of the cloak are anisotropic and inhomogeneous.

An acoustic cloak with an irregular shape is designed with Equations (3.2)-(3.3). The properties of the cloak are derived by substituting the functions of the exterior and interior boundaries into these equations. The numerical simulation of a plane wave with amplitude of 1 Pa for the field with the cloak is conducted with COMSOL Multiphysics. The result is shown in Figure 3.2.

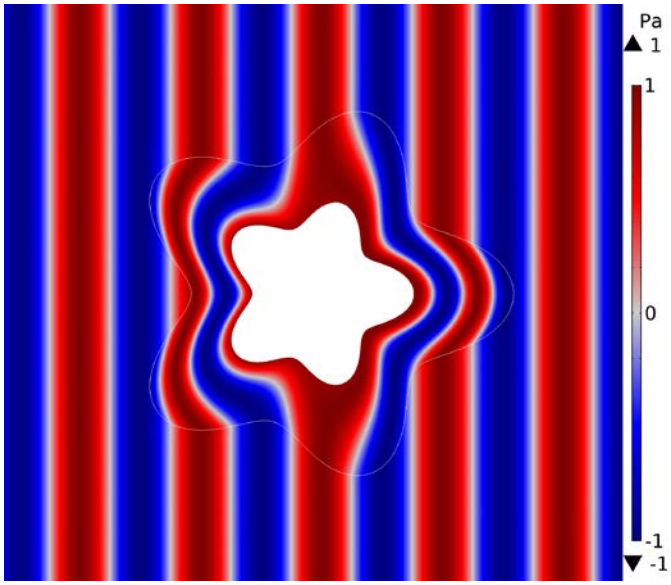

Figure 3.2 Simulation of a plane wave with amplitude of 1 Pa through the field with an arbitrarily shaped acoustic cloak with exact required properties

The results show that despite the odd shape of the cloak, it works well in reducing reflections and shadows. The acoustic field outside the cloak is homogeneous as if the wave propagated in the background medium.

3.2 BUILDING THE CLOAKS WITH LAYERED STRUCTURES

Circular cloaks can be designed with concentric layered structures because their density tensors are diagonal and their properties are only functions of radius. In contrast, the properties of cloaks with arbitrary shapes are inhomogeneous and anisotropic. What's more, the density tensor has off-diagonal elements, and the density tensor and bulk modulus are functions of r and θ.

The anisotropy can be partially addressed by dividing the cloak into small sections (Li & Vipperman, 2014). For example, a square cloak (Figure 3.3a) is divided into five-degree sections (Figure 3.3b).

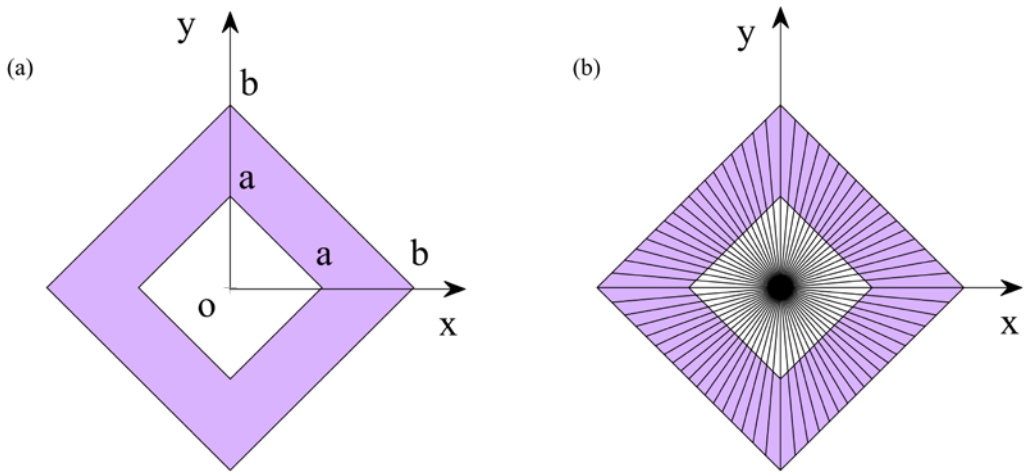

Figure 3.3 Configuration and division of a square cloak: (a) configuration (b) division

If expressed in polar coordinate system, the interior and exterior boundaries are functions of θ, which are

$$R_{in} = \frac{a}{\cos(\theta)+\sin(\theta)}, \tag{3.4}$$

$$R_{ex} = \frac{b}{\cos(\theta)+\sin(\theta)}, \tag{3.5}$$

where *a* and *b* are dimensions of the cloak shown in Figure 3.3.

The properties of the square cloak can be derived with Equations (3.2)-(3.5). The properties are functions of *r* and θ. However, since each section is small, θ can be treated as constant within each section. If the properties in the middle of the each section are used as approximation of the whole section, the properties are now only functions of *r*. Although the derived density tensor in each section is now a function of *r* only, it has off-diagonal elements. Since the matrix is symmetric, it can be diagonalized by an orthogonal matrix. That is

$$\overline{\overline{\boldsymbol{\rho}_A}} = \boldsymbol{Q}^T \overline{\overline{\boldsymbol{\rho}}} \boldsymbol{Q} \tag{3.6}$$

where, $\boldsymbol{Q}$ is an unitary matrix, the columns of which are eigenvectors of $\overline{\overline{\boldsymbol{\rho}}}$; the elements of the diagonal matrix $\overline{\overline{\boldsymbol{\rho}_A}}$ are the corresponding eigenvalues. Matrix $\overline{\overline{\boldsymbol{\rho}_A}}$ can be expressed as

$$\overline{\overline{\boldsymbol{\rho}_A}} = \begin{bmatrix} \rho_{\parallel} & 0 \\ 0 & \rho_{\perp} \end{bmatrix} \tag{3.7}$$

where $\rho_{\parallel}$ And $\rho_{\perp}$ are densities in the principal directions. Then layered structures can be used to approximate the properties along principal directions.

The properties of each section of the cloak are calculated and layered structures are used within each section along principal directions. The properties of the layers are calculated with Equations (2.21). A blowup of the first quadrant of the cloak more clearly shows the layered structures in Figure 3.4. The structures in the other three quadrants are equivalent due to symmetry.

The cloaking effect of the square cloak with layered structures is simulated with COMSOL Multiphysics finite element software. A plane wave with amplitude of 1 Pa through a space with a square obstacle is simulated. The results in two directions with and without the

cloaks are shown in Figure 3.5. From the results we can see that the cloak works well in the two chosen directions since it is an omni-directional 2D cloak.

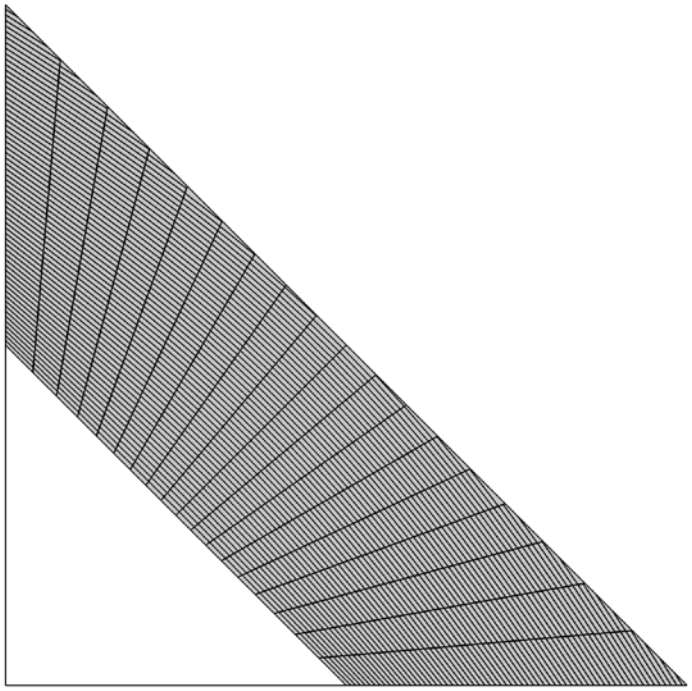

Figure 3.4 Layered structures of the square cloak in the first quadrant

For cloaks with curvilinear boundaries, they can also be divided into small sections. An elliptical cloak and its division are shown in Figure 3.6. The elliptical cloak is divided into five-degree sections.

If expressed in Polar coordinate system, the interior and exterior boundaries are functions of θ, which are given by

$$R_{in} = r_0, \tag{3.8}$$

$$R_{ex} = \frac{1}{\sqrt{\frac{\cos^2(\theta)}{a^2} + \frac{\sin^2(\theta)}{b^2}}}, \tag{3.9}$$

where a, b and r_0 are dimensions of the cloak shown in Figure 3.6.

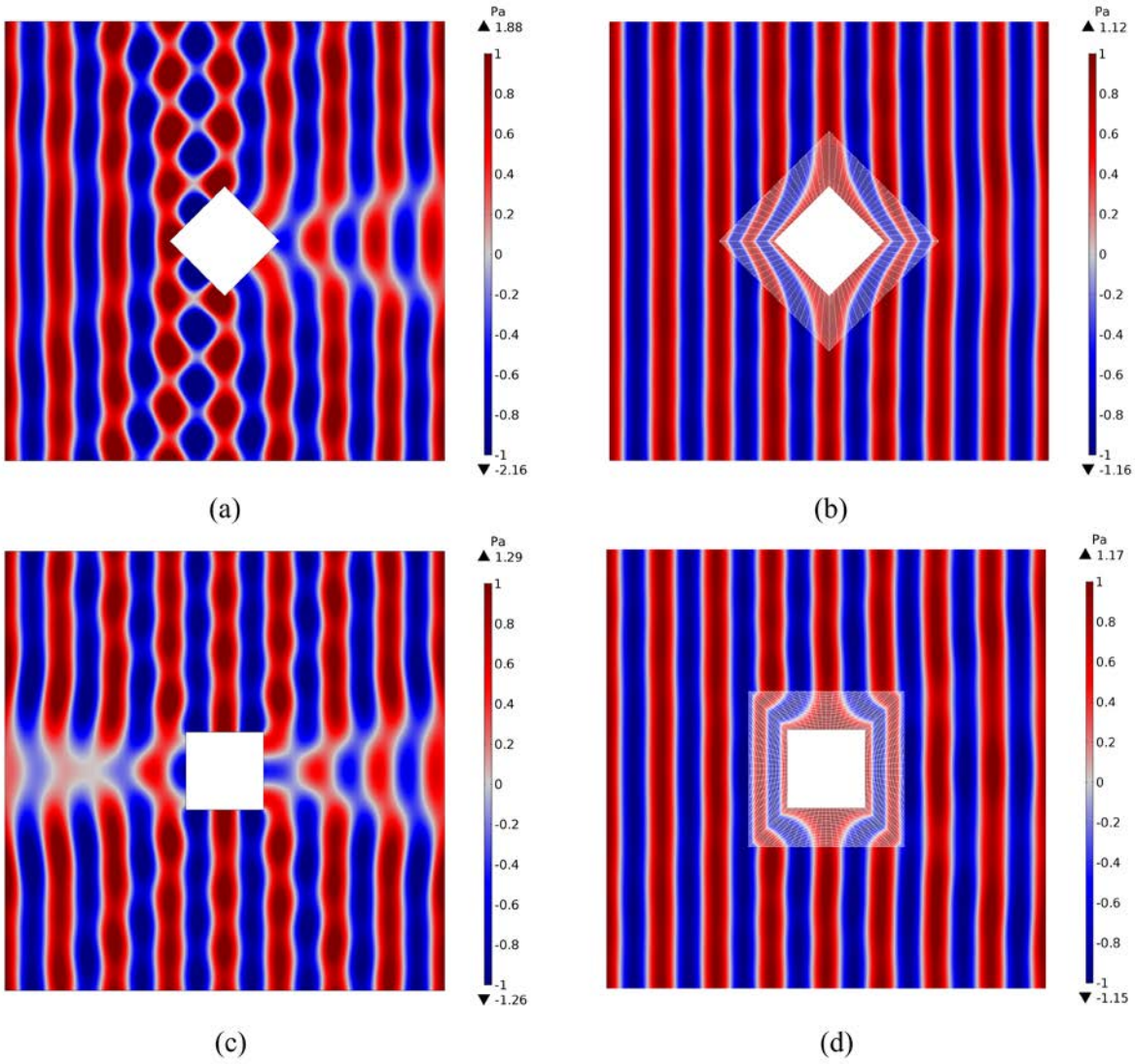

Figure 3.5 Simulation of a plane wave with amplitude of 1 Pa in two directions (a) without cloak in direction 1 (b) with square cloak in direction 1 (c) without cloak in direction 2 (d) with square cloak in direction 2

The interior and exterior boundaries are curves. But the curvilinear segments within each section can be approximated piecewise linear. The properties within each section can be derived with the linear boundaries and calculated along the middle of each section. Similar procedures are adopted as the square cloak from the previous example. The layered structures of the

elliptical cloak in the first quadrant are shown in Figure 3.7. The structures in the other quadrants are the same by symmetry.

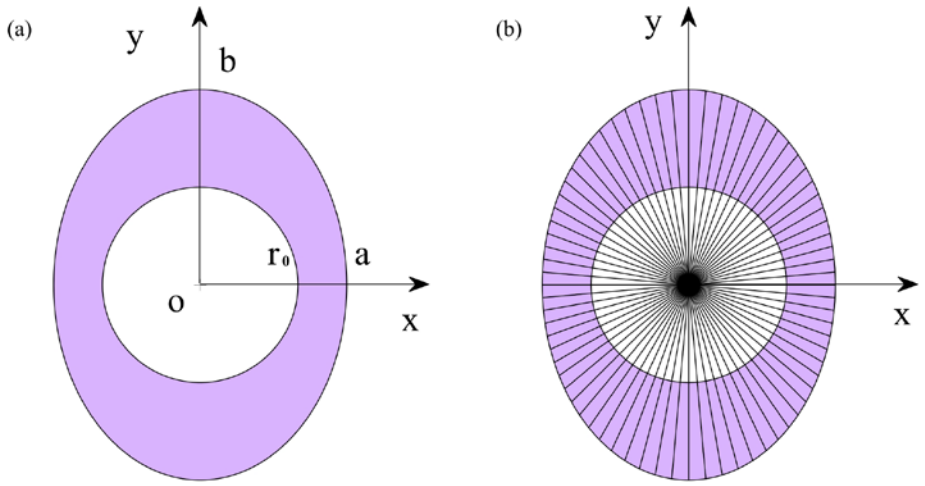

Figure 3.6 Configuration and division of the elliptical cloak: (a) configuration (b) division

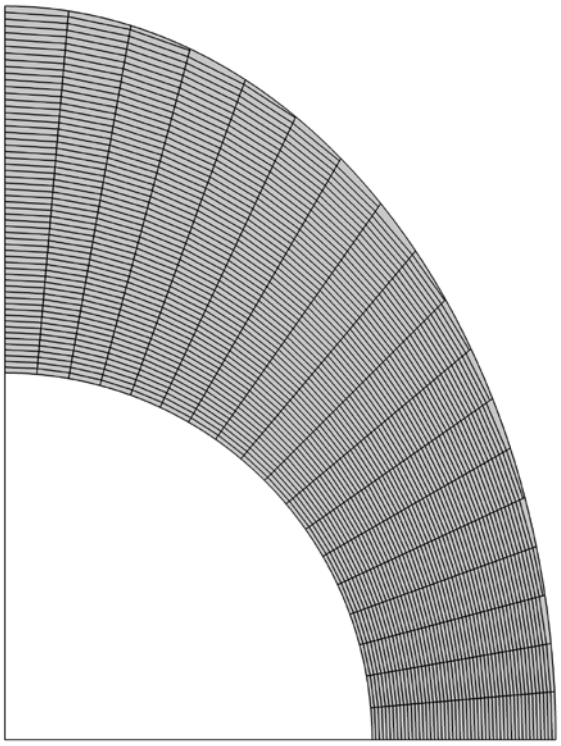

Figure 3.7 Layered structures of the elliptical cloak in the first quadrant

The effect of the elliptical cloak with layered structures is simulated with COMSOL Multiphysics finite element software. A plane wave with amplitude of 1 Pa and wavelength of r_0 is set to pass through the space. The results with and without the layered elliptical cloak are shown in Figure 3.8. The results show that the reflections and shadows due to an object in the acoustic field are greatly reduced, rendering the object almost undetectable in acoustic field. The cloak works well no matter from which direction the plane wave propagates.

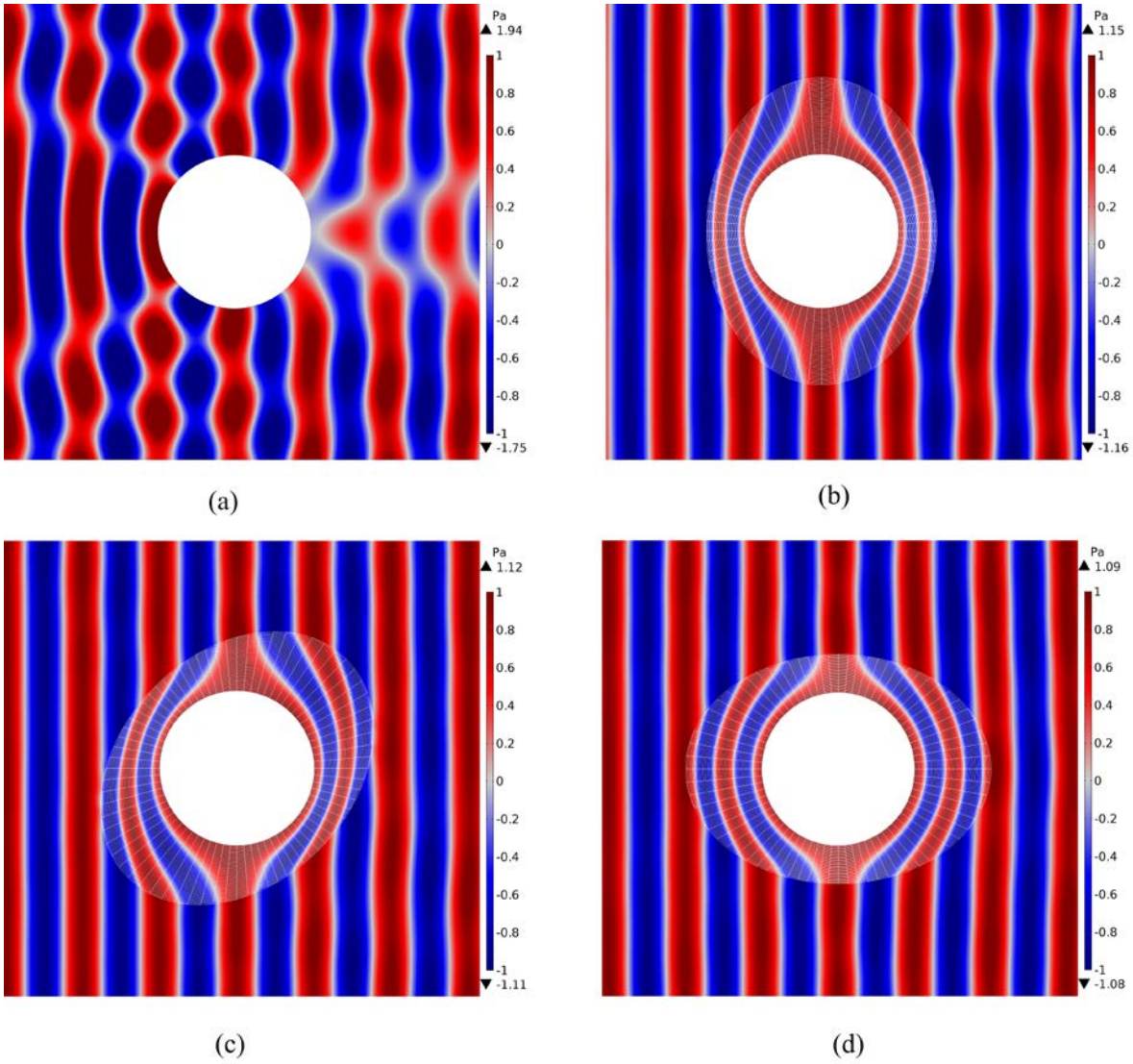

Figure 3.8 Simulation of a plane wave with an amplitude of 1 Pa in three directions (a) without cloak (b) with elliptical cloak in direction 1 (c) with elliptical cloak in direction 2 (d) with elliptical cloak in direction 3

3.3 ANALYSIS OF THE ELLIPTICAL CLOAK

The full wave simulations in Section 3.2 have shown the effect of the cloaks built with layered structures. In this section, the elliptical cloak in Section 3.2 is taken as an example to be studied in detail.

When a plane wave collides with an obstacle, it will cause scattered waves. When surrounded by a cloak, the amplitude of the scattered waves will be diminished. The scattered fields are defined as

$$P_{\text{cloaked,scat}} = P_{\text{cloaked,tot}} - P_{\text{plane-wave,tot}},$$
$$P_{\text{uncloaked,scat}} = P_{\text{uncloaked,tot}} - P_{\text{plane-wave,tot}}, \tag{3.10}$$

where $P_{\text{cloaked,tot}}$, $P_{\text{uncloaked,tot}}$ and $P_{\text{plane-wave,tot}}$ are the total field for the cloaked model, the bare obstacle model and the plane-wave. The amplitude of the scattered waves can be normalized by the amplitude of the plane-wave.

The normalized amplitudes of the scattered waves in the cases of Figure 3.8 are calculated for all directions at a distance of $r=5\lambda_b$. λ_b is the wavelength in the background medium. The comparisons of the normalized amplitudes of the scattered field without (blue curves) and with (red curves) the elliptical cloak are shown in the radar plot of Figure 3.9. Without cloaks, the cylinder scatters to a large extent with the maximum almost equal to 1 Pa. The amplitudes of the scattered waves are greatly reduced with the help of the cloak. The cloak works in all the three directions, but the cloaking effects are different when the incident waves strike the cloak from different directions.

The reduced total radar cross section (RCS) is introduced to quantitatively evaluate the cloaking performance of EM cloaks, and represents ratio of scattered field in the cloaked model

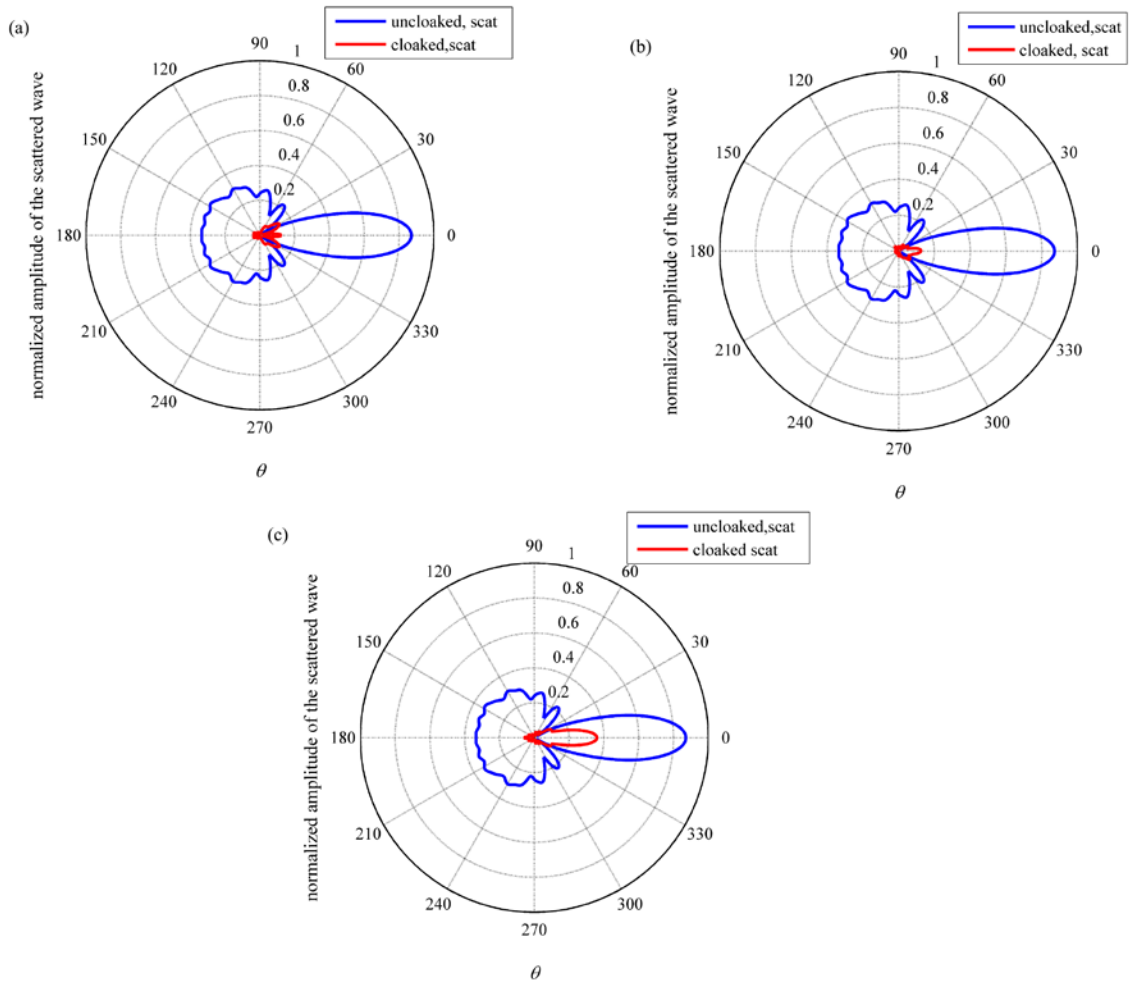

Figure 3.9 Normalized amplitude of the scattered waves without and with the elliptical cloak at $r=5\lambda_b$ for incident waves from three directions (as in Figure 3.8)

to the scattered field in the uncloaked model. (Yang, et al., 2016) It was later adapted for acoustic fields. (Bi, Jia, Lu, Ji, & Yang, 2017). For the acosutic cloak, it can be defined as

$$\sigma_{\text{reduced}} = \frac{\sigma_{\text{cloaked}}}{\sigma_{\text{uncloaked}}} = \oint_{\Omega} \left(\frac{|P_{\text{cloaked,scat}}|^2}{|P_{\text{uncloaked,scat}}|^2} \right) d\Omega , \tag{3.11}$$

where $P_{\text{cloaked,scat}}$, and $P_{\text{uncloaked,scat}}$ are defined in Equation (3.10). The smaller this value, the better the performance of the cloak. The reduced total RCS of the elliptical cloak over an area of $8r_0 \times 6r_0$ (where r_0 is inner radius of the cloak) excluding the cloak is calculated for three angles

of incidence for a series of normalized frequencies (r_0/λ_b, where λ_b is the wavelength of sound). The results are shown in Figure 3.10.

It can be seen from Figure 3.10 that the cloak works well when r_0/λ_b is relatively small, i.e. at relatively low frequencies. The reduced total RCS is lower than 0.2 when r_0/λ_b is smaller than 1.5. The full wave simulation for cases at r_0/λ_b =0.5, r_0/λ_b =1 and r_0/λ_b =1.5 are shown in Figure 3.11. The acoustic waves outside the cloak are disturbed a little, and still remains a plane-wave in total. The cloaking effect becomes worse with the increase of r_0/λ_b, which can also be seen from Figure 3.10

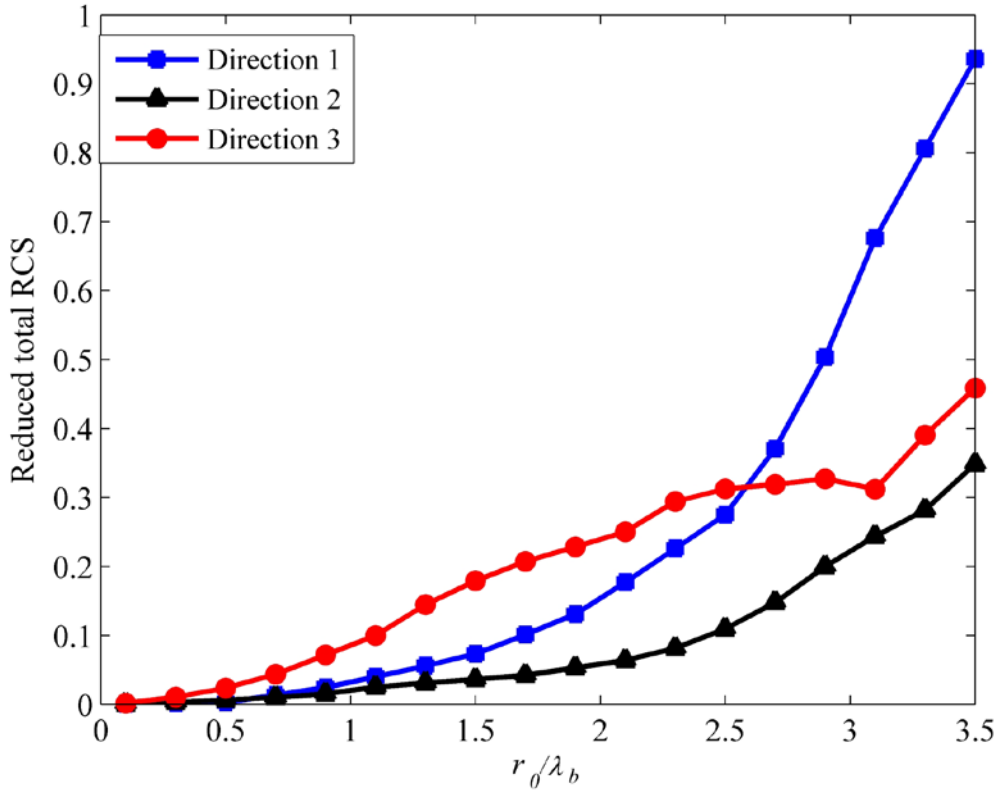

Figure 3.10 Reduced total RCS of the elliptical cloak for three angles of incidence (as in Figure 3.8)

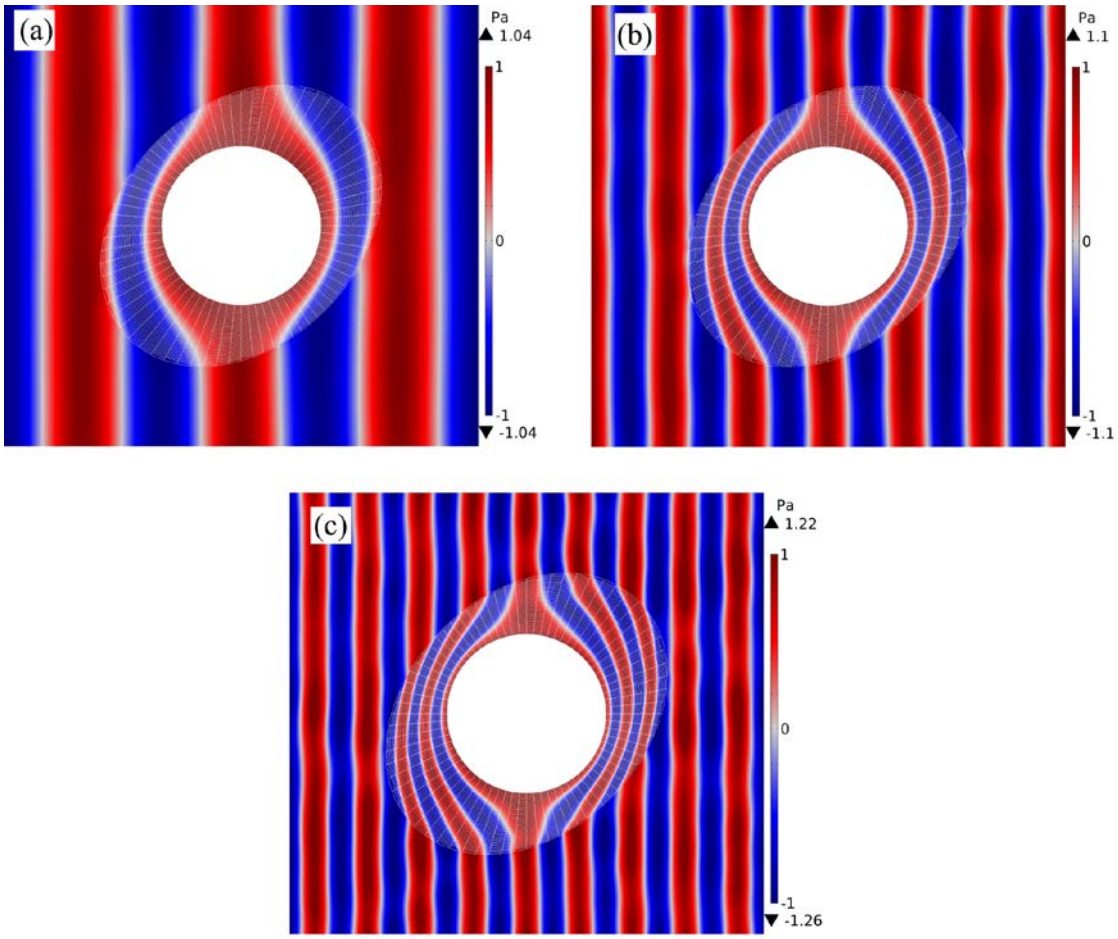

Figure 3.11 The effect of the elliptical cloak at different frequencies (a) r_0/λ_b =0.5 (b) r_0/λ_b =1 (c) r_0/λ_b =1.5

The cloaks are built with layered structures. When the wavelength is much larger than the thickness of the layers, the layers are effectively homogenized. The results show that the cloak works across a wide bandwidth, but does degrade as frequency is increased further.

The properties within each section are inhomogeneous. Thus the properties of the two layers derived with Equations (2.21) are changing. The relative densities (to the background medium) of the layered materials for each section of the elliptical cloak are shown in Figure 3.12. Extreme densities are noted as the inner boundary is approached. Even with the plot

truncated, the densities of the two layers deviate from that of the background by a few orders of magnitude in opposite directions, as radius is decreased toward the inner boundary. Near the outer boundary, the relative densities are within an order of magnitude of the background medium. The widely varying densities pose a challenge for fabrication

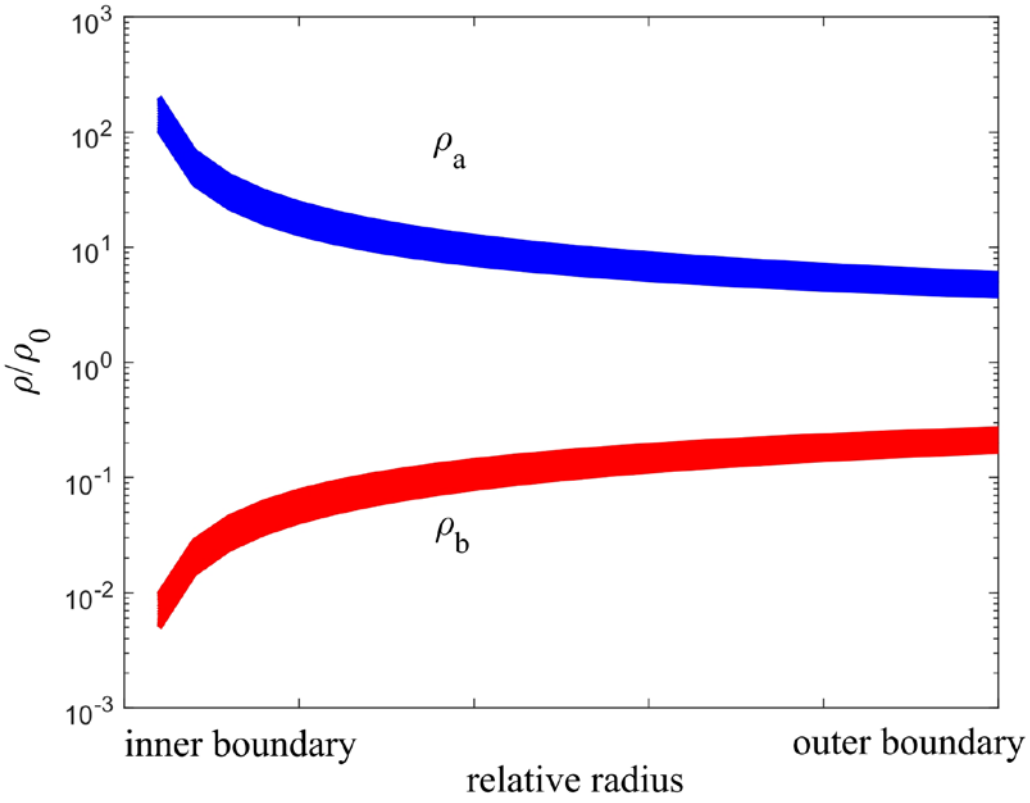

Figure 3.12 Densities of the layered materials along radial directions for all sections

The relative bulk moduli (to the background medium) for each section of the elliptical cloak are shown in Figure 3.13. The bulk moduli for the two layers are the same and, like the densities, become more extreme near the inner boundary of the cloak.

It has been demonstrated that acoustic cloaks with arbitrary shapes can be realized with layered structures. The cloaks are observed to be broadband and omnidirectional. However,

fabrication is a challenge, since the required properties of the layers are changing within each section, and the properties near the interior boundary are extremely large or small.

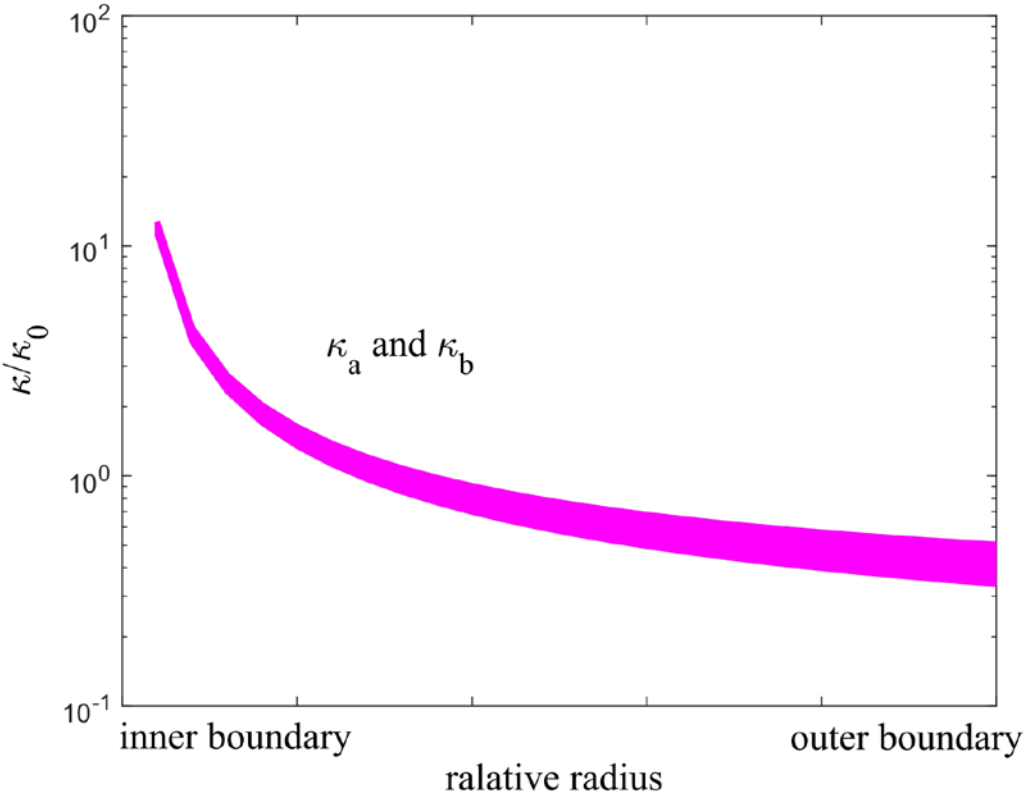

Figure 3.13 Bulk moduli of the layered materials along radial directions

4.0 TWO DIMENSIONAL ARBITRARILY SHAPED ACOUSTIC CLOAKS DERIVED WITH TWO-STEP TRANSFORMATION

As discussed in the previous chapter, acoustic cloaks with arbitrary shapes can be designed with transformation acoustics by compressing along radial directions. But the materials properties end up being functions of both r and θ. By dividing the cloaks into small sections, the cloaks can be built with layered structures. The properties of the layers vary layer by layer.

There are a few reports of step-transformations in the literature that can lead to homogeneous properties. However they are limited to a few specific cloak geometries. (Li, Huang, Yang, Lan, & Sun, 2012) (Zhu, et al., 2016) As will be shown next, any arbitrarily shaped 2D acoustic cloak can be designed with two-step transformation that leads to sections composed of two homogeneous parts.

4.1 DERIVATION OF THE HOMOGENEOUS PROPERTIES WITH A TWO-STEP TRANSFORMATION

An acoustic cloak with an arbitrary shape is shown in Figure 4.1. As before, it can be divided into sections by drawing radial lines from the origin. These sections, in turn, will be divided into two parts with homogeneous properties. A section of the cloak (OCD) is shown in the figure. The inner and outer boundaries of each section can be approximated as linear segments (e.g. BE

and CD in section OCD). Without loss of generality, analysis is conducted for this section. For simplicity, a local coordinate system is defined with O as the origin and OC as the *x*-axis, as shown.

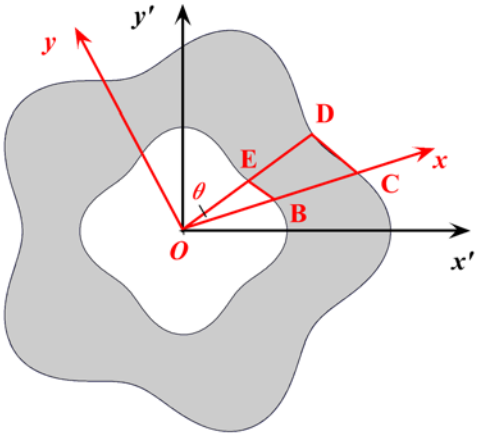

Figure 4.1 An arbitrarily shaped acoustic cloak with a section as an example

Recall that for transformation acoustics, the cloak occupies the physical space, and the virtual space is an imaginary space filled with background medium. A two-step transformation is performed from virtual space ACDF (Figure 4.2a) to physical space BCDE (Figure 4.2c). In the first step, OAD (Figure 4.2a) is expanded to OBD (Figure 4.2b) and ACD (Figure 4.2a) is compressed to BCD (Figure 4.2b) with a linear transform along *x* direction. In the second step, the FBD (Figure 4.2b) obtained in the first step is compressed to EBD (Figure 4.2c) with a linear transform along the OD direction. After the two steps, points in the physical space BCDE are mapped from those in the virtual space ACDF. The area OBE corresponds to the area OAF. Particularly, when |OF| is zero, the area OBE corresponds to the short line OA. The area OAF is the effective obstacle. Smaller lengths of |OA| and |OF| correspond to better cloaking performance. (Li & Vipperman, 2017)

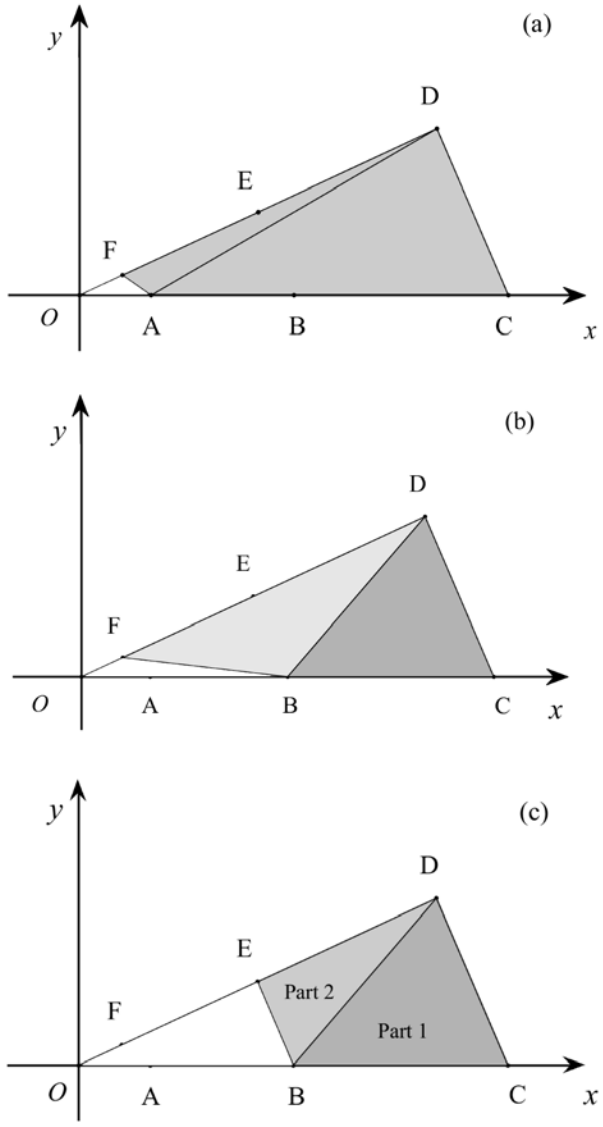

Figure 4.2 Schematics of the two-step transformation of a section from virtual space to physical space (a) virtual space (b) intermediate space (c) physical space

In the first step, the points in ACD of Figure 4.2a are mapped to the points in BCD of Figure 4.2b using

$$\begin{bmatrix} x \\ y \end{bmatrix} = \underbrace{\begin{bmatrix} a_1 & a_2 \\ 0 & 1 \end{bmatrix}}_{\boldsymbol{A_1}} \begin{bmatrix} X \\ Y \end{bmatrix} + \begin{bmatrix} a_3 \\ 0 \end{bmatrix} \tag{4.1}$$

where

$$a_1 = \frac{x_C - x_B}{x_C - x_A},$$

$$a_2 = \frac{x_D - x_B}{y_D} - \frac{x_C - x_B}{x_C - x_A}\frac{x_D - x_A}{y_D},$$

$$a_3 = x_B - \frac{x_C - x_B}{x_C - x_A}x_A.$$

Next, the points in OAD of Figure 4.2a are mapped to the points in OBD of Figure 4.2b using

$$\begin{bmatrix} x_m \\ y_m \end{bmatrix} = \underbrace{\begin{bmatrix} a_4 & a_5 \\ 0 & 1 \end{bmatrix}}_{\boldsymbol{A_2}} \begin{bmatrix} X \\ Y \end{bmatrix} \tag{4.2}$$

where

$$a_4 = \frac{x_B}{x_A},$$

$$a_5 = \left(1 - \frac{x_B}{x_A}\right)\frac{x_D}{y_D}.$$

In the second step, the points in FBD of Figure 4.2b are then mapped to EBD of Figure 4.2c by

$$\begin{bmatrix} x \\ y \end{bmatrix} = \underbrace{\begin{bmatrix} a_6 & a_7 \\ a_9 & a_{10} \end{bmatrix}}_{\boldsymbol{A_3}} \begin{bmatrix} x_m \\ y_m \end{bmatrix} + \begin{bmatrix} a_8 \\ a_{11} \end{bmatrix} \tag{4.3}$$

where

$$a_6 = 1 + \frac{x_D\left(x_F - x_E\right)}{x_B\left(x_D - x_F\right)},$$

$$a_7 = \frac{x_D\left(x_D - x_B\right)\left(x_E - x_F\right)}{x_B y_D\left(x_D - x_F\right)},$$

$$a_8 = \frac{x_D(x_E - x_F)}{x_D - x_F},$$

$$a_9 = \frac{y_E - y_D}{y_F - y_D}\frac{y_F}{x_B} - \frac{y_E}{x_B},$$

$$a_{10} = \frac{x_B(y_E - y_D) + x_D(y_F - y_E)}{x_B(y_F - y_D)},$$

$$a_{11} = \frac{y_D(y_F - y_E)}{y_F - y_D}.$$

The points in ADF of Figure 4.2a are finally mapped to points in BDE of Figure 4.2c, using

$$\begin{bmatrix} x \\ y \end{bmatrix} = \boldsymbol{A}_3\boldsymbol{A}_2 \begin{bmatrix} X \\ Y \end{bmatrix} + \begin{bmatrix} a_8 \\ a_{11} \end{bmatrix}, \tag{4.4}$$

where $\boldsymbol{A}_2$ and $\boldsymbol{A}_3$ are matrices in Equations (4.2) and (4.3).

The Jacobian matrix for BCD is

$$\boldsymbol{J}_1 = \boldsymbol{A}_1 \tag{4.5}$$

The Jacobian matrix for BDE is

$$\boldsymbol{J}_2 = \boldsymbol{A}_3\boldsymbol{A}_2 \tag{4.6}$$

Using the two Jacobian matrices, the properties of the two parts of the section can be derived with Equations (2.13). Since the Jacobian matrices are constant, the derived properties are constant. The properties of layers within each section can be derived using Equations (2.21).

The process is repeated for the other sections. Any symmetry in the device will reduce the total number of homogenous parts in the device. For example, a regular polygonal cloak could be built of just four materials.

Polygonal cloaks can be divided into sections according to their boundaries. As an example, a hexagonal cloak shown in Figure 4.3 is designed. The interior and exterior

boundaries of the cloak are both regular hexagons. The side length of the exterior hexagon is twice that of the interior hexagon.

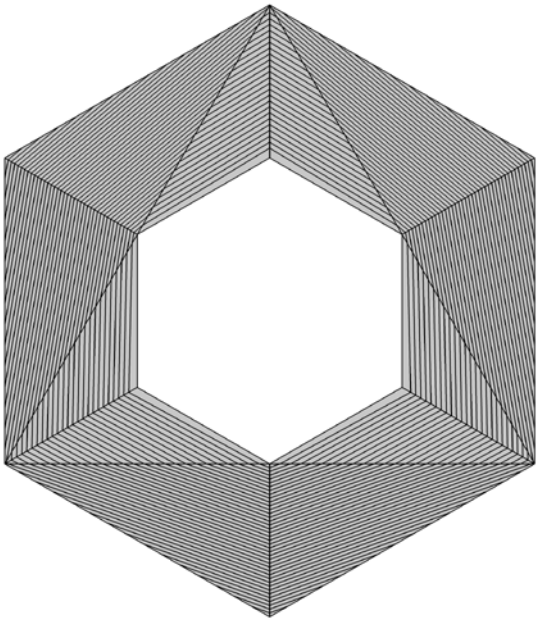

Figure 4.3 A hexagonal cloak composed of homogeneous parts built with layered structures

The cloak can be divided into six or more sections. By dividing the cloak into six sections, the angle for each section is $\pi/3$. All the sections are equivalent. Letting |OA|/|OB| and |OF|/|OE| be equal to 0.1, the properties of each part can be derived as outlined in Section 4.1. The properties can then be transformed to the principal directions. The principal densities and bulk moduli of the two parts are

$$\begin{cases} \rho_{||1} = 0.4785\rho_b, \quad \rho_{\perp 1} = 2.0899\rho_b, \quad \kappa_1 = 0.5263\kappa_b \\ \rho_{||2} = 0.0405\rho_b, \quad \rho_{\perp 2} = 24.6964\rho_b, \quad \kappa_2 = 5.2632\kappa_b \end{cases}.$$

Each part can be approximated by layered structures. The layered structure of the hexagonal cloak is shown in Figure 4.3. Each part can be built with only two materials. Because all the sections are equivalent, the cloak can be built with only four materials.

Full wave simulations of a plane wave with amplitude of 1 Pa for a space with an obstacle were conducted with COMSOL Multiphysics. The results with and without the hexagonal cloak in two directions are shown in Figure 4.4. It can be seen that the cloak reduces the reflections and shadows significantly and is omnidirectional.

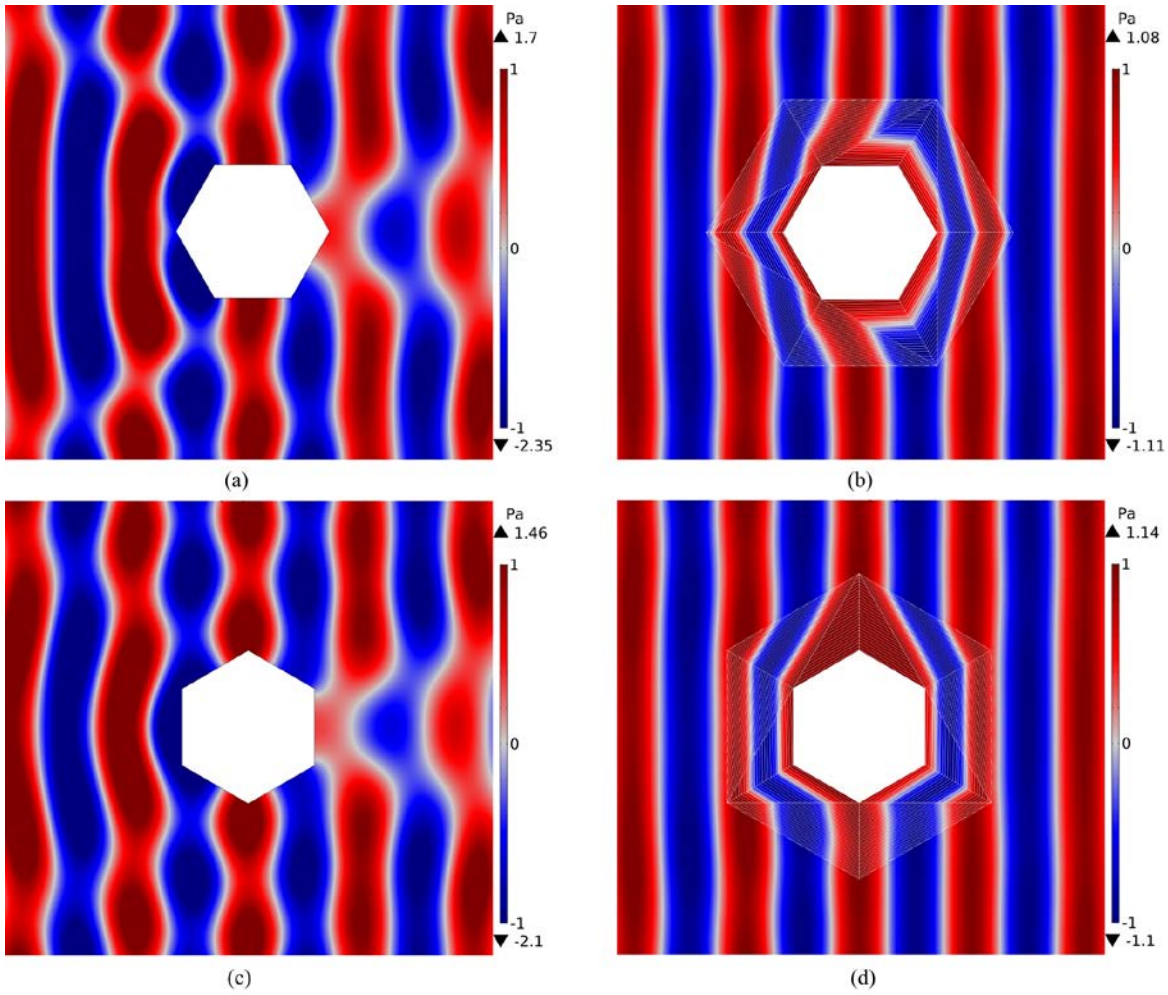

Figure 4.4 Simulation of a plane wave with amplitude of 1 Pa through a space with an object (a) without cloak in direction 1 (b) with the hexagonal cloak in direction 1(c) without cloak in direction 2 (d) with hexagonal cloak in direction 2

The method can be adapted for cloaks with curvilinear boundaries by approximating the curved boundary segments with piece-wise linear segments. To illustrate, a cloak is designed in the shape shown in Figure 4.5. The cloak was first divided into sections by radial lines starting from the center. A total of 32 sections are created. The section angles are not the same (more divisions are added in regions of higher curvature). The properties of each section are derived as before. |OA|/|OB| and |OF|/|OE| are both set to 0.1 for every section. The cloak built with layered structures is shown in Figure 4.5.

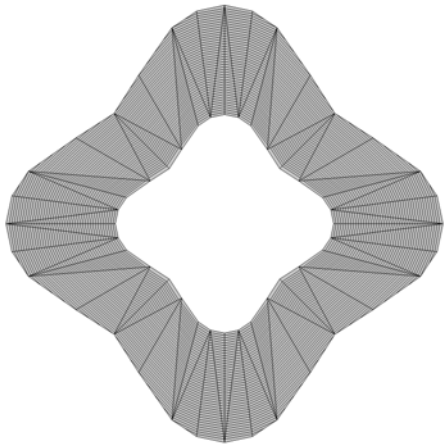

Figure 4.5 A non-regular cloak built with layered structures

Full wave simulations of a plane wave with amplitude of 1 Pa for a space with an obstacle are conducted with COMSOL Multiphysics. The results without and with the irregular cloak are shown in Figure 4.6. It can be seen from the figure that the cloak works well in reducing reflections and shadows. The obstacle is acoustically undetectable from the acoustic field outside the cloak, as if the acoustic wave propagated unimpeded through the homogeneous background medium.

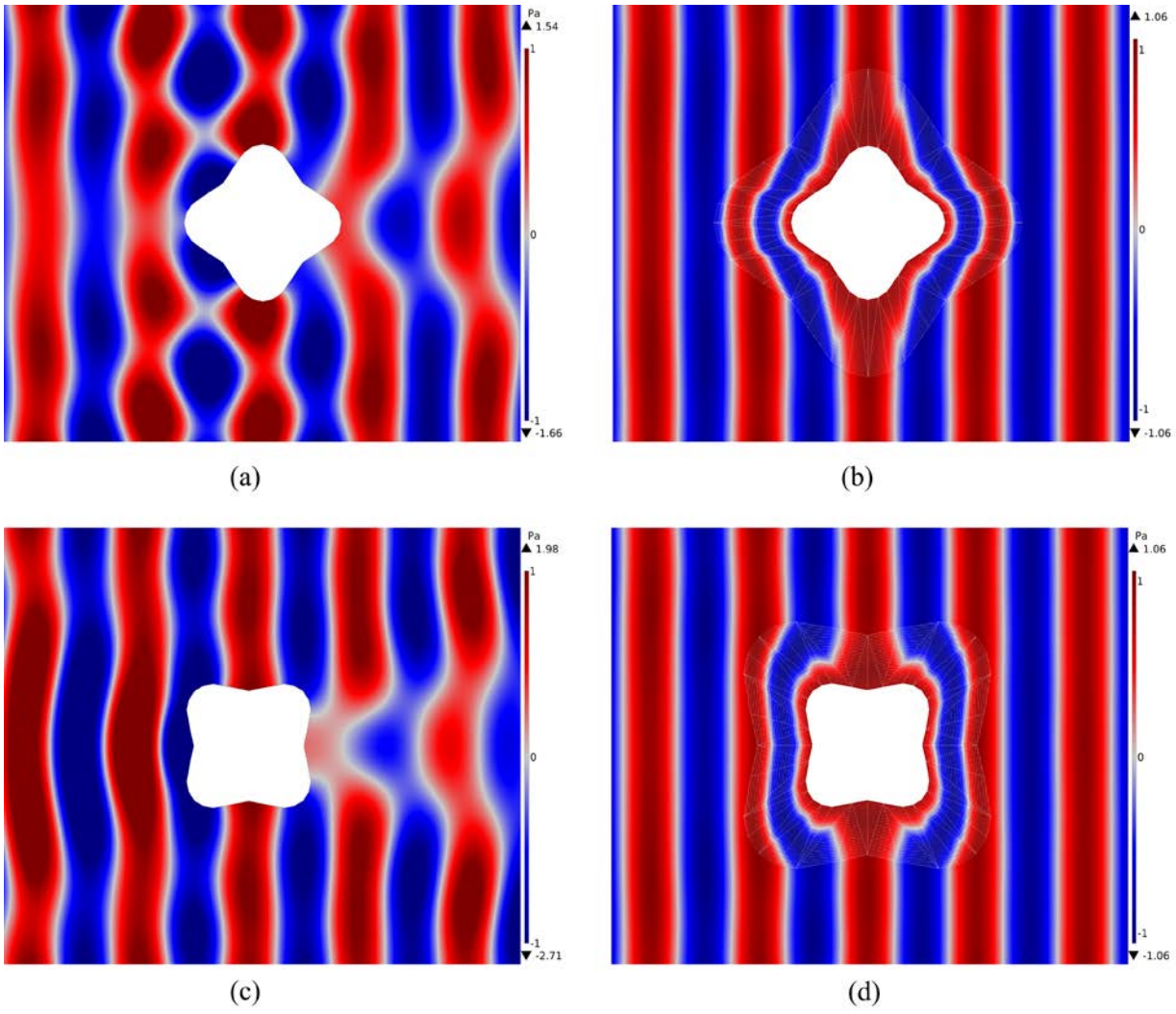

Figure 4.6 Simulation of a plane wave with amplitude of 1 Pa for a space with an object (a) without cloak, direction 1 (b) with the irregular cloak, direction 1 (c) without cloak, direction 2 (d) with the irregular cloak, direction 2

4.2 ANALYSIS OF THE CLOAKING PERFORMANCE

The full wave simulations in Section 4.1 have demonstrated that the cloaks designed with the two-step method work well in reducing reflections and shadows.

The normalized amplitudes of the scattered waves of the irregular cloak in Figure 4.6 are shown in Figure 4.7. The normalized amplitudes of the scattered waves are defined with Equation (3.10). The cloak significantly reduces the scattered waves (red curves as compared to the blue curves in Figure 4.7).

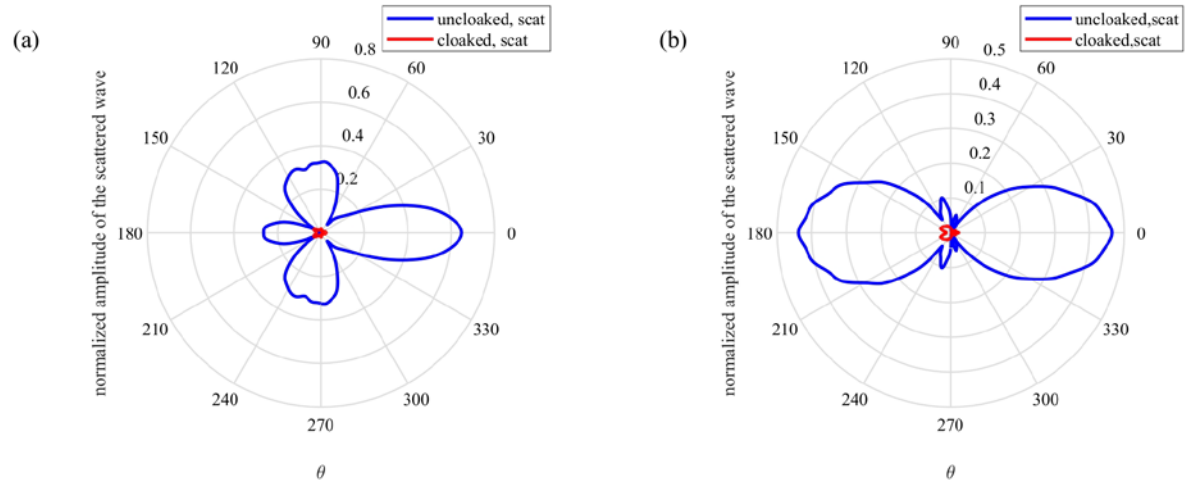

Figure 4.7 Normalized amplitudes of the scattered waves without and with the irregular cloak at $r=5\lambda_b$ for incident waves in two directions

The reduced total RCS of the irregular cloak for two angles of incidence over an area of $11r_m \times 11r_m$ excluding the cloak is shown in Figure 4.8, as defined by Equation (3.11). In the figure, r_m is the maximum radius of the cloaked area. It can be seen that the cloak works well when r_m/λ_b is relatively small, that is, at relatively low frequencies.

The bandwidth is limited by two factors. First, the thickness of the layers must be much smaller than the wavelength to satisfy the long-wavelength limit. (Torrent & Sánchez-Dehesa, 2008) (Cheng, Yang, Xu, & Liu, 2008) Second, the wavelength must be much larger than the

lengths of OA and OF. What's more, the lengths of OA cannot be extremely small to avoid extreme properties.

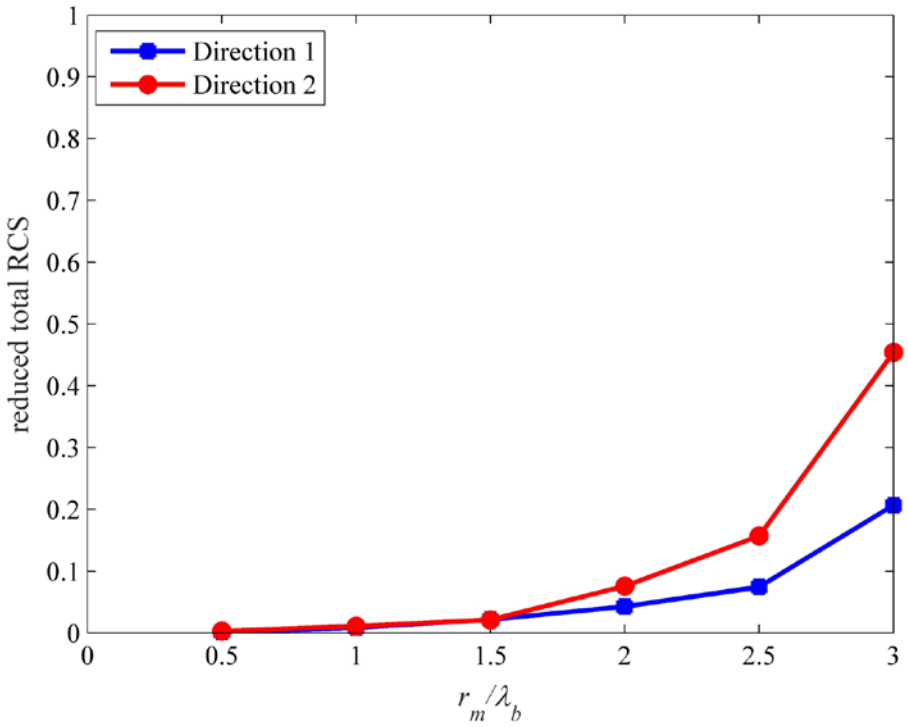

Figure 4.8 Reduced total RCS of the irregular cloak for various normalized frequencies for two angles of incidence (as in Figure 4.6)

4.3 ANALYSIS OF THE FACTORS THAT AFFECT THE MATERIAL PROPERTIES

The required material properties to build cloaks are usually beyond those of natural materials. That limits the realization of cloaks. Since the geometric parameters in the transformation acoustics affect the properties of each section, they may be tailored to make the properties easier to realize.

For a regular polygonal cloak, all the sections are equivalent. One section of a regular polygonal cloak with |OB|=|OE|=1 and |OC|=|OD|=2 is used for a sample analysis, as shown in Figure 4.9. There are three parameters that go into determining the properties of the cloak: the lengths of OA and OF, and the angle θ. The variation of the principal densities and bulk moduli of the two parts with θ, |OA| and the ratio of |OF|/|OA| are investigated.

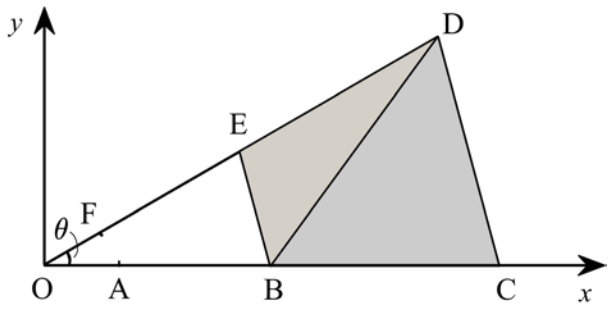

Figure 4.9 One section of a regular polygonal cloak for two-step transformation

When $\theta=\pi/10$ and |OA|=|OF|, the material properties vary with |OA|, as shown in Figure 4.10. The deviation of the principal densities and bulk moduli decreases with the increase of |OA|. However, larger |OA| and |OF| means larger size of the equivalent scattering cross section, thus worse cloaking performance. When |OA|=|OF|=0.1, the material properties vary with θ, as shown in Figure 4.11. The principal densities and bulk moduli deviate from that of the background medium with the increase of θ. The variations of material properties with the ratio of |OF|/|OA| at different arc angles are shown in Figure 4.12. Since |OF| only affects the properties of Part BDE, |OF| can be used to optimize the properties of Part BDE to make it easier to realize. For sections with a small θ, |OF|≈|OA| is preferred.

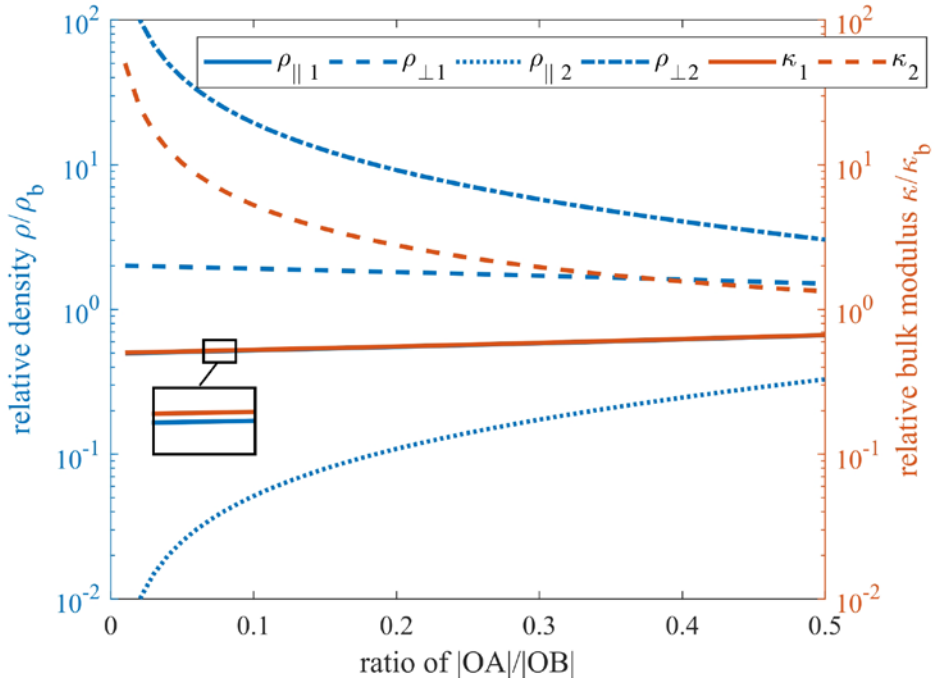

Figure 4.10 Variation of material properties with |OA/|OB| at $\theta=\pi/10$ and |OF|/|OA|=1

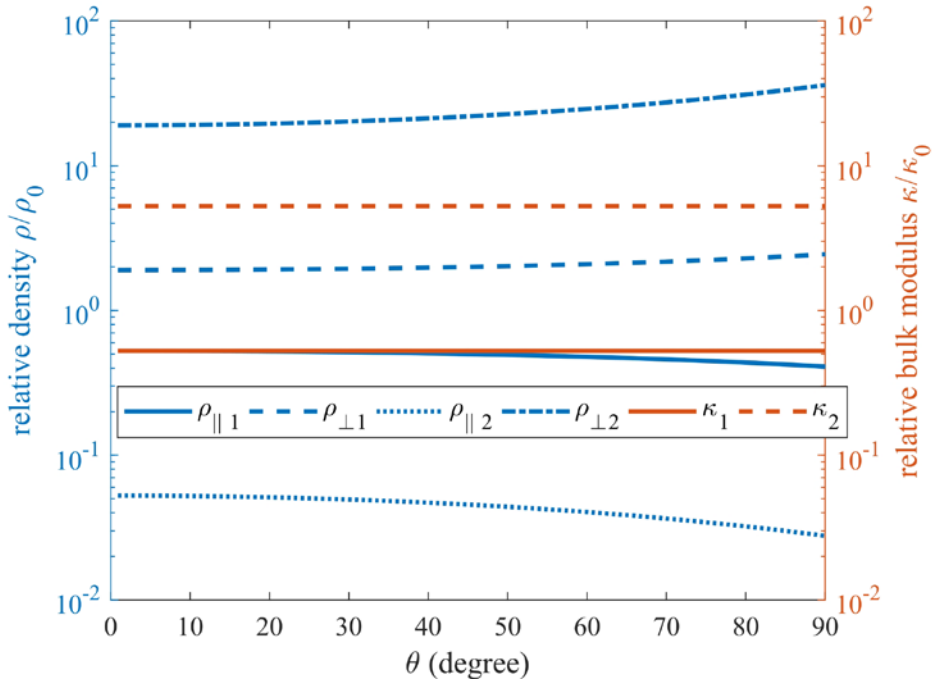

Figure 4.11 Variation of material properties with θ at |OA|=|OF|=0.1

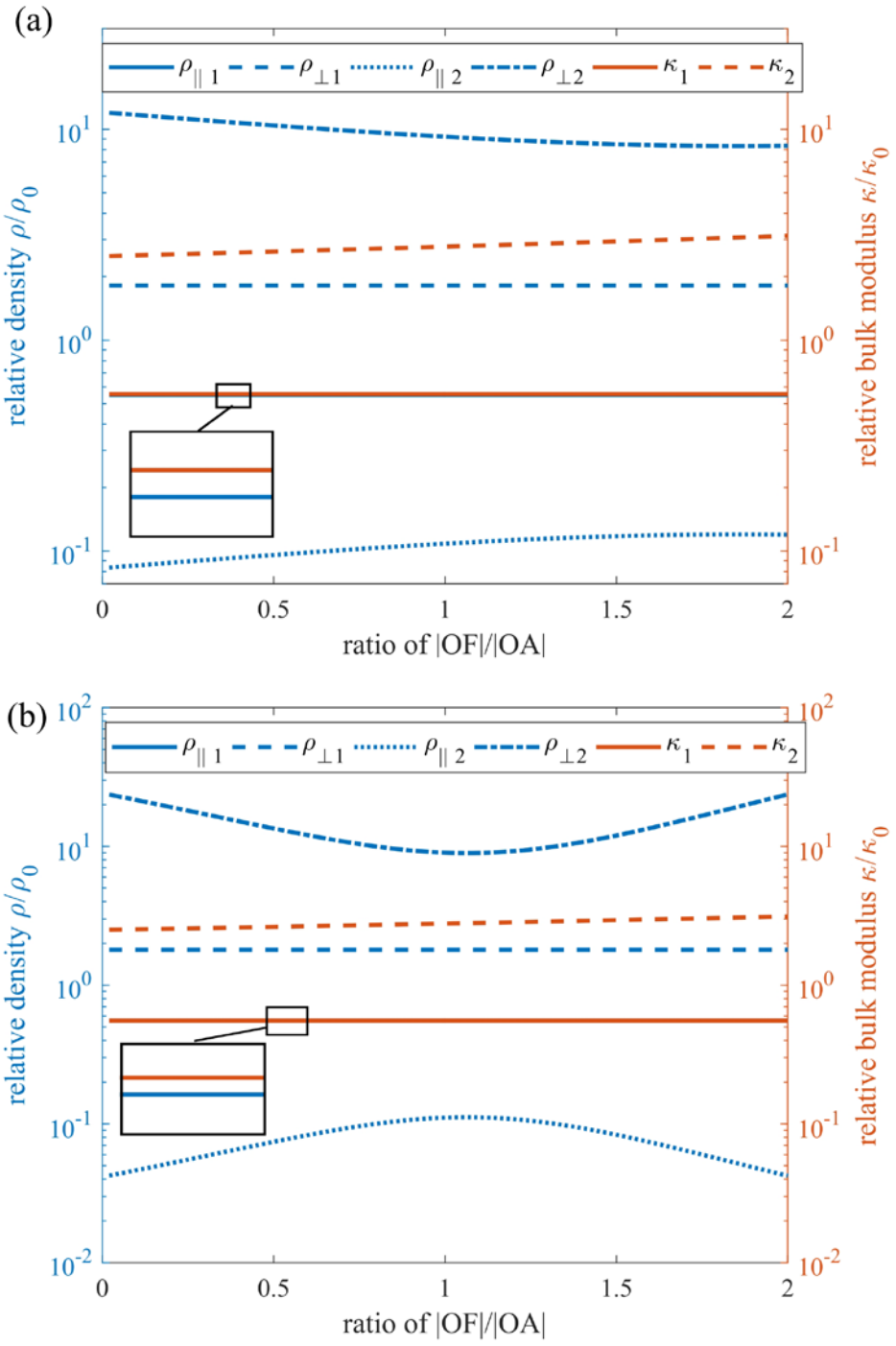

Figure 4.12 Variation of material properties with |OF|/|OA| at |OA|=0.2 and (a) $\theta=\pi/9$ (b) $\theta=\pi/36$

In order to guarantee good cloaking performance, the values of |OA| and |OF| should be as small as possible. But extremely small values correspond to extreme properties which are

difficult to realize. A balance can be found between cloaking performance and realizable properties.

4.4 FABRICATION FEASIBILITY OF THE CLOAK

When |OA| and |OF| are too small, it is difficult to find materials to build the cloak; when |OA| and |OF| are too large, the cloaking effect is degraded. A balance is required.

Using the analysis presented in Section 4.2, a regular polygonal cloak is designed. All the sections are equivalent with $\theta=\pi/36$, |OA|=|OF|=0.2, |OB|=|OE|=1 and |OC|=|OD|=2. The required properties of each section are shown in Table 4.1. Although there are significant disparities among the relative densities (two orders of magnitude), no extreme values are required. The cloak built with layered structures of equal thickness is shown in Figure 4.13.

Table 4.1 Required properties of one section for a realizable cloak

	Principal properties	Relative values (ρ_b, κ_b)
Part BCD	Density 1 ($\rho_{\|\|}$)	0.5553
	Density 2 ($\rho_{\perp}$)	1.8010
	Bulk modulus (κ)	0.5556
Part BDE	Density 1 ($\rho_{\|\|}$)	0.1109
	Density 2 ($\rho_{\perp}$)	9.0137
	Bulk modulus (κ)	2.7778

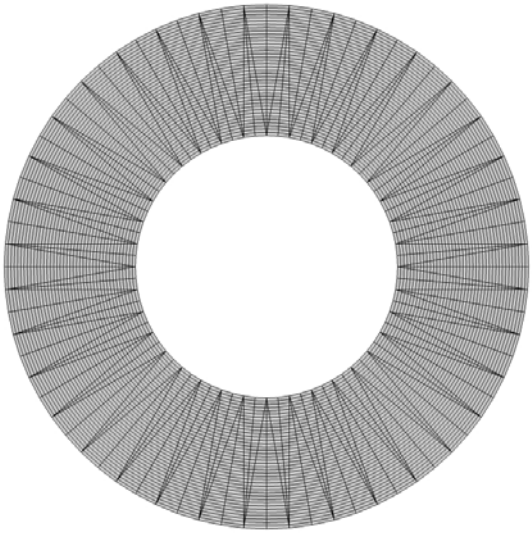

Figure 4.13 An approximately circular cloak with layered structures

The cloaking effect of the approximately circular cloak with layered structures is simulated with COMSOL Multiphysics finite element software. A plane wave with amplitude of 1 Pa through a space with an obstacle is simulated. The results without and with the cloak are shown in Figure 4.14. The results show that the cloak guides the waves around the obstacle. The cloaking effect is not perfect, but reflections and shadows are significantly reduced.

The reduced total RCS of the cloak over an area of $10r_0 \times 10r_0$ (where r_0 is the inner radius of the cloak) is shown in Figure 4.15. When $r_0/\lambda_b<1.5$, the reduced total RCS is less than 0.2. Therefore, at relatively low frequencies, that is, when r_0/λ_b, is small, the cloak significantly reduces the effect of the obstacle. When frequency increases, the cloaking effect decreases. When $r_0/\lambda_b=2$, the reduced total RCS goes to 0.8. There is little cloaking effect.

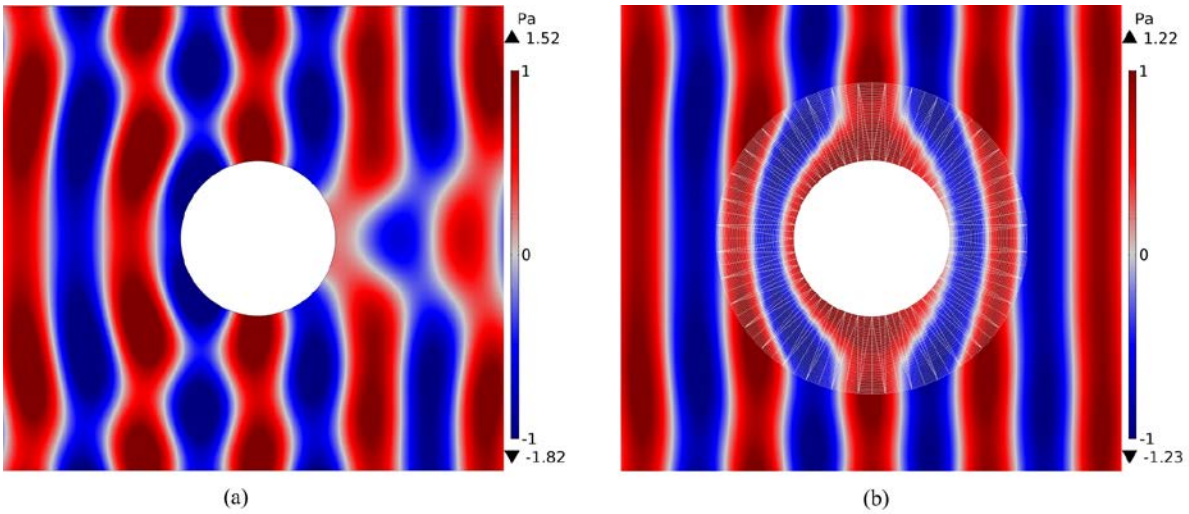

Figure 4.14 Simulation of a plane wave with amplitude of 1Pa through a space with an object (a) without cloak (b) with the approximately circular cloak

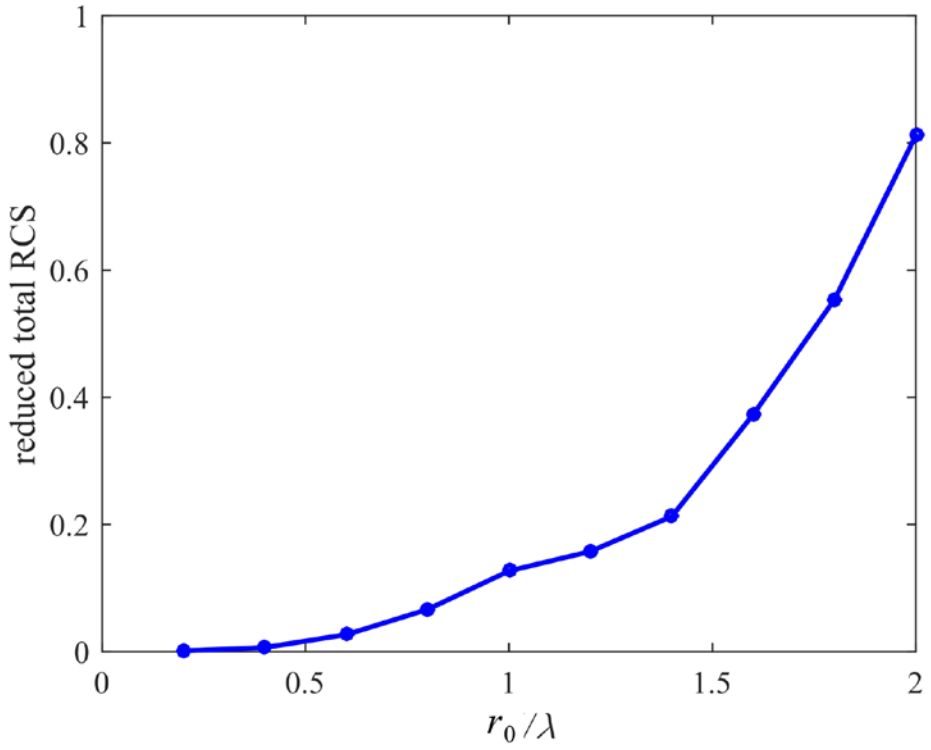

Figure 4.15 Reduced total RCS of the circular cloak built with two-part sections

It is difficult to satisfy the requirements for both densities and bulk moduli given in Table 4.1 with natural materials. It is easier to satisfy the requirement of velocities only. Such cloaks are not impedance matched, which are called eikonal cloaks (Urzhumov, Ghezzo, Hunt, & Smith, 2010).

Given that the cloak is radial-symmetric, all the sections are equivalent and the cloak is composed of just two different parts. The required relative velocities of the two parts in the approximately circular cloak are shown in Table 4.2. These velocities are attainable for water and air background media. Since it is not impedance matched, there would be more scattering than the one with properties in Table 4.1.

Table 4.2 The required velocities of the approximately circular cloak

	Principal velocities	Relative values (c_b)
Part BCD	Velocity_1 ($c_{\|\|}$)	1.0003
	Velocity_2 ($c_{\perp}$)	0.5554
Part BDE	Velocity_1 ($c_{\|\|}$)	5.0038
	Velocity_2 ($c_{\perp}$)	0.5551

5.0 TWO DIMENSIONAL ACOUSTIC CLOAKS WITH ARBITRARY HOMOGENEOUS PATTERNS

In Chapter 4.0, acoustic cloaks were designed by dividing the cloak into sections, which were further divided into two triangular parts. A two-step transformation was then applied, resulting in homogeneous properties.

Transformation from one triangle to another leads to cloak that is composed of arbitrary homogeneous triangular patterns. The geometric division of a cloak affects the properties of each triangular part dramatically, which can be used to tailor the properties of each triangular part. Simulations for models based on this method show good cloaking performance.

5.1 DERIVATION OF THE PROPERTIES

The properties of acoustic cloaks are derived with transformation acoustics. The mapping relation in the transformation determines the properties of the cloaks. A 2D cloak can be divided into arbitrary patterns composed of triangles. A cloak in triangular pattern can be mapped from another pattern, as shown in Figure 5.1. The triangles are mapped one to one. The exterior boundaries of the physical space and the virtual space are the same, and they are divided into the same pattern and mapped accordingly.

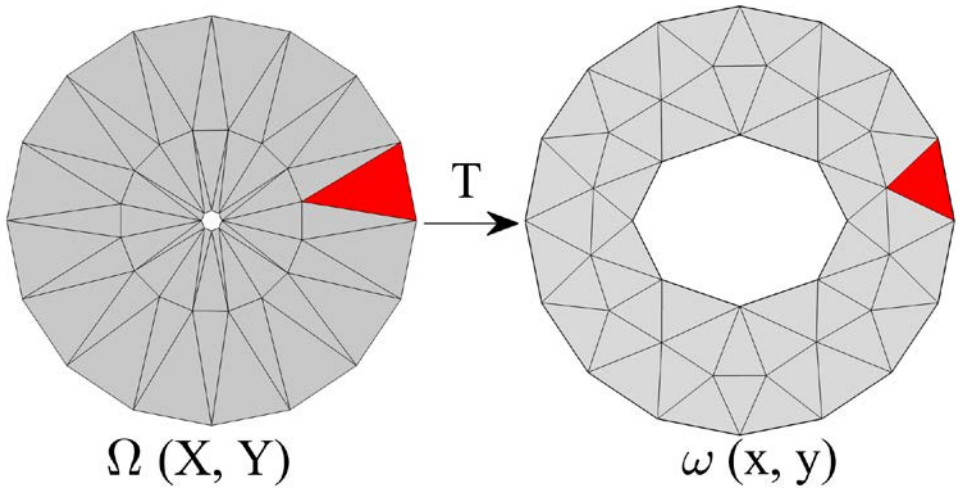

Figure 5.1 Mapping relations from the virtual space (Ω) to the physical space (ω) in triangular patterns

A mapping from one triangle to another is shown in Figure 5.2. The Triangle ABC is in virtual space, Ω, and the Triangle DEF is in physical space, ω. First, assume a mapping relation in the form:

$$\begin{bmatrix} x \\ y \end{bmatrix} = \begin{bmatrix} b_1 & b_2 \\ b_4 & b_5 \end{bmatrix} \begin{bmatrix} X \\ Y \end{bmatrix} + \begin{bmatrix} b_3 \\ b_6 \end{bmatrix}, \tag{5.1}$$

where the coefficients are constant.

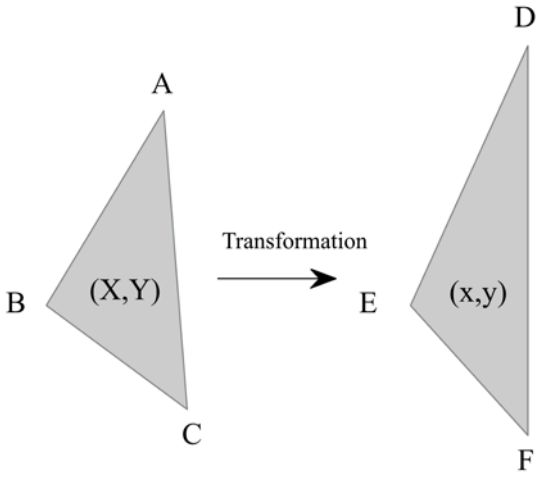

Figure 5.2 Transformation from a triangular area to another

The Jacobian matrix for this transformation is then given by:

$$\boldsymbol{J} = \begin{bmatrix} b_1 & b_2 \\ b_4 & b_5 \end{bmatrix}. \tag{5.2}$$

It is a constant matrix.

Substituting the three groups of corresponding vertices into Equation (5.1), we get

$$\begin{bmatrix} x_D \\ y_D \end{bmatrix} = \boldsymbol{J} \begin{bmatrix} X_A \\ Y_A \end{bmatrix} + \begin{bmatrix} b_3 \\ b_6 \end{bmatrix}, \tag{5.3}$$

$$\begin{bmatrix} x_E \\ y_E \end{bmatrix} = \boldsymbol{J} \begin{bmatrix} X_B \\ Y_B \end{bmatrix} + \begin{bmatrix} b_3 \\ b_6 \end{bmatrix}, \tag{5.4}$$

$$\begin{bmatrix} x_F \\ y_F \end{bmatrix} = \boldsymbol{J} \begin{bmatrix} X_C \\ Y_C \end{bmatrix} + \begin{bmatrix} b_3 \\ b_6 \end{bmatrix}. \tag{5.5}$$

Subtracting Equation (5.3) with (5.4) and (5.5), and combining, we get

$$\boldsymbol{A} = \boldsymbol{J}\ \boldsymbol{B}, \tag{5.6}$$

where,

$$\boldsymbol{A} = \begin{bmatrix} x_D - x_E & x_D - x_F \\ y_D - y_E & y_D - y_F \end{bmatrix},$$

$$\boldsymbol{B} = \begin{bmatrix} X_A - X_B & X_A - X_C \\ Y_A - Y_B & Y_A - Y_C \end{bmatrix}.$$

Since the Point *D*, *E*, and *F* are vertices of a triangle, the determinant of Matrix $\boldsymbol{B}$ cannot be zero. The Jacobian matrix can be derived as

$$\boldsymbol{J} = \boldsymbol{A}\,\boldsymbol{B}^{-1}. \tag{5.7}$$

Since the Matrices $\boldsymbol{A}$ and $\boldsymbol{B}$ are independent of *x* and *y*, the Jacobian matrix is constant.

Again, the resulting Jacobian matrix is constant, meaning that the required material properties are independent of x and y. The properties for each triangular area are thus homogeneous. The density tensor can be transposed to the principal directions with Equation (3.6) and layered structures can be used to build each part with Equations (2.21). Since the properties of each part are homogeneous, only two different materials in layered structures are used to build each part.

5.2 SIMULATION AND ANALYSIS OF AN APPROXIMATELY CIRCULAR CLOAK WITH THREE-PART SECTIONS

The division of a cloak into triangular patterns can be arbitrary. One method is, as done in Chapter 4.0, dividing the cloak into radial sections. For symmetric models, this division will lead to equivalent sections to reduce the calculation.

There are two differences between this method and Chapter 4.0. First, the section is divided into more than two parts and multiple transformations are not performed on these parts. The method still results in homogenous parts. As an example, one section from a circular cloak with three triangles in virtual and physical space is shown in Figure 5.3.

In the figure, the triangle OA_1B_1 is the cloaked area. Accordingly, the triangle OA_0B_0 is the mapped area in virtual space. The cloaking effect gets better when $|OA_0|$ and $|OB_0|$ get smaller. Particularly, when $|OB_0|=0$, the cloaked area is mapped to a short line. Since all the points are located at the two edges, it can be noted as: $|OA_0|=\delta_1|OA_2|$, $|OB_0|=\delta_2|OB_2|$, $|OP|=\alpha|OB_2|$, $|OA_1|=\gamma_1|OA_2|$, $|OB_1|=\gamma_2|OB_2|$, and $|OQ|=\beta|OB_2|$. The ranges of the scaling constants are: $0<\delta_1<1$, $0\leq\delta_2<\alpha<1$, $\delta_1<\gamma_1<1$, $\delta_2<\gamma_2<\beta<1$.

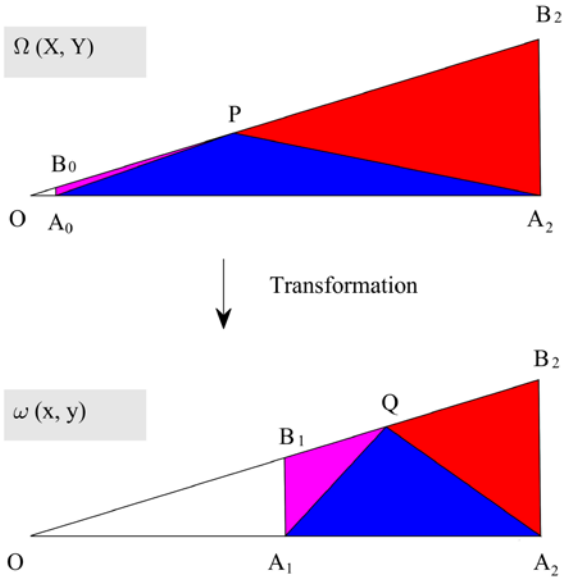

Figure 5.3 Transformation of a section with three triangles from virtual space to physical space

If γ_1, γ_2, δ_1 and δ_2 are constrained, there still are degrees of freedom that can be used to tune the effective properties. They are α and β. For a five-degree section from a circle, when $\delta_1 = \delta_2 = 0.05$ and $\gamma_1 = \gamma_2 = 0.5$, the variation of principal densities and bulk moduli with α and β are shown in Figure 5.4-Figure 5.5. As can be observed, the effective properties change dramatically with the two parameters. Extreme properties will result if the parameters α or β approaches the boundaries.

The variation of principal velocities of each part with α and β is shown in Figure 5.6. Some velocities are observed to change dramatically, while the others change little. Variations in velocities are required no matter how to tune α and β.

The parameters α and β affect the properties of each part. But the properties cannot be controlled arbitrarily with just the two parameters, but they are observed to be quite effective at tailoring materials properties in the cloak.

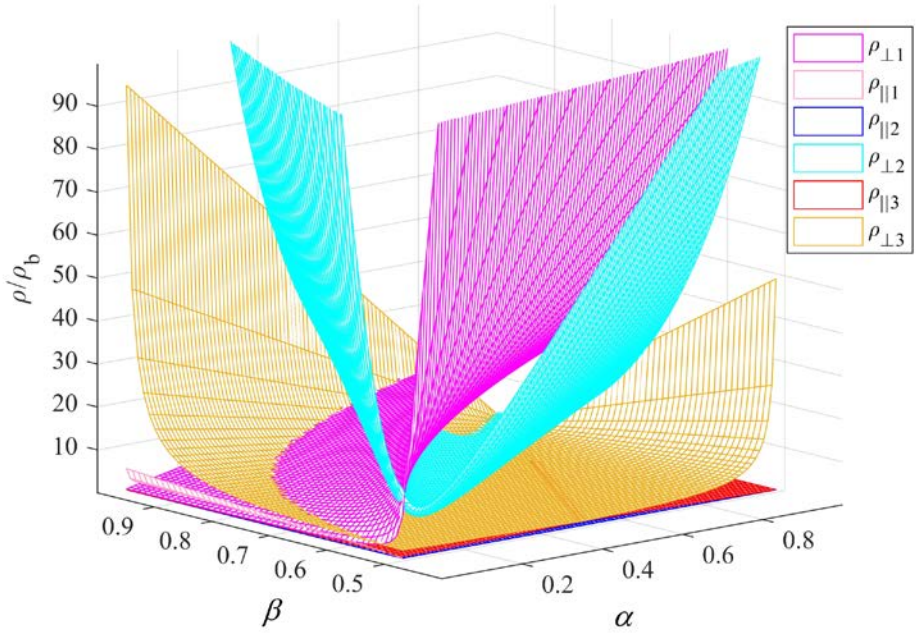

Figure 5.4 Variation of principal densities of each part with parameters α and β

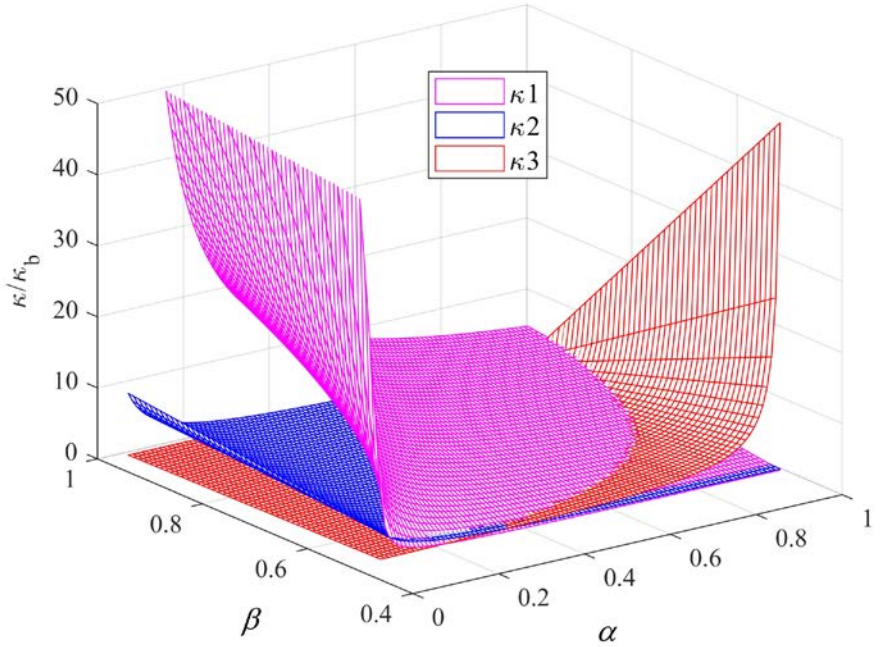

Figure 5.5 Variation of bulk modulus of each part with parameters α and β

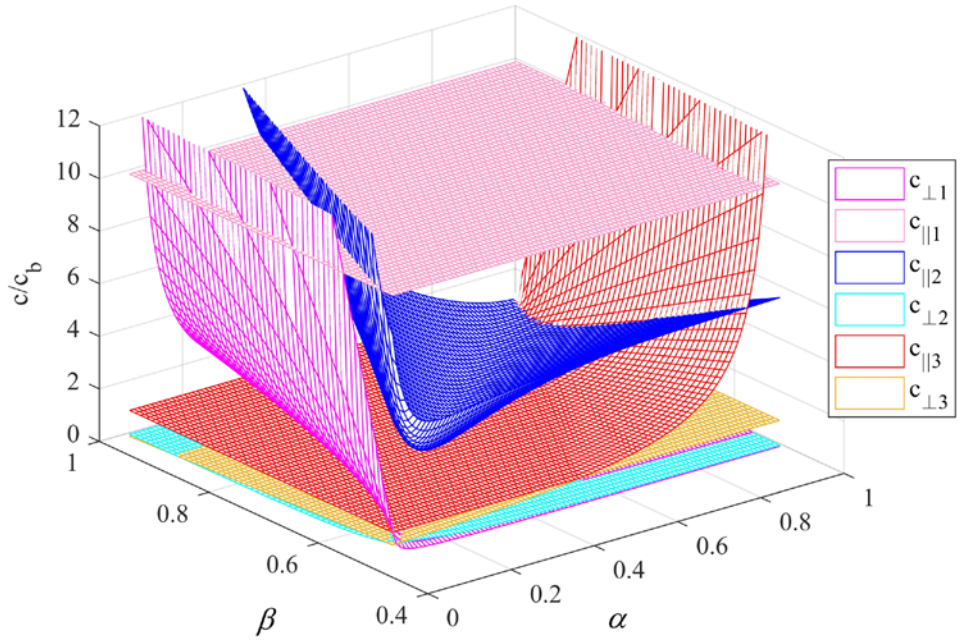

Figure 5.6 Variation of velocities of sound of each part with parameters α and β

There are three bulk moduli and 6 principal density elements in one section with 3 parts. A parameter ζ is defined as

$$\zeta = \sigma(\boldsymbol{\rho}) + \sigma(\boldsymbol{\kappa}), \tag{5.8}$$

where, σ() is the standard deviation, $\boldsymbol{\rho}$ is the vector containing all the principal density elements in the section, and $\boldsymbol{\kappa}$ is the vector containing all the bulk moduli in the section.

The minimum of ζ is reached when α=0.19 and β=0.6. The principal densities and bulk moduli of each part are

$$\begin{cases} \rho_{||1} = 0.4935\rho_b, \quad \rho_{\perp 1} = 2.0263\rho_b, \quad \kappa_1 = 0.4938\kappa_b \\ \rho_{||2} = 0.1363\rho_b, \quad \rho_{\perp 2} = 7.3381\rho_b, \quad \kappa_2 = 1.6620\kappa_b \\ \rho_{||3} = 0.0713\rho_b, \quad \rho_{\perp 3} = 14.0231\rho_b, \quad \kappa_3 = 7.1429\kappa_b \end{cases}$$

Each part can be built by just two alternating layers of material. The layered structure of the whole cloak is shown in Figure 5.7.

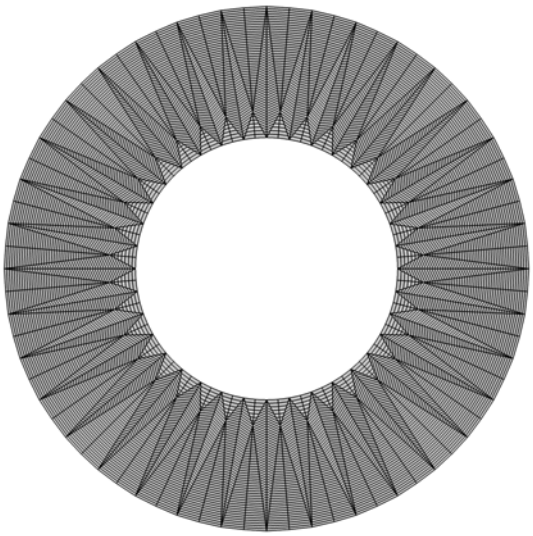

Figure 5.7 A circular cloak composed of three-part sections built with layered structures

The cloaking effect of the approximately circular cloak with layered three-part sections is simulated with COMSOL Multiphysics finite element software. The total pressure fields for a plane wave with amplitude of 1 Pa without and with the cloak are simulated. The results are shown in Figure 5.8. It can be seen from the figures that the cloak reduces scattering and shadows noticeably.

The normalized amplitudes of the scattered waves without and with the circular cloak at $r=5\lambda_b$ are shown in Figure 5.9. As discussed in Figure 5.8, there is strong scattering for the bare obstacles. The scattering is significantly reduced with the cloak. Thus, the cloak works well at this frequency.

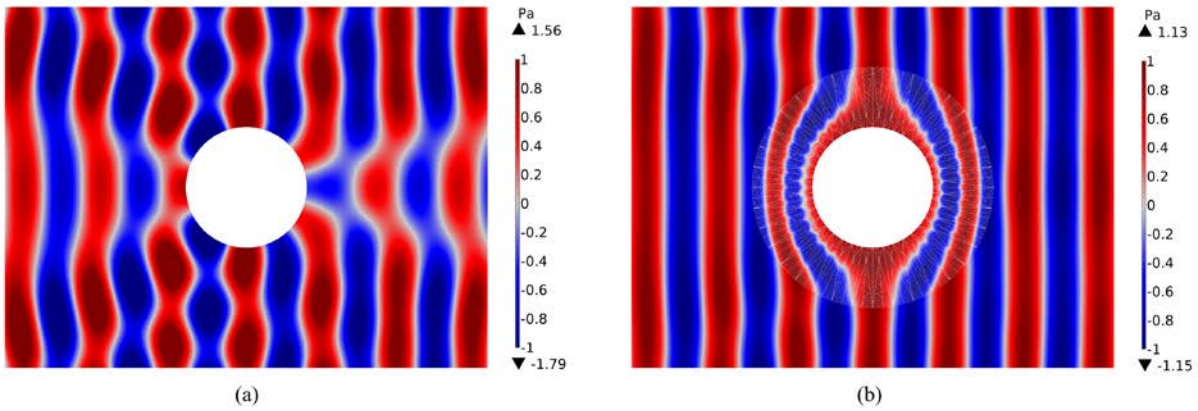

Figure 5.8 Simulation of a plane wave with amplitude of 1Pa propagating through a space with the circular cloak with triangular pattern (a) without cloak (b) with the cloak

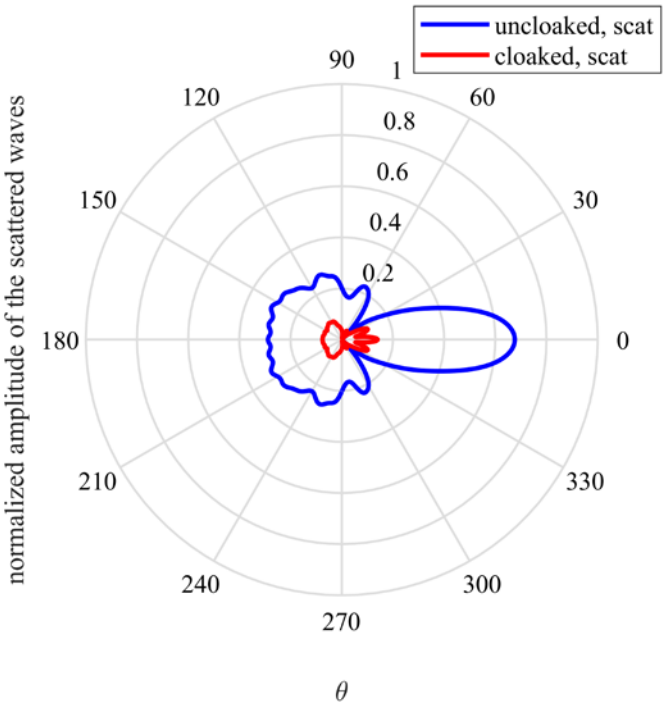

Figure 5.9 Normalized amplitude of the scattered waves without and with the circular cloak at $r=5\lambda_b$

The reduced total RCS of the cloak over an area of $8r_0 \times 6r_0$ (r_0 is the inner radius of the cloak) excluding the cloak is shown in Figure 5.10. When r_0/λ is relatively small, that is, at

relatively low frequencies, the reduced total RCS is small. The cloaking performance decreases with the increase of r_0/λ.

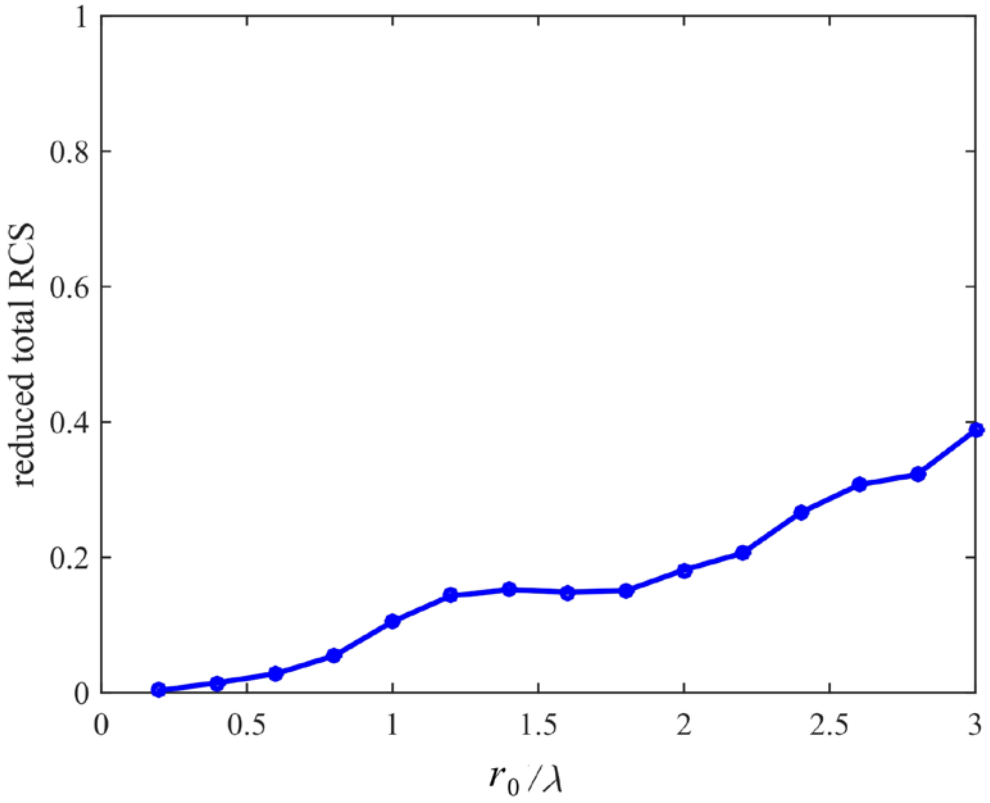

Figure 5.10 Reduced total RCS of the circular cloak

5.3 SIMULATION OF A RECTANGULAR CLOAK WITH FIVE-PART SECTIONS

A cloak can be divided into any number of arbitrary triangular patterns. Therefore, a section can be divided into more triangular parts. As an example, a 45-degree section of a square cloak with five parts is shown in Figure 5.11. The five triangles in physical space are mapped from five triangles in virtual space accordingly.

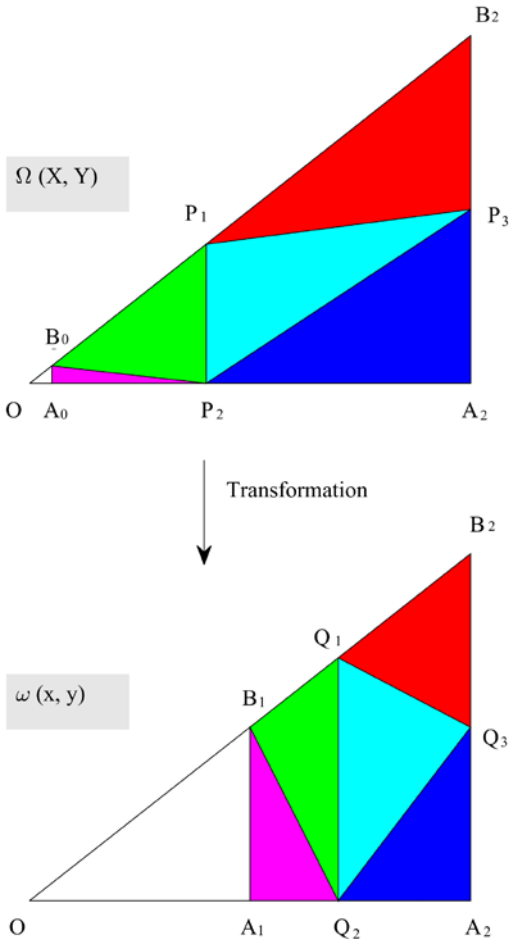

Figure 5.11 Mapping of a section with five parts from virtual space to physical space

The triangle OA_1B_1 is the cloaked area, and the triangle OA_0B_0 is the mapped area in virtual space. When they are constrained, there still are degrees of freedom in affecting the properties of the section. They are positions of P_i and Q_i. The properties of each part are calculated and built with layered structures. The layered structure of the whole cloak is shown in Figure 5.12. The parameters are: $|OA_0|=0.05|OA_2|$, $|OB_0|=0.05|OB_2|$, $|OP_1|=0.25|OB_2|$, $|OP_2|=0.25|OA_2|$, $|A_2P_3|=0.5|A_2B_2|$, $|OA_1|=0.5|OA_2|$, $|OB_1|=0.5|OB_2|$, $|OQ_1|=0.7|OB_2|$, $|OQ_2|=0.7|OA_2|$, $|A_2Q_3|=0.5|A_2B_2|$.

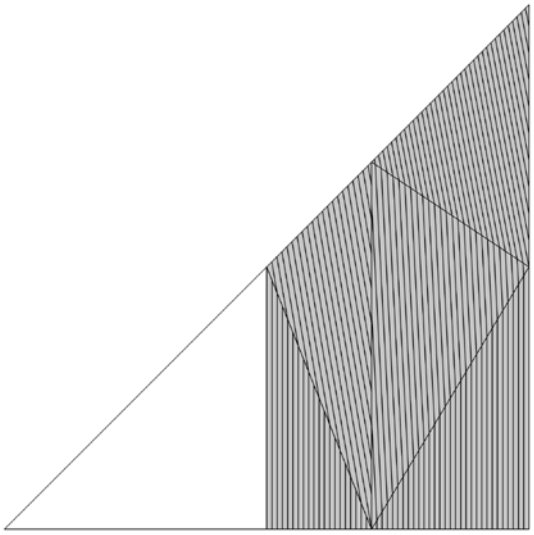

Figure 5.12 A rectangular cloak with triangular pattern built with layered structures

The cloaking effect of the square cloak with layered five-part sections is simulated with COMSOL Multiphysics finite element software. The total pressure fields for a plane wave with amplitude of 1 Pa without and with the cloak are simulated. The results are shown in Figure 5.13. It can be seen from the figures that the cloak reduces scattering and shadows noticeably.

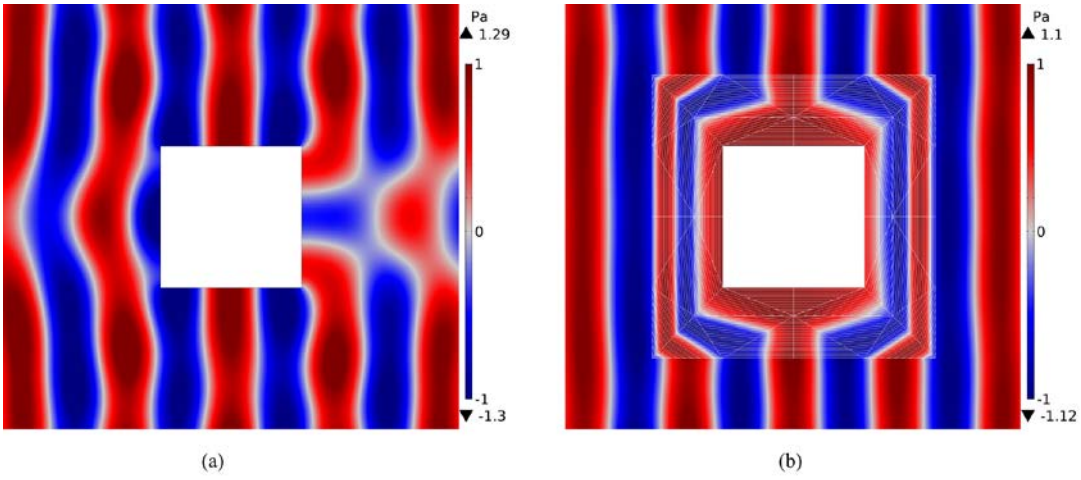

Figure 5.13 Simulation of a plane wave with amplitude of 1Pa propagating through a space with the rectangular cloak (a) without cloak (b) with cloak

The reduced total RCS of the square cloak is shown in Figure 5.14. The cloak works well when $0.5l/\lambda$ is small. l is the side length of cloaked obstacle. That is, the cloaking effect is good at relatively low frequencies.

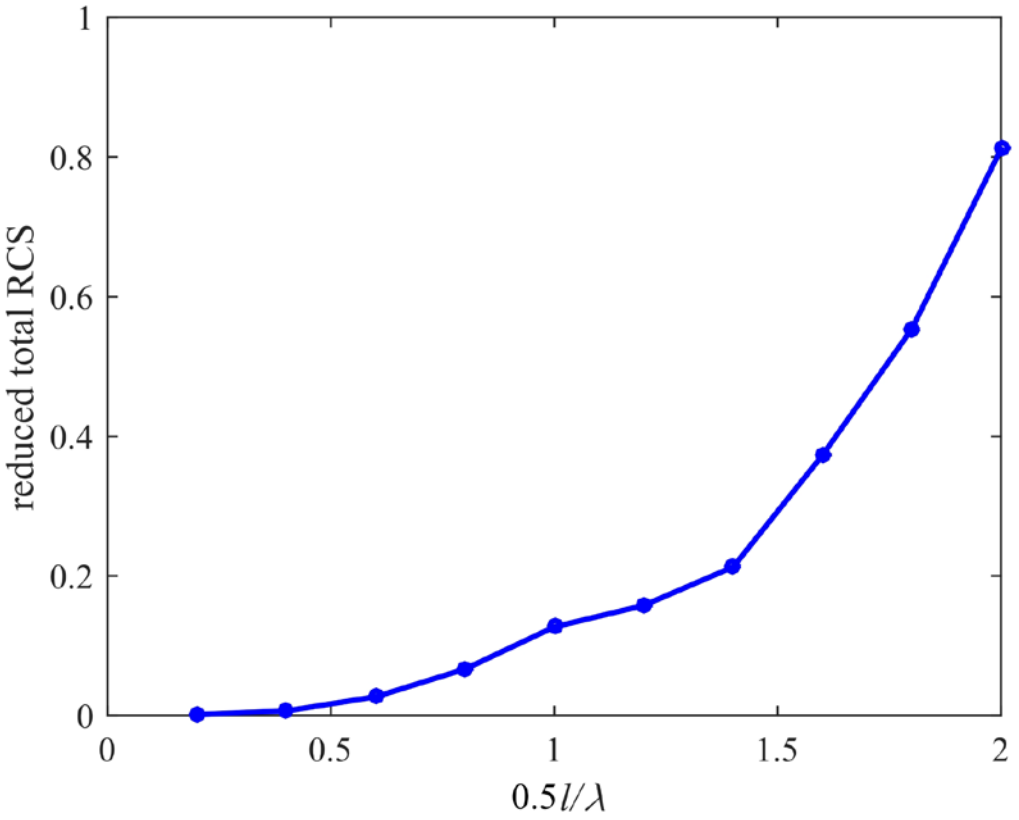

Figure 5.14 Reduced total RCS of the square cloak

The results demonstrate that cloaks can be divided into any number of arbitrary triangular parts with homogeneous properties. The properties of each part can be controlled by the division to some extent.

6.0 THREE DIMENSIONAL ARBITRARILY SHAPED ACOUSTIC CLOAKS COMPOSED OF HOMOGENEOUS PARTS

The methods of dividing a 2D cloak into homogeneous parts presented in Chapter 4.0 and Chapter 5.0 are extended to 3D. Three dimensional acoustic cloaks can also be mapped along radial directions. A cubic cloak is designed with transformation acoustics by mapping along radial directions, as shown in Figure 6.1. The resulting properties are inhomogeneous and anisotropic. However, homogeneous parts can be realized by using other transformations in space.

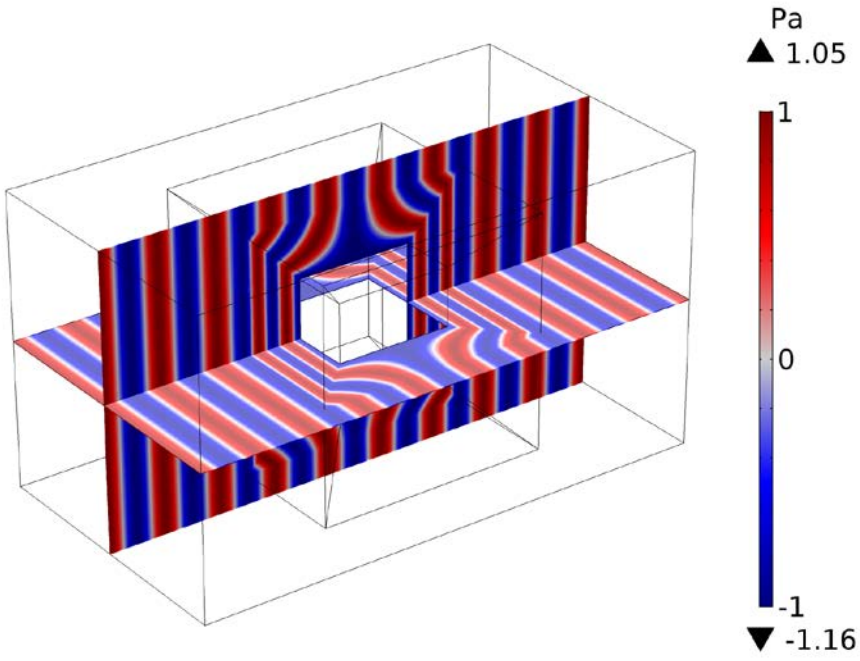

Figure 6.1 Cubic cloak by mapping along radial directions

The 3D multi-transform method begins by dividing the cloak into tetrahedral sections. Each section is then further divided into three more tetrahedral parts. A three-step transformation can be used to derive the properties of each part of the section, which are homogeneous. More generally, transformation from a tetrahedron to another leads to homogenous properties. 3D cloaks can be either realized or at least approximated with arbitrary tetrahedral sections. For example, a spherical cloak could be approximated as a polyhedron, with faceted inner and outer boundaries.

6.1 DERIVATION OF THE PROPERTIES OF THE CLOAKS WITH A THREE-STEP TRANSFORMATION

Most cloaks can be divided into sections. The composite of the cloak and its cloaked space can be divided into tetrahedral sections, one of which is shown in Figure 6.2. The shadowed part is the section of the cloak. The Tetrahedron $OA_1B_1C_1$ represents a section of the cloaked space. A_0, B_0 and C_0 are virtual points which are used to derive the required material properties. Without loss of generality, the edge OA_2 is selected as the *x*-axis, and the face OA_2B_2 lies on the *xy* plane.

Multi-step transformation acoustics will be used to derive the properties of the general section of a cloak. The transformation from the virtual space to the physical space takes three steps, as shown in Figure 6.3. (Li & Vipperman, 2018)

In the first step (Figure 6.3a), Tetrahedron $OA_0B_2C_2$ is expanded to $OA_1B_2C_2$ and $A_0A_2B_2C_2$ is compressed to $A_1A_2B_2C_2$ with a linear transform along OA_2. The second step (Figure 6.3b) continues after the first step. The $OA_1C_2B_0$ is expanded to $OA_1C_2B_1$ and $B_0A_1B_2C_2$ is compressed to $B_1A_1B_2C_2$ with a linear transform along OB_2. After the second step, the third

step (Figure 6.3c) continues. In the third step, $C_0A_1B_1C_2$ is compressed to $C_1A_1B_1C_2$ along OC_2. Part 1 undergoes the first transformation, Part 2 undergoes the first two transformations, and Part 3 undergoes all three transformations. After the three steps, the cloaked space $OA_1B_1C_1$ has been mapped from the virtual space $OA_0C_0B_0$. In particular, when $OC_0=0$, the virtual space becomes an area OA_0B_0.

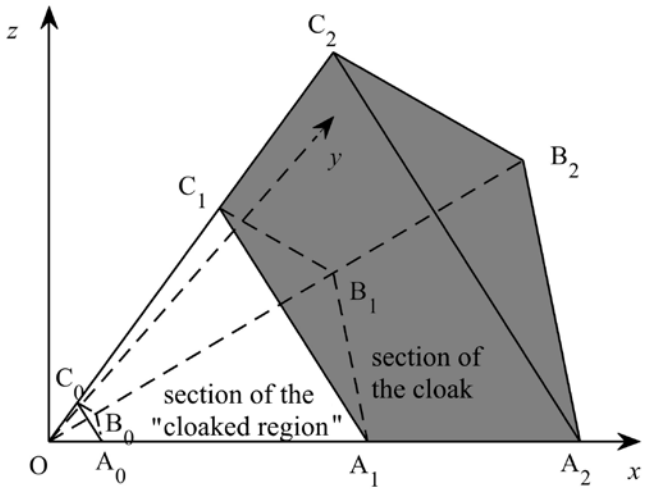

Figure 6.2 A section from a 3D acoustic cloak with arbitrary shapes

Since all the points are located on three edges, letting $OA_0= \lambda_1 OA_2$, $OA_1= \lambda_2 OA_2$, $OB_0= \mu_1 OB_2$, $OB_1= \mu_2 OB_2$, $OC_0= \xi_1 OC_2$, $OC_1= \xi_2 OC_2$, where λ_i, μ_i and ξ_i are all constants.

In the first step, the transformation from points in Tetrahedron $A_0A_2B_2C_2$ to points in Tetrahedron $A_1A_2B_2C_2$ is represented by

$$\begin{bmatrix} x \\ y \\ z \end{bmatrix} = \underbrace{\begin{bmatrix} c_1 & c_2 & c_3 \\ 0 & 1 & 0 \\ 0 & 0 & 1 \end{bmatrix}}_{\boldsymbol{C_1}} \begin{bmatrix} X \\ Y \\ Z \end{bmatrix} + \begin{bmatrix} c_4 \\ 0 \\ 0 \end{bmatrix}, \tag{6.1}$$

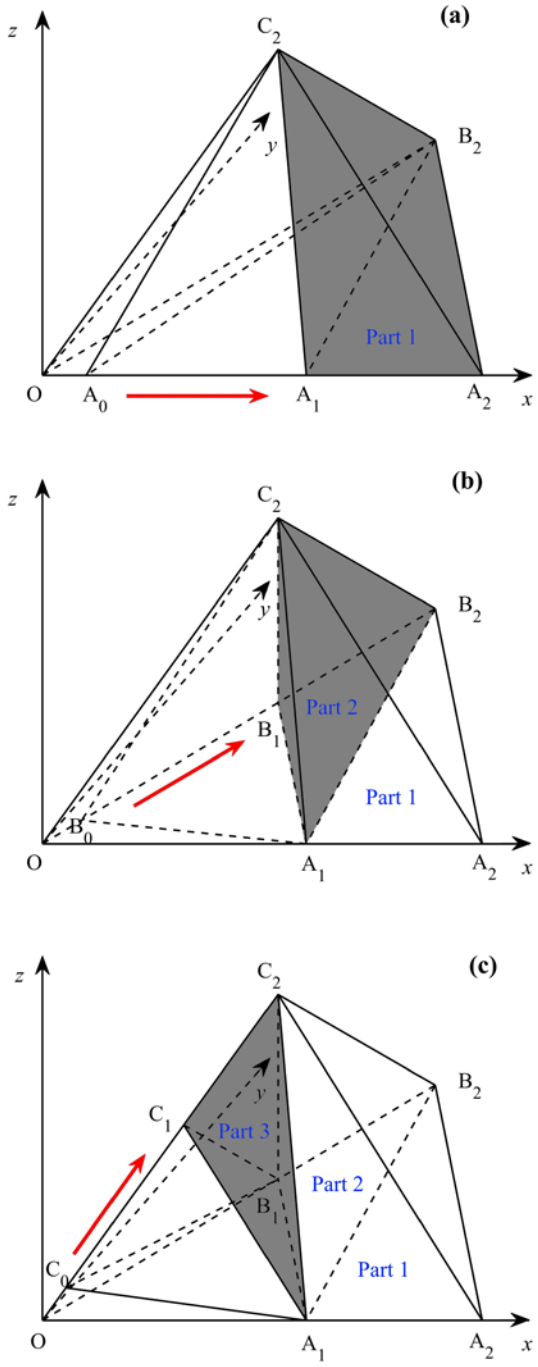

Figure 6.3 Schematic diagram of the three-step mapping (a) first step (b) second step (c) third step

where,

$$c_1 = \frac{1-\lambda_2}{1-\lambda_1},$$

$$c_2 = \frac{\lambda_2-\lambda_1}{1-\lambda_1}\frac{x_{B_2}-x_{A_2}}{y_{B_2}},$$

$$c_3 = -\frac{\lambda_2-\lambda_1}{1-\lambda_1}\frac{x_{B_2}y_{C_2}-x_{C_2}y_{B_2}+x_{A_2}\left(y_{B_2}-y_{C_2}\right)}{y_{B_2}z_{C_2}}, \text{ and}$$

$$c_4 = \frac{\lambda_2-\lambda_1}{1-\lambda_1}x_{A_2}.$$

At the same time, the points in Tetrahedron $OA_0B_2C_2$ are mapped to Tetrahedron $OA_1B_2C_2$ using

$$\begin{bmatrix} x_I \\ y_I \\ z_I \end{bmatrix} = \underbrace{\begin{bmatrix} c_5 & c_6 & c_7 \\ 0 & 1 & 0 \\ 0 & 0 & 1 \end{bmatrix}}_{\boldsymbol{C_2}} \begin{bmatrix} X \\ Y \\ Z \end{bmatrix}, \tag{6.2}$$

where,

$$c_5 = \frac{\lambda_2}{\lambda_1},$$

$$c_6 = \frac{\lambda_1-\lambda_2}{\lambda_1}\frac{x_{B_2}}{y_{B_2}}, \text{ and}$$

$$c_7 = -\frac{\lambda_1-\lambda_2}{\lambda_1}\frac{x_{B_2}y_{C_2}-x_{C_2}y_{B_2}}{y_{B_2}z_{C_2}}.$$

The second step takes place in the Tetrahedron $OA_1B_2C_2$ derived in the first step, and also contains two transformations. The points in Tetrahedron $B_0A_1B_2C_2$ are mapped to tetrahedron $B_1A_1B_2C_2$ using

$$\begin{bmatrix} x \\ y \\ z \end{bmatrix} = \underbrace{\begin{bmatrix} c_8 & c_9 & c_{10} \\ c_{12} & c_{13} & c_{14} \\ 0 & 0 & 1 \end{bmatrix}}_{\boldsymbol{C_3}} \begin{bmatrix} x_I \\ y_I \\ z_I \end{bmatrix} + \begin{bmatrix} c_{11} \\ c_{15} \\ 0 \end{bmatrix}, \tag{6.3}$$

where,

$$c_8 = \frac{\mu_1 - \mu_2}{1-\mu_1} \frac{x_{B_2}}{\lambda_2 x_{A_2}} + 1,$$

$$c_9 = \frac{\mu_1 - \mu_2}{1-\mu_1} \frac{x_{B_2}}{y_{B_2}} \left(1 - \frac{x_{B_2}}{\lambda_2 x_{A_2}} \right),$$

$$c_{10} = \frac{\mu_2 - \mu_1}{1-\mu_1} \left[\frac{x_{B_2}}{z_{C_2}} \left(\frac{x_{C_2}}{\lambda_2 x_{A_2}} - 1 \right) + \frac{x_{B_2} y_{C_2}}{y_{B_2} z_{C_2}} \left(1 - \frac{x_{B_2}}{\lambda_2 x_{A_2}} \right) \right], c_{11} = \frac{\mu_2 - \mu_1}{1-\mu_1} x_{B_2},$$

$$c_{12} = \frac{\mu_1 - \mu_2}{1-\mu_1} \frac{y_{B_2}}{\lambda_2 x_{A_2}},$$

$$c_{13} = \frac{\mu_1 - \mu_2}{1-\mu_1} \left(1 - \frac{x_{B_2}}{\lambda_2 x_{A_2}} \right) + 1,$$

$$c_{14} = \frac{\mu_2 - \mu_1}{1-\mu_1} \left[\frac{y_{B_2}}{z_{C_2}} \left(\frac{x_{C_2}}{\lambda_2 x_{A_2}} - 1 \right) + \frac{y_{C_2}}{z_{C_2}} \left(1 - \frac{x_{B_2}}{\lambda_2 x_{A_2}} \right) \right], \text{ and}$$

$$c_{15} = \frac{\mu_2 - \mu_1}{1-\mu_1} y_{B_2}.$$

At the same time, the points from Tetrahedron $OA_1C_2B_0$ are mapped to Tetrahedron $OA_1C_2B_1$ using

$$\begin{bmatrix} x_{II} \\ y_{II} \\ z_{II} \end{bmatrix} = \underbrace{\begin{bmatrix} 1 & c_{16} & c_{17} \\ 0 & c_{18} & c_{19} \\ 0 & 0 & 1 \end{bmatrix}}_{\boldsymbol{C_4}} \begin{bmatrix} x_I \\ y_I \\ z_I \end{bmatrix}, \tag{6.4}$$

where,

$$c_{16} = -\frac{\mu_1 - \mu_2}{\mu_1}\frac{x_{B_2}}{y_{B_2}},$$

$$c_{17} = \frac{\mu_1 - \mu_2}{\mu_1}\frac{x_{B_2} y_{C_2}}{y_{B_2} z_{C_2}},$$

$$c_{18} = \frac{\mu_2}{\mu_1}, \text{ and}$$

$$c_{19} = \frac{\mu_1 - \mu_2}{\mu_1}\frac{y_{C_2}}{z_{C_2}}.$$

Finally, the third step takes place in the Tetrahedron $OA_1B_1C_2$ derived in the second step. The mapping of points from Tetrahedron $C_0A_1B_1C_2$ to Tetrahedron $C_1A_1B_1C_2$ is given by

$$\begin{bmatrix} x \\ y \\ z \end{bmatrix} = \underbrace{\begin{bmatrix} c_{20} & c_{21} & c_{22} \\ c_{24} & c_{25} & c_{26} \\ c_{28} & c_{29} & c_{30} \end{bmatrix}}_{\boldsymbol{C_5}} \begin{bmatrix} x_{II} \\ y_{II} \\ z_{II} \end{bmatrix} + \begin{bmatrix} c_{23} \\ c_{27} \\ c_{31} \end{bmatrix}, \tag{6.5}$$

where,

$$c_{20} = 1 - \frac{\xi_2 - \xi_1}{1 - \xi_1}\frac{x_{C_2}}{\lambda_2 x_{A_2}},$$

$$c_{21} = \frac{\xi_2 - \xi_1}{1 - \xi_1}\frac{x_{C_2}}{\mu_2 y_{B_2}}\left(\frac{\mu_2 x_{B_2}}{\lambda_2 x_{A_2}} - 1\right),$$

$$c_{22} = \frac{\xi_2 - \xi_1}{1 - \xi_1}\frac{x_{C_2}}{z_{C_2}}\left[\frac{x_{C_2}}{\lambda_2 x_{A_2}} - \frac{y_{C_2}}{\mu_2 y_{B_2}}\left(\frac{\mu_2 x_{B_2}}{\lambda_2 x_{A_2}} - 1\right) - 1\right],$$

$$c_{23} = \frac{\xi_2 - \xi_1}{1 - \xi_1} x_{C_2},$$

$$c_{24} = -\frac{\xi_2 - \xi_1}{1-\xi_1}\frac{y_{C_2}}{\lambda_2 x_{A_2}},$$

$$c_{25} = \frac{\xi_2 - \xi_1}{1-\xi_1}\frac{y_{C_2}}{\mu_2 y_{B_2}}\left(\frac{\mu_2 x_{B_2}}{\lambda_2 x_{A_2}} - 1\right) + 1,$$

$$c_{26} = \frac{\xi_2 - \xi_1}{1-\xi_1}\frac{y_{C_2}}{z_{C_2}}\left[\frac{x_{C_2}}{\lambda_2 x_{A_2}} - \frac{y_{C_2}}{\mu_2 y_{B_2}}\left(\frac{\mu_2 x_{B_2}}{\lambda_2 x_{A_2}} - 1\right) - 1\right],$$

$$c_{27} = \frac{\xi_2 - \xi_1}{1-\xi_1} y_{C_2},$$

$$c_{28} = -\frac{\xi_2 - \xi_1}{1-\xi_1}\frac{z_{C_2}}{\lambda_2 x_{A_2}},$$

$$c_{29} = \frac{\xi_2 - \xi_1}{1-\xi_1}\frac{z_{C_2}}{\mu_2 y_{B_2}}\left(\frac{\mu_2 x_{B_2}}{\lambda_2 x_{A_2}} - 1\right),$$

$$c_{30} = \frac{\xi_2 - \xi_1}{1-\xi_1}\left(\frac{x_{C_2}}{\lambda_2 x_{A_2}} - \frac{y_{C_2}}{\mu_2 y_{B_2}}\left(\frac{\mu_2 x_{B_2}}{\lambda_2 x_{A_2}} - 1\right) - 1\right) + 1, \text{ and}$$

$$c_{31} = \frac{\xi_2 - \xi_1}{1-\xi_1} z_{C_2}.$$

From Equations (6.1) and (2.4), the Jacobian matrix for Tetrahedron $A_1A_2B_2C_2$ is

$$\boldsymbol{J}_1 = \boldsymbol{C}_1. \tag{6.6}$$

Equations (6.2), (6.3), and (2.4) can be used to find the Jacobian matrix for Tetrahedron $B_1A_1B_2C_2$ as

$$\boldsymbol{J}_2 = \boldsymbol{C}_3\boldsymbol{C}_2. \tag{6.7}$$

For Tetrahedron $C_1A_1B_1C_2$, the Jacobian matrix is computed using equations (6.2), (6.4), (6.5) and (2.4) as

$$\boldsymbol{J}_3 = \boldsymbol{C}_5 \boldsymbol{C}_4 \boldsymbol{C}_2 . \tag{6.8}$$

Since $\boldsymbol{C}_i$ (i=1, 2, 3, 4, 5) are not functions of neither x nor y, all the Jacobian matrices are constant. As such, the properties of the cloaks derived with Equations (2.13) are homogeneous.

6.2 DERIVATION OF THE HOMOGENEOUS PROPERTIES WITH A GENERAL TRANSFORMATION

Three dimensional acoustic cloaks can be composed of homogeneous parts with a three-step transformation, as discussed in Section 6.1. Finally, each tetrahedral part is transformed from another tetrahedron in virtual space. A general transformation can be found from a tetrahedron to another directly, as shown in Figure 6.4. The Tetrahedron ABCD in virtual space is mapped to the Tetrahedron EFGH in physical space.

A linear transformation from virtual space to physical space is desired, which is noted as

$$\begin{bmatrix} x \\ y \\ z \end{bmatrix} = \begin{bmatrix} d_1 & d_2 & d_3 \\ d_5 & d_6 & d_7 \\ d_9 & d_{10} & d_{11} \end{bmatrix} \begin{bmatrix} X \\ Y \\ Z \end{bmatrix} + \begin{bmatrix} d_4 \\ d_8 \\ d_{12} \end{bmatrix}, \tag{6.9}$$

where all the coefficients are constant.

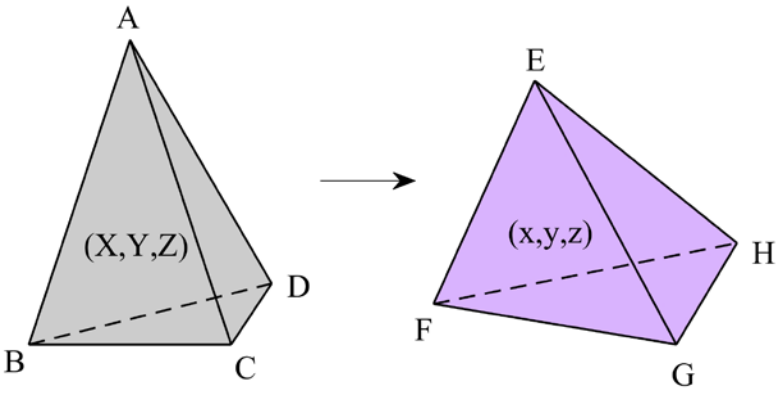

Figure 6.4 Transformation from one tetrahedron in virtual space to another in physical space

The Jacobian matrix for this transformation is constant, which is

$$\boldsymbol{J} = \begin{bmatrix} d_1 & d_2 & d_3 \\ d_5 & d_6 & d_7 \\ d_9 & d_{10} & d_{11} \end{bmatrix} \tag{6.10}$$

Substituting the four groups of corresponding vertices into Equation (6.9), and simplifying, we get

$$\boldsymbol{A} = \boldsymbol{J}\ \boldsymbol{B}\,, \tag{6.11}$$

where

$$\boldsymbol{A} = \begin{bmatrix} x_E - x_F & x_E - x_G & x_E - x_H \\ y_E - y_F & y_E - y_G & y_E - y_H \\ z_E - z_F & z_E - z_G & z_E - z_H \end{bmatrix},$$

$$\boldsymbol{B} = \begin{bmatrix} X_A - X_B & X_A - X_C & X_A - X_D \\ Y_A - Y_B & Y_A - Y_C & Y_A - Y_D \\ Z_A - Z_B & Z_A - Z_C & Z_A - Z_D \end{bmatrix}.$$

Because Point *A*, *B*, *C* and *D* are vertices of a tetrahedron, the determinant of $\boldsymbol{B}$ is not zero. The Jacobian matrix is derived as

$$\boldsymbol{J} = \boldsymbol{A}\,\boldsymbol{B}^{-1}. \tag{6.12}$$

Matrices $\boldsymbol{A}$ and $\boldsymbol{B}$ are free of *x* and *y*, and thus the Jacobian matrix $\boldsymbol{J}$ is constant. As such, the properties of the cloaks derived with Equations (2.13) are homogeneous when using these Jacobian matrices.

6.3 NUMERICAL SIMULATION OF TWO POLYHEDRAL CLOAKS COMPOSED OF HOMOGENEOUS PARTS

Similar to two-dimensional versions, three-dimensional cloaks can be divided into any number of arbitrary tetrahedral patterns, which will impact how extreme the material properties become. The physical space and the virtual space are divided into the same number of tetrahedral patterns such that each tetrahedron in the cloak can be mapped to one in virtual space. One method first divides the composite of the cloak and its cloaked space into a series of tetrahedral sections by forming radial lines starting from the origin. Then each part is further subdivided into the three tetrahedra illustrated in Figure 6.3a-c. One such section is shown in Figure 6.5. Tetrahedron $A_0A_2B_2C_2$ is mapped to $A_1A_2B_2C_2$, $A_0B_0B_2C_2$ is mapped to $A_1B_1B_2C_2$ and $A_0B_0C_0C_2$ is mapped to $A_1B_1C_1C_2$. The properties of each tetrahedral part can be derived with the methods given in Section 6.1 or Section 6.2.

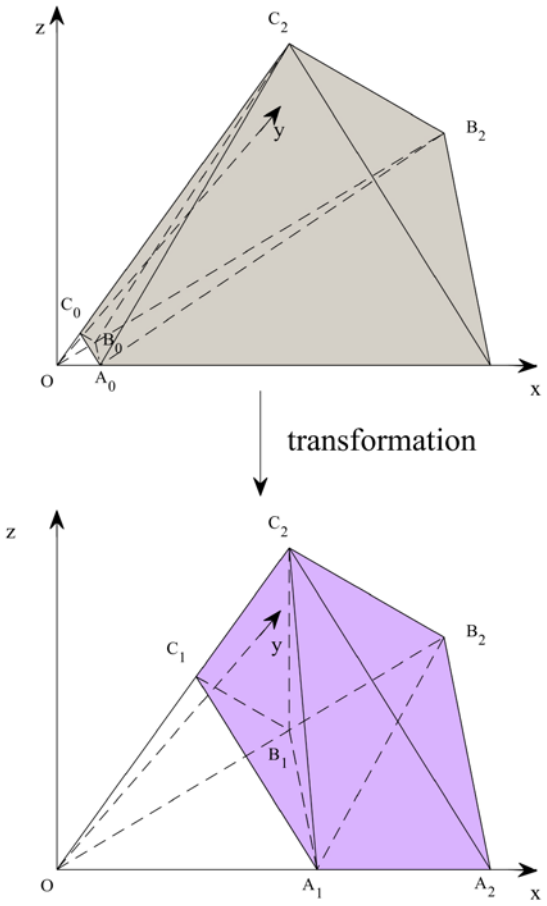

Figure 6.5 Transformation of corresponding tetrahedra from the virtual space to the physical space

Since all the points are located on three edges for this division, in the general case, we will let $OA_0 = \lambda_1 OA_2$, $OA_1 = \lambda_2 OA_2$, $OB_0 = \mu_1 OB_2$, $OB_1 = \mu_2 OB_2$, $OC_0 = \xi_1 OC_2$, $OC_1 = \xi_2 OC_2$, where λ_i, μ_i and ξ_i are all constants that determine the degree of stretch along their respective directions.

When OA_2, OB_2 and OC_2 are perpendicular to each other, an octahedral cloak is formed. Letting $\lambda_1 = \mu_1 = \xi_1 = 0.05$, and $\lambda_2 = \mu_2 = \xi_2 = 0.5$. The outline of the cloak is shown in Figure 6.6. The cloaked space is mapped to a smaller virtual space. The properties of the three parts in one section are

$$\begin{cases} \overline{\overline{\boldsymbol{\rho}}}_1^{pr} = \mathrm{diag}([0.3403 \quad 0.5263 \quad 2.9389]), \kappa_1 = 0.5263 \\ \overline{\overline{\boldsymbol{\rho}}}_2^{pr} = \mathrm{diag}([0.0277 \quad 4.6377 \quad 40.962]), \kappa_2 = 5.2632 \\ \overline{\overline{\boldsymbol{\rho}}}_3^{pr} = \mathrm{diag}([0.1882 \quad 0.5263 \quad 530.33]), \kappa_3 = 52.6316 \end{cases}.$$

The properties are homogeneous and the density tensors are anisotropic in three directions.

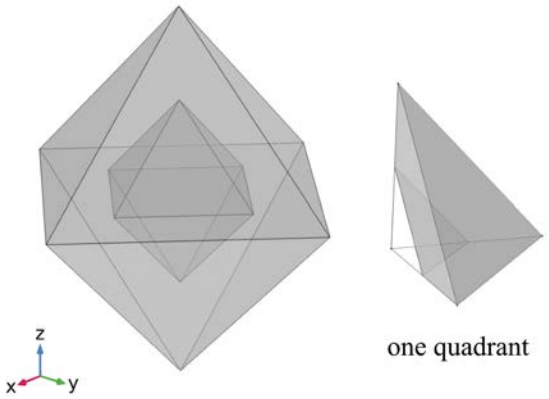

Figure 6.6 An octahedral cloak model

Helmholtz equations for the space containing an obstacle are solved with COMSOL Multiphysics finite element software. The results are shown in Figure 6.7. It can be seen from the numerical simulation that the cloak reduces the effects of the cloaked obstacle. From the outside of the cloak, the wave appears to propagate unimpeded through the homogeneous background medium.

More complicated polyhedral cloaks can also be designed with this method. Given that most 3D cloaks can be approximated as polyhedra, the method applies to a wide range of geometries. For example, a polyhedron is shown in Figure 6.8, which is an approximation of a sphere with $|OA_2|=|OB_2|=|OC_2|$ for every section. Letting $\lambda_1 = \mu_1 = \xi_1 = 0.05$, and $\lambda_2 = \mu_2 = \xi_2 = 0.5$, the properties of each section are calculated.

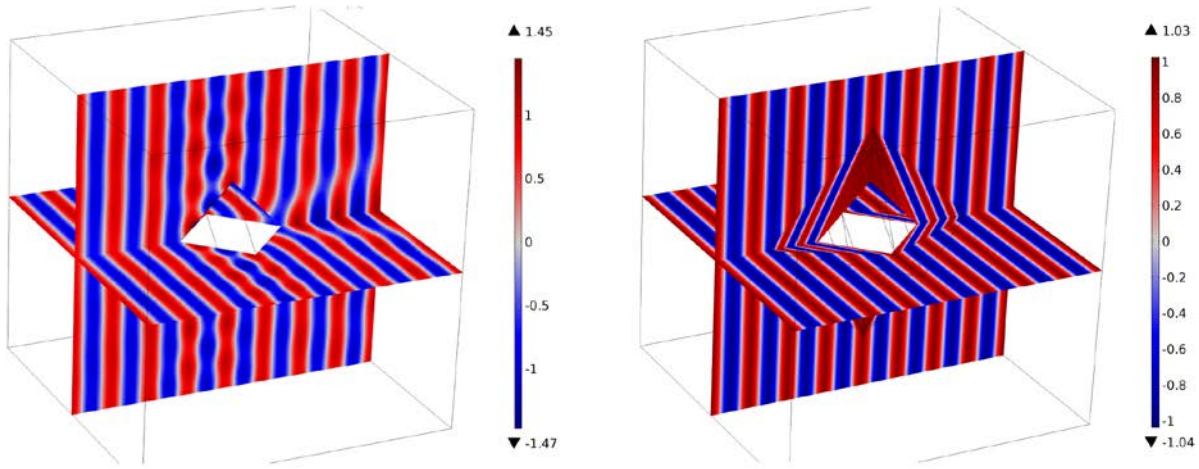

Figure 6.7 Simulation of a space with an obstacle (a) without cloak (b) with the octahedral cloak

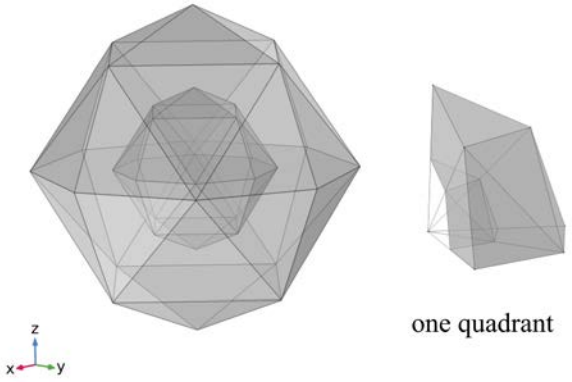

Figure 6.8 A polyhedral cloak model with 32 faces

Helmholtz equations are solved using COMSOL Multiphysics finite element software for a space with a polyhedral obstacle. The cloaking effect is shown in Figure 6.9. It can be seen from the figure that the cloak works well at concealing the cloaked object.

The reduced total RCS of the polyhedral cloak for a space of $6r_m \times 6r_m \times 6r_m$ (r_m is the maximum radius of cloaked space) is shown in Figure 6.10. When r_m/λ is relatively small, that is, at relatively low frequencies, the reduced total RCS is small. When r_m/λ becomes larger, the

reduced total RCS is large. Therefore, the cloak works best at relatively low frequencies. However, the working frequency range can be adjusted by the dimensions of the cloak.

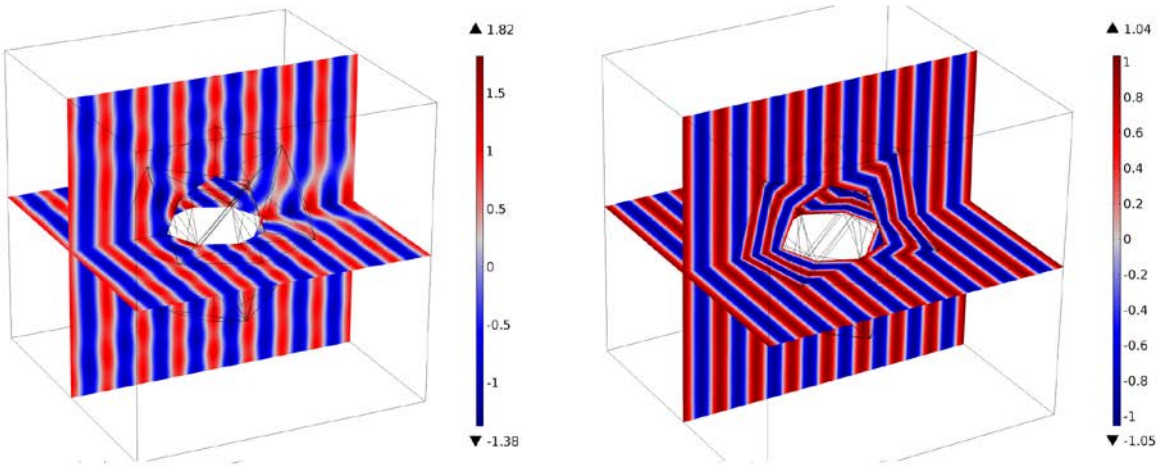

Figure 6.9 Simulation of a space with an obstacle (a) without cloak (b) with the polyhedral cloak

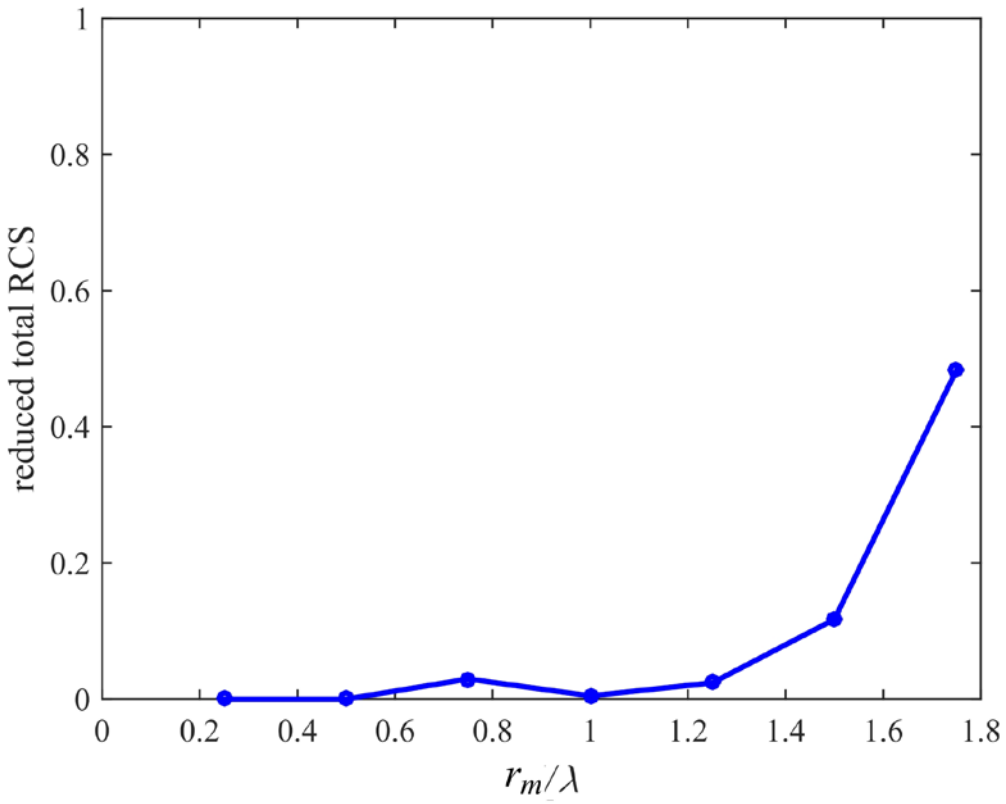

Figure 6.10 Reduced total RCS of the polyhedral cloak

Two examples of cloaks with homogeneous tetrahedral parts were given by dividing into sections. There is a virtually limitless number of ways to divide a 3D cloak into tetrahedra to produce homogenous parts. Smooth boundaries can be approximated by first changing the shape to a polyhedron. Next, the impact of parameters on material properties is analyzed.

6.4 GEOMETRICAL FACTORS THAT AFFECT THE PROPERTIES

The geometries in the transformation acoustics affect the properties. All the factors may affect the properties and they can vary independently. One section from a regular polyhedral cloak is used for analysis, as shown in Figure 6.11. For simplicity, only two factors are analyzed. Since all the points are located on three edges, one can let $OA_0= \lambda_1 OA_2$, $OA_1= \lambda_2 OA_2$, $OB_0= \mu_1 OB_2$, $OB_1= \mu_2 OB_2$, $OC_0= \xi_1 OC_2$, $OC_1= \xi_2 OC_2$, where λ_i, μ_i and ξ_i are all constants. Letting $|OA_2|=|OB_2|=|OC_2|$, $\lambda_2 = \mu_2 = \xi_2 = 0.5$, $\lambda_1 = \mu_1 = \xi_1 = \eta$, and $\angle A_2OB_2=\angle B_2OC_2=\angle C_2OA_2=\theta$, the effects of θ and η are analyzed separately. The effect of θ and η on the properties of the cloak section are shown in Figure 6.12 and Figure 6.13.

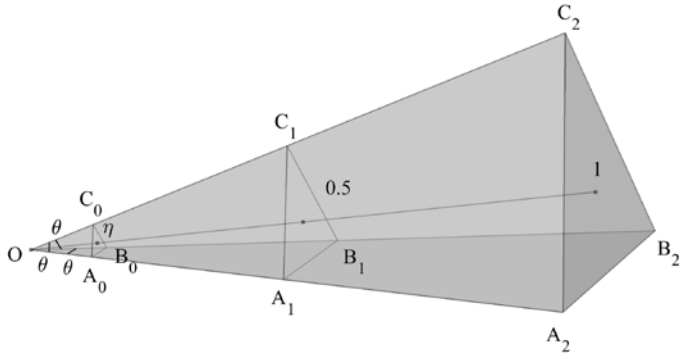

Figure 6.11 A simplified section from a regular polygonal cloak

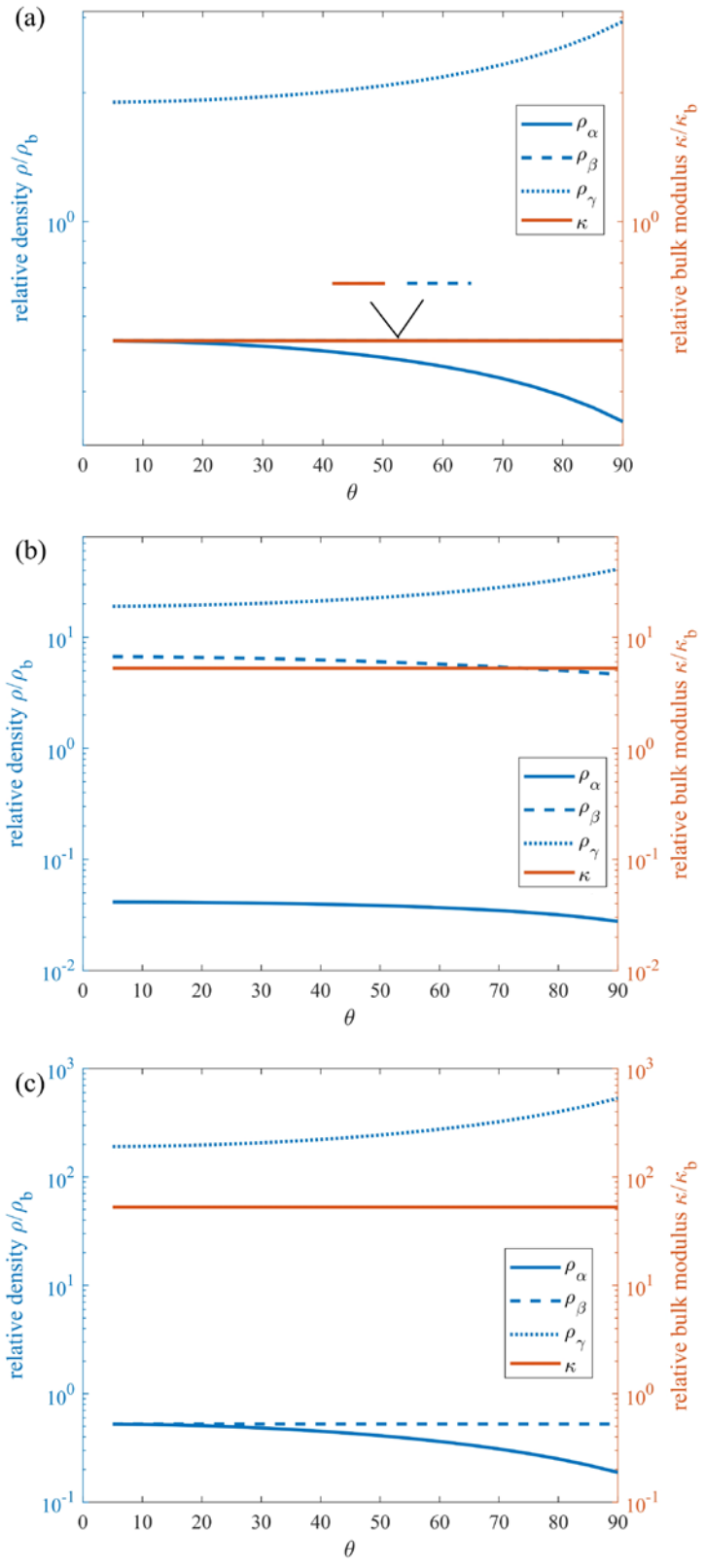

Figure 6.12 Effects of θ on the principal velocities when η=0.05 for (a) Part 1 (b) Part 2 (c) Part 3.

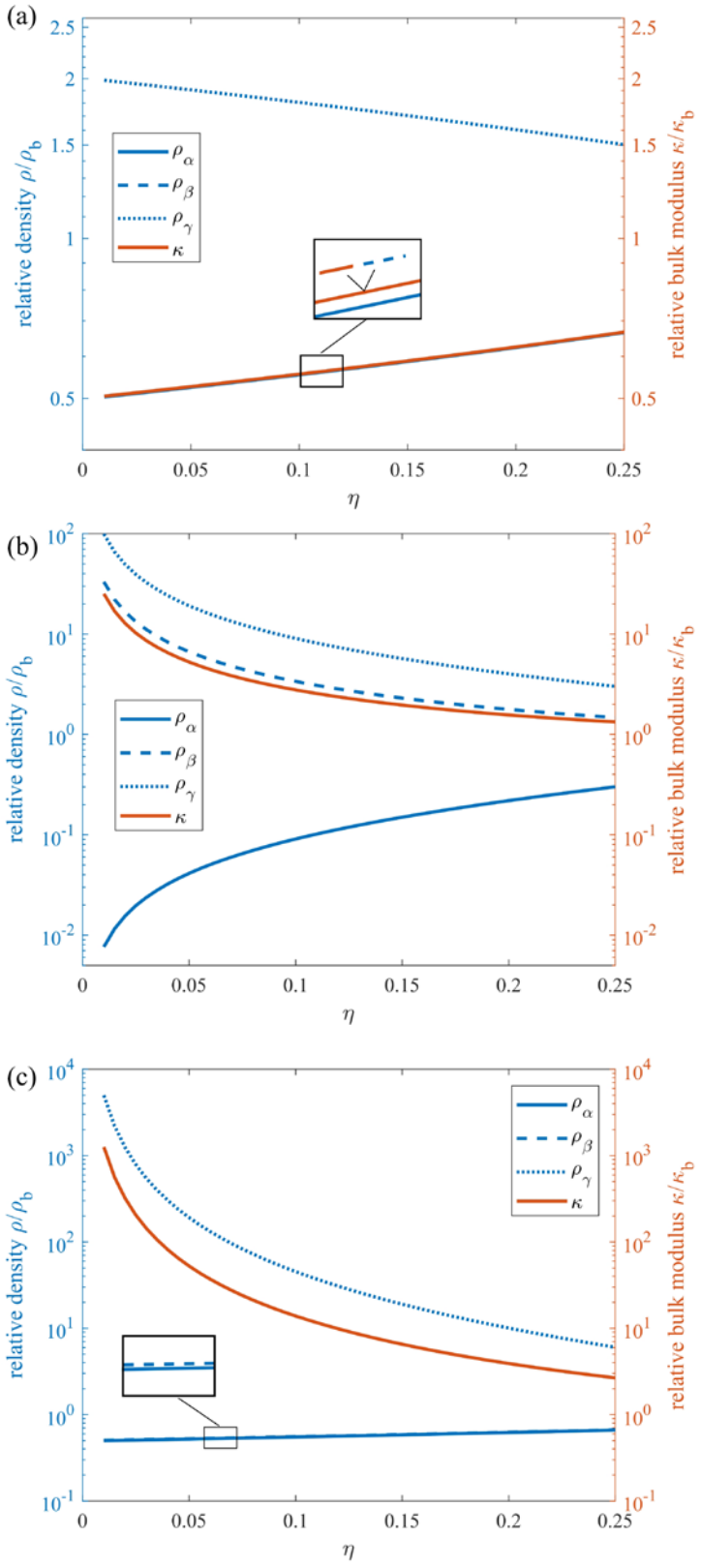

Figure 6.13 Effects of η on the principal velocities when θ=10° for (a) Part 1 (b) Part 2 (c) Part 3

When η=0.05, the principal densities and bulk moduli are given as a function of θ in Figure 6.12. It can be seen from the figures that the deviation of some material properties of each part increases with the increase of θ, while the others are insensitive to θ.

Next, fixing θ=10°, how the principal densities and bulk moduli of each part vary with η, is shown in Figure 6.13. Some properties deviate from those of the background by a few orders of magnitude if η is small. The deviation of all the material properties of each part decreases with the increase of η.

It is observed that both θ and η can be used to tune the principal densities and bulk moduli of each part. Smaller θ and larger η leads to more attainable material properties. Note that η is the size of tetrahedron to which the cloaked space is mapped. An increase of η corresponds to a decrease in cloaking performance, since the scattering cross section in the virtual space is larger. In summary, small θ (<20°) should be used and for η, a balance must be struck between cloaking performance and attainable material properties.

7.0 THREE-DIMENSIONAL PENTAMODE ACOUSTIC CLOAKS COMPOSED OF HEXAGONAL UNIT CELLS

Bimode and pentamode material were first proposed by Milton & Cherkaev (1995). A bimode material is the counterpart of pentamode material in 2D. Norris (2008) presented pentamode cloaks based on pentamode materials. In contrast with inertial acoustic cloaks, pentamode materials possess anisotropic stiffness instead of anisotropic density. 2D bimode cloaks have been designed (Chen, Liu, & Hu, 2015), but 3D pentamode cloaks are more challenging to design.

In the previous studies, face-centered-cubic (FCC) unit cell composed of double-cone structures (DCSs) (see Figure 2.12) were always used for 3D pentamode materials. In order to build a 3D shape that is spherical, a hexagonal unit cell is proposed in this dissertation. Its properties for various parameters are studied, and the unit cells for a spherical pentamode cloak are explored.

7.1 DIVISION OF A SPHERICAL SURFACE

Division of a spherical surface must satisfy Euler's polyhedral formula (Cessna & Bewley, 2009) which states that the number of vertices V, faces F, and edges E in a convex three dimensional polyhedron, satisfy

$$V + F - E = 2 \tag{7.1}$$

For one hexagonal surface in a polyhedron, V=2, F=1, and E=3. However, a polyhedron cannot be composed of just hexagonal surfaces.

This problem was solved by adding 4 triangular faces, 6 square faces, or 12 pentagonal faces embedded within an otherwise honeycomb graph. (Cessna & Bewley, 2009) The polyhedra with 6 square faces are special. One such "spherical" polyhedra is shown in Figure 7.1. Half of the points are made red and the other half black to make the shape easier to view. As such, the red points only connect to neighboring black points and the black points only connect to neighboring red points. The two groups of vertices can be located at different radii, forming layers of the pattern connected together in specific ways to form a hollow sphere made of pentamode materials.

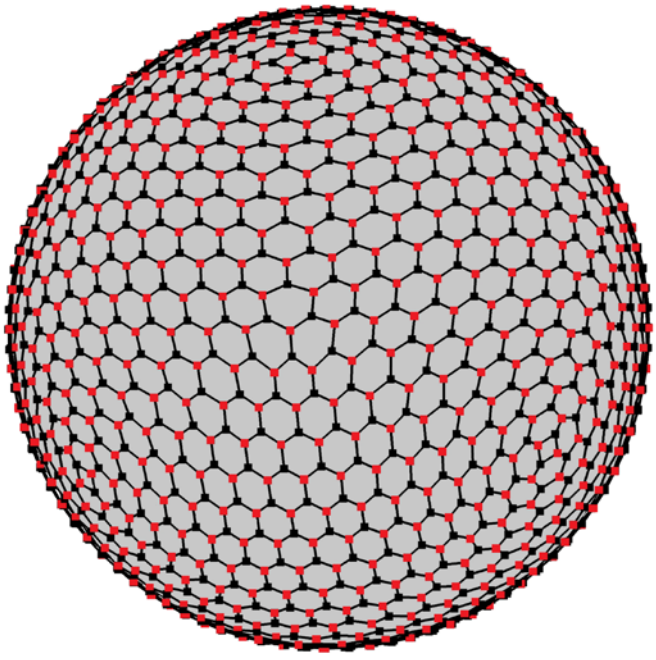

Figure 7.1 A polyhedron with hexagonal surfaces and square faces

7.2 HAXAGONAL PENTAMODE UNIT CELL

Previously studied pentamode unit cells in 3D are FCC unit cells, which cannot form a curved 3D geometry. As discussed in Section 7.1, a spherical surface cannot be divided into hexagonal surfaces. A hexagonal unit cell with double-cone structures is presented for the approximately spherical model shown in Figure 7.1. Its primitive cell is shown in Figure 7.2. The side length of the bottom rhombus is *l*. Note that the Eigen-frequencies of the metamaterial are scalable with the reciprocal of *l*.

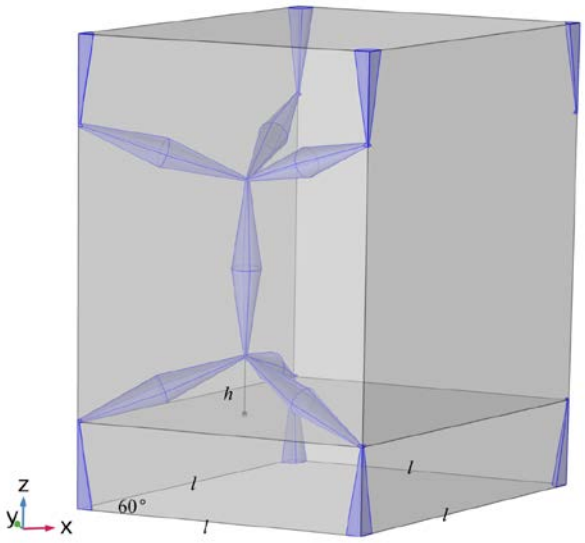

Figure 7.2 Primitive cell of a hexagonal unit cell composed of double-cone structures

There are four arms of DCSs at every connection point. A close up of the DCS from the unit cell is shown in Figure 7.3. The dimension of the thin end, *d*, is not zero to maintain the structural stability. The dimensions of the DCS, *d* and *D*, can be varied to alter the effective material properties of the structure. In this dissertation, the lengths of all the double-cone structures in a particular cell are the same. The length of the double-cone structure changes with

the parameter *h* shown in Figure 7.2. Moving the connection point (e.g. vertically) will affect the structure of the cell, and thus the effective properties.

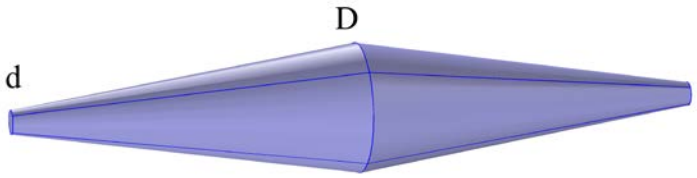

Figure 7.3 Double-cone structure used in designing the pentamode materials

The parameter *h* is found to have a dramatic effect on the effective properties. There is a critical point for *h*, given by

$$h_c = \frac{\sqrt{6}}{12} l \,. \tag{7.2}$$

When $h=h_c$, the connection point is at the center of the regular tetrahedron where the four double-cones connect. When $h>h_c$ or $h<h_c$, anisotropy is introduced. If $h=0$, the three bottom double-cones are on the same plane, and the velocity in the vertical direction is zero. If $h<0$, the structure is auxetic, which is not studied in the dissertation.

The properties of the structures can be derived from the dispersion relations of the first Brillouin zone of the primitive cell, which is shown in Figure 7.4. The first Brillouin zone is a uniquely defined primitive cell in reciprocal space. The irreducible zone is also illustrated in the figure. All the properties of the structure can be derived from the irreducible zone.

The DCSs are made of aluminum with Young's modulus 76GPa, Poisson's ratio 0.3 and density 2700kg/m^3. The space in the unit cell other than the double-cones is a vacuum. The side length of the bottom rhombus is set l=1cm.

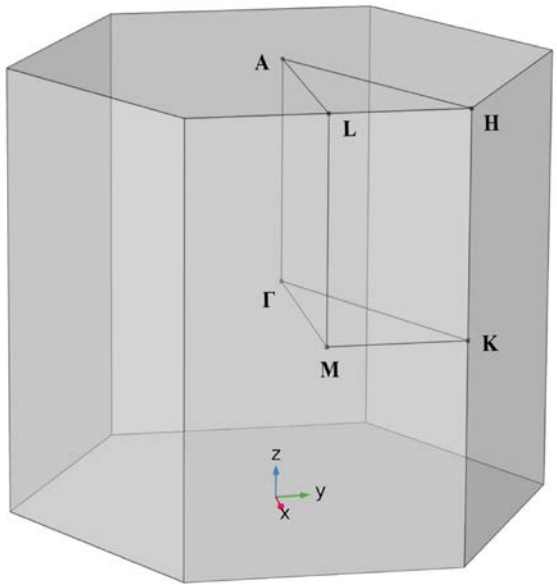

Figure 7.4 Brillouin zone of the hexagonal unit cell

The connection point is the center of the tetrahedron where the four double-cones connect when $h=h_c$. The primitive cell with $h=h_c$ is shown in Figure 7.5. The angles between any two of the double-cone arms connected together are the same. The dimensions of the DCS are d=0.01l and D=0.07l.

The dispersion relations for the Brillouin zone of the primitive cell along the ΓM direction are shown in Figure 7.6. There are three modes starting from the origin. There should be one compressional mode and two shear modes. There are two flexural modes at relatively low frequencies. Shear modes exist as a result of the finite dimension, d. The five modes are shown in Figure 7.7. The black lines show the original cell and the colored shape shows the deformation. Propagation is along the x direction. It is observed that, ⑤ is the compressional mode, ①② are shear modes and ③④ are flexural modes.

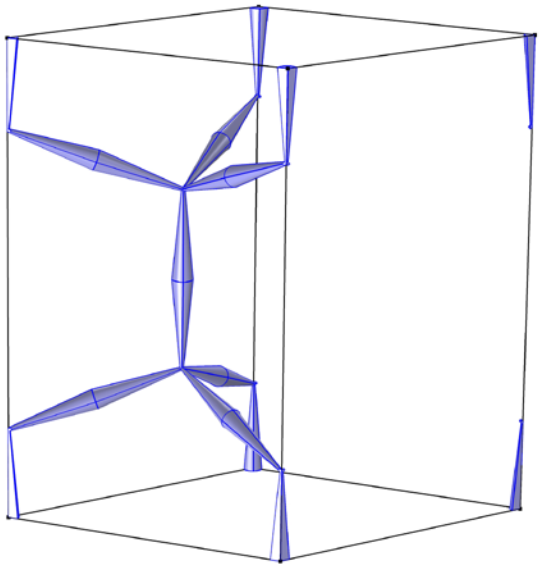

Figure 7.5 Primitive cell composed of double-cone structures when $h=h_c$ (D=0.07l, d=0.01l)

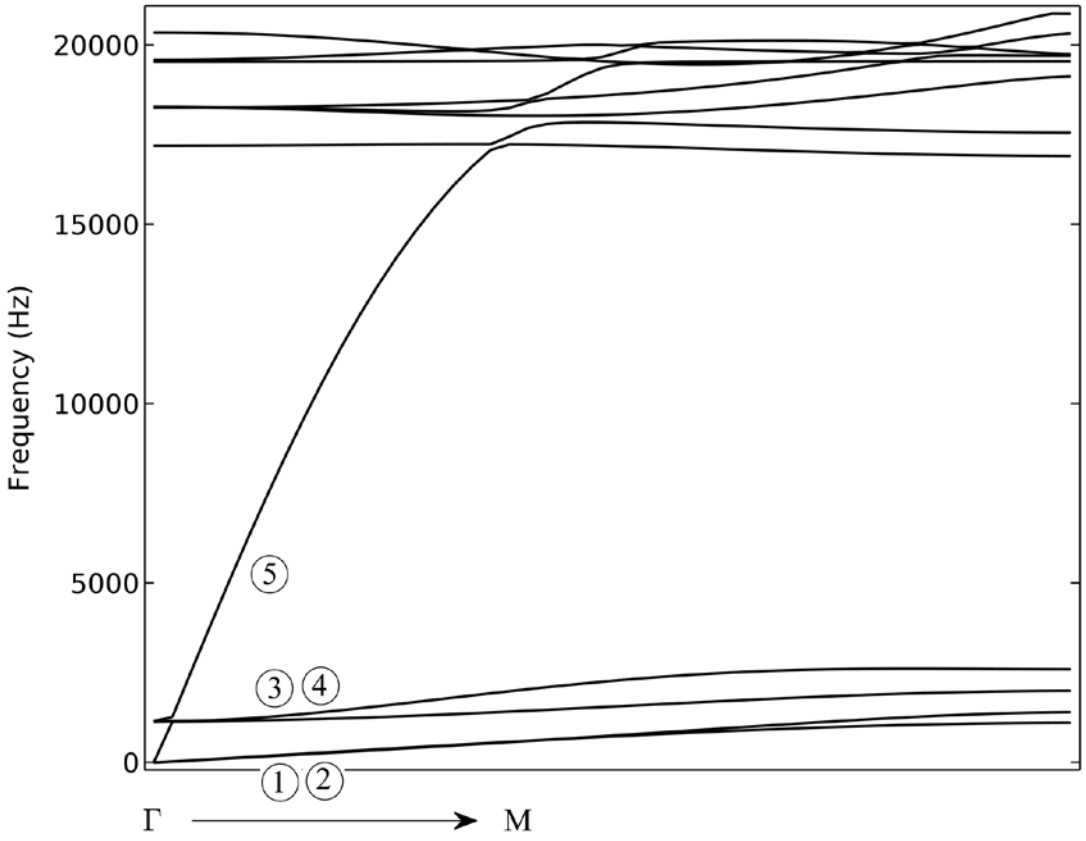

Figure 7.6 Dispersion relations along ΓM direction of the Brillouin zone of the primitive cell

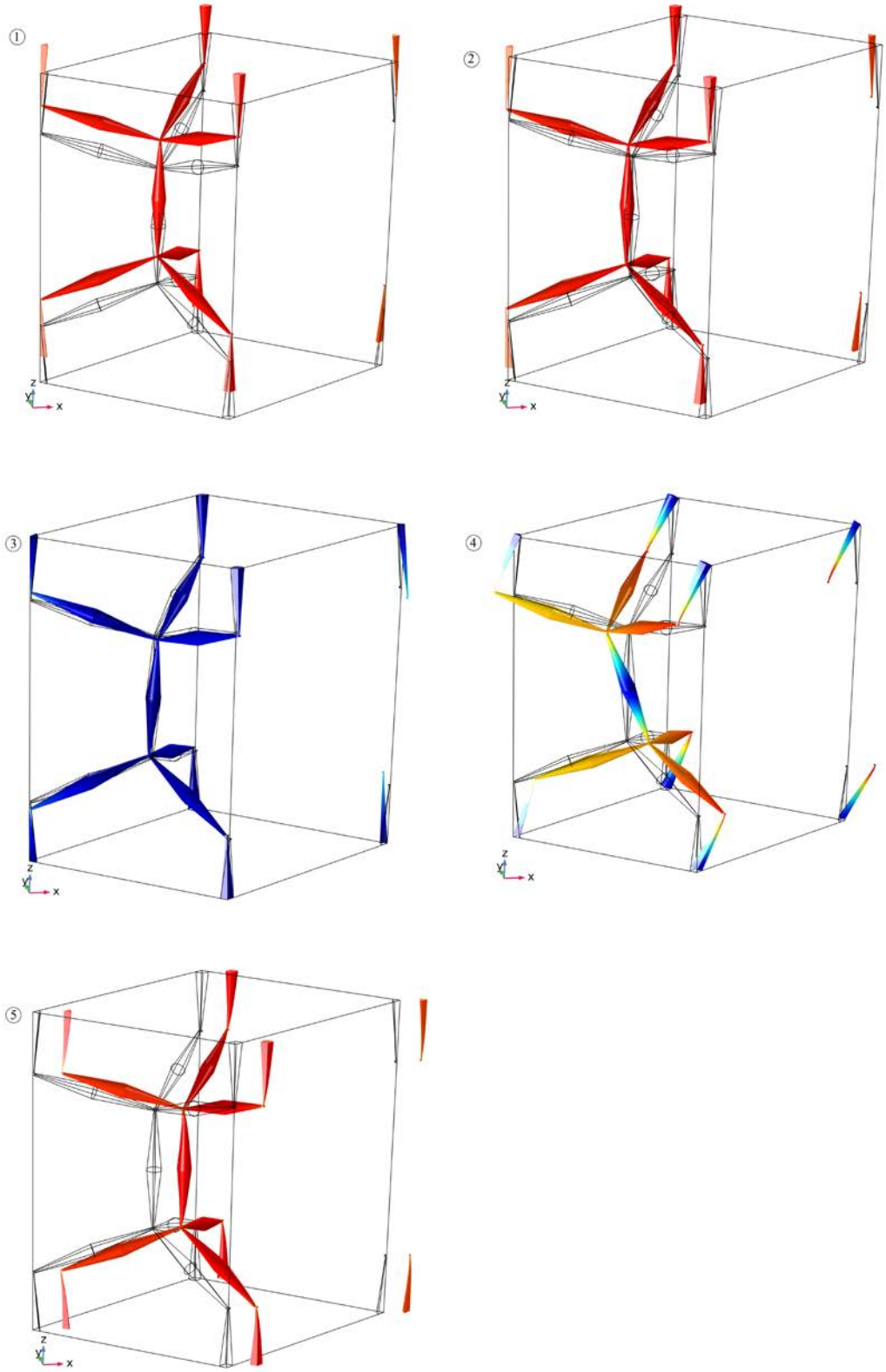

Figure 7.7 The five modes along the ΓM direction (x) at relatively low frequencies

Similarly, the dispersion relations for the Brillouin zone of the primitive cell along ΓA direction are shown in Figure 7.8. There are three modes starting from the origin. As before, there should be one compressional mode and two shear modes. There are two other modes at relatively low frequencies that are flexural modes. The five modes are shown in Figure 7.9. The black lines show the original cell and the colored shape shows the deformation. The propagation is now along *z* direction. Again, ⑤ is observed to be the compressional mode, ①② are shear modes and ③④ are flexural modes.

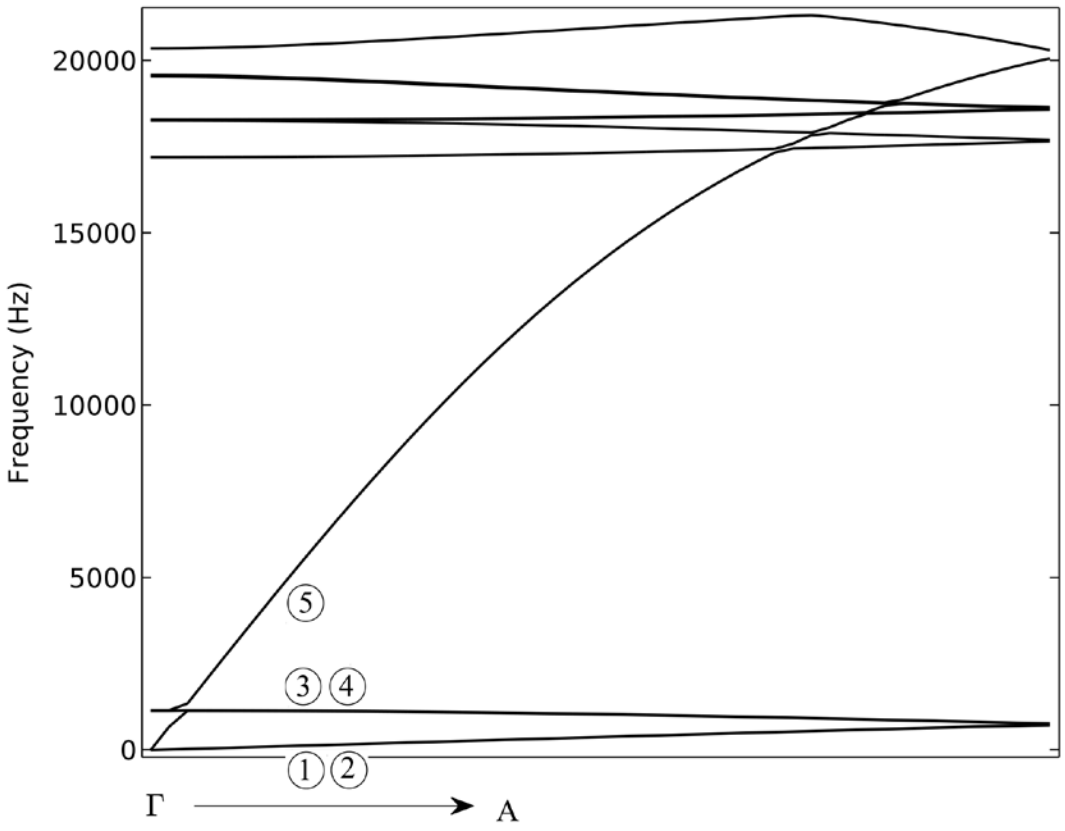

Figure 7.8 Dispersion relations along ΓA direction for the primitive cell

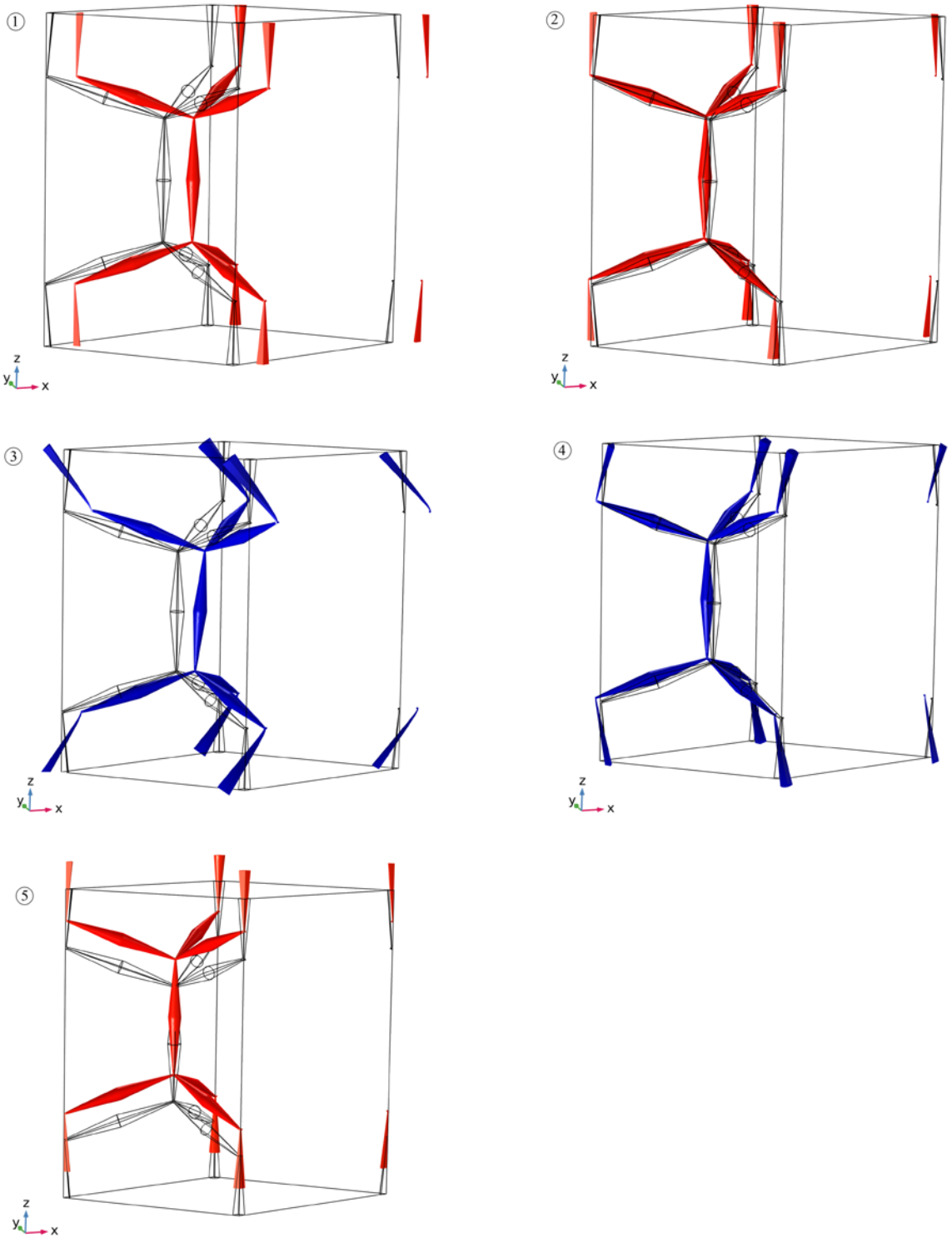

Figure 7.9 The five modes along the ΓA direction (*z*) at relatively low frequencies

The dispersion relations for the Brillouin zone of the primitive cell of Figure 7.5 are calculated with COMSOL Multiphysics finite element software along the edges of the entire irreducible zone. The results are shown in Figure 7.10. The *x*-axis just shows the route, since the scale is not proportional. It can be seen from the figure that there is a frequency band where only the compressional modes exist. Thus, the materials made with this primitive cell are pentamode materials within this frequency band, which is relatively broadband (~3-17 kHz).

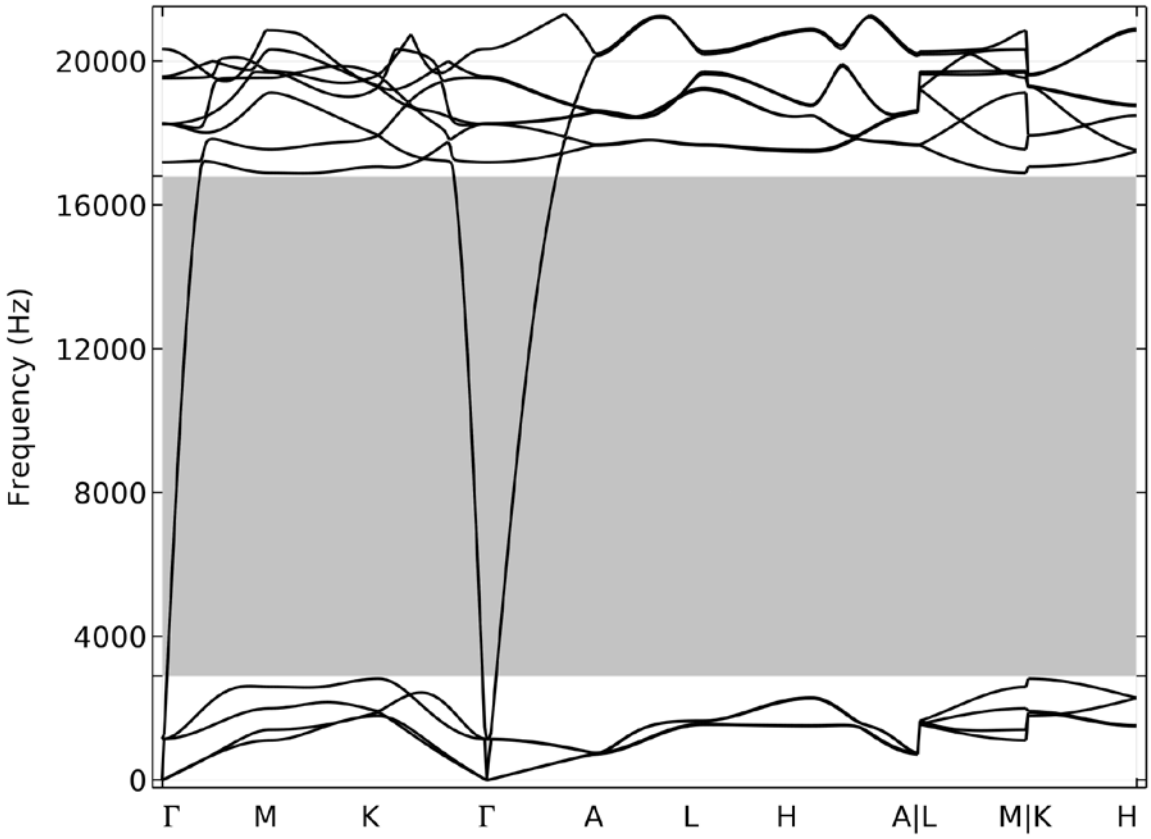

Figure 7.10 Dispersion relations of the primitive cell when $h=h_c$ (D=0.07l, d=0.01l)

7.3 DISPERSION RELATIONS OF THE HEXAGONAL UNIT CELL WITH VARYING GEOMETRIES

The primitive cell of Figure 7.5 is the basic primitive cell. When h is not equal to h_c, the primitive cell becomes taller or shorter. The primitive cell with h=4.16h_c is shown in Figure 7.11. The unit cell is taller than the one with h=h_c.

The dispersion relations for the Brillouin zone of the primitive cell of Figure 7.11 are calculated with COMSOL Multiphysics finite element software along the edges of the entire irreducible zone. The results are shown in Figure 7.12. It can be seen from the figure that there is also a frequency band where only compressional modes exist. Since the structure of the unit cell changes, the pentamode frequency range has changed to roughly 1-6 kHz.

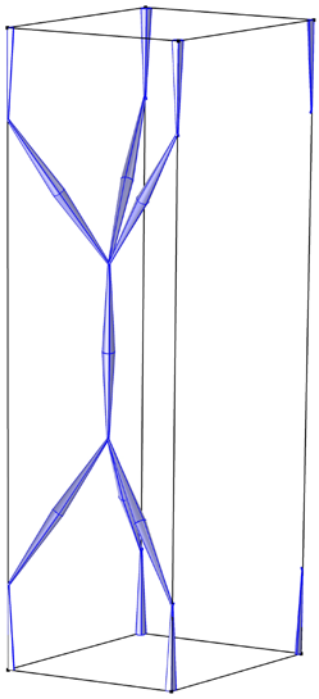

Figure 7.11 Primitive cell composed of double-cone structure when h=4.16h_c (D=0.07l, d=0.01l)

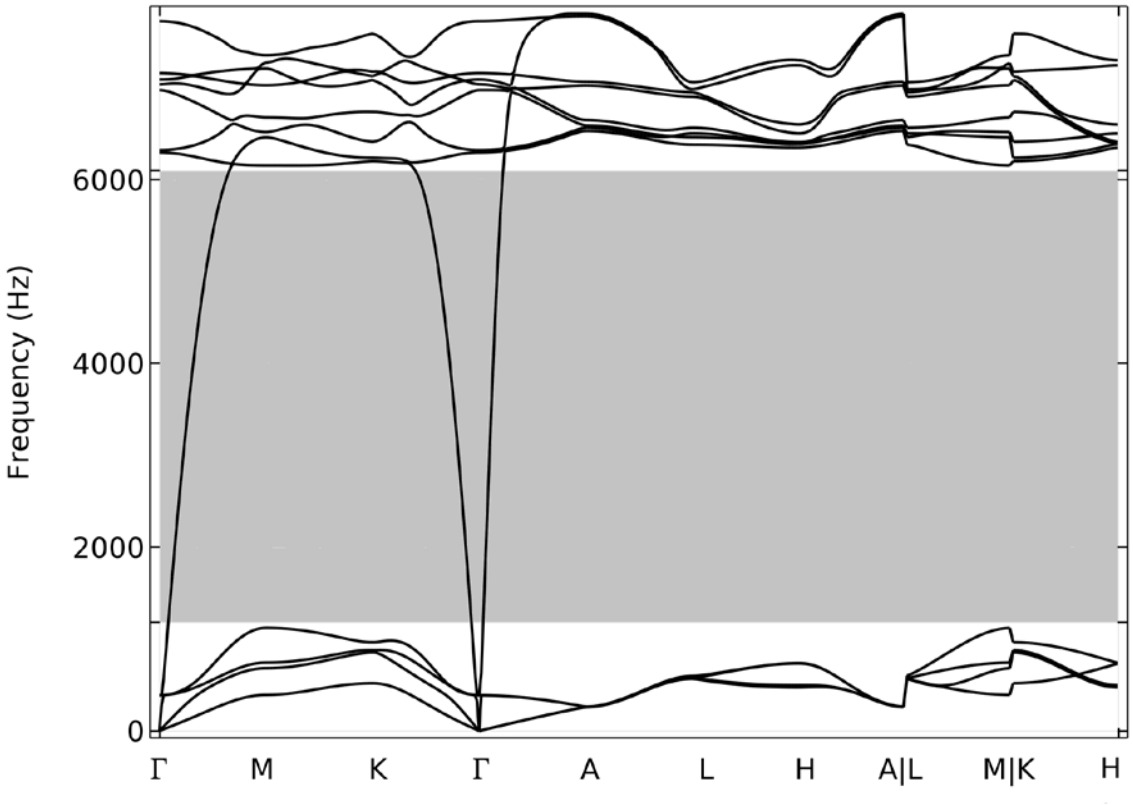

Figure 7.12 Dispersion relations of the primitive cell when h=4.16h_c (D=0.07l, d=0.01l)

When 0<h<h_c, it is different. The primitive cell with h=0.372h_c is shown in Figure 7.13. The unit cell is shorter than the one with h=h_c.

The dispersion relations for the Brillouin zone of the primitive cell of Figure 7.13 are calculated with COMSOL Multiphysics finite element software along the edges of the irreducible zone. The results are shown in Figure 7.14. It can be seen from the figure that there is also a frequency band where only compressional waves exist. Since the structure of the unit cell changes, the frequency range changes to roughly 3.5-15 kHz.

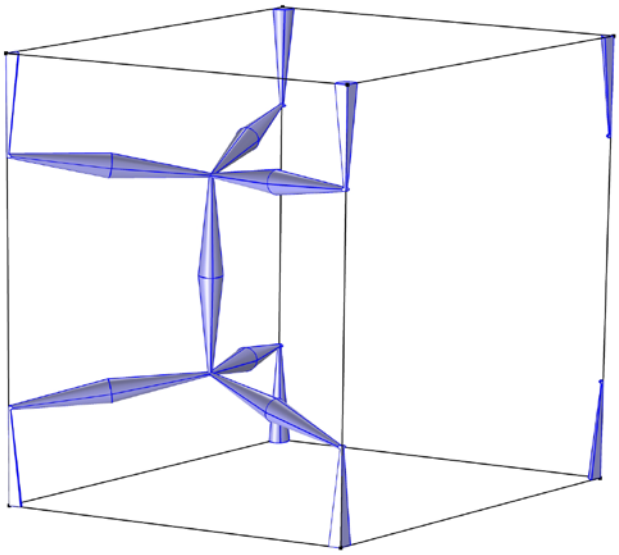

Figure 7.13 Primitive cell composed of double-cone structure when h=0.372h_c (D=0.07l, d=0.01l)

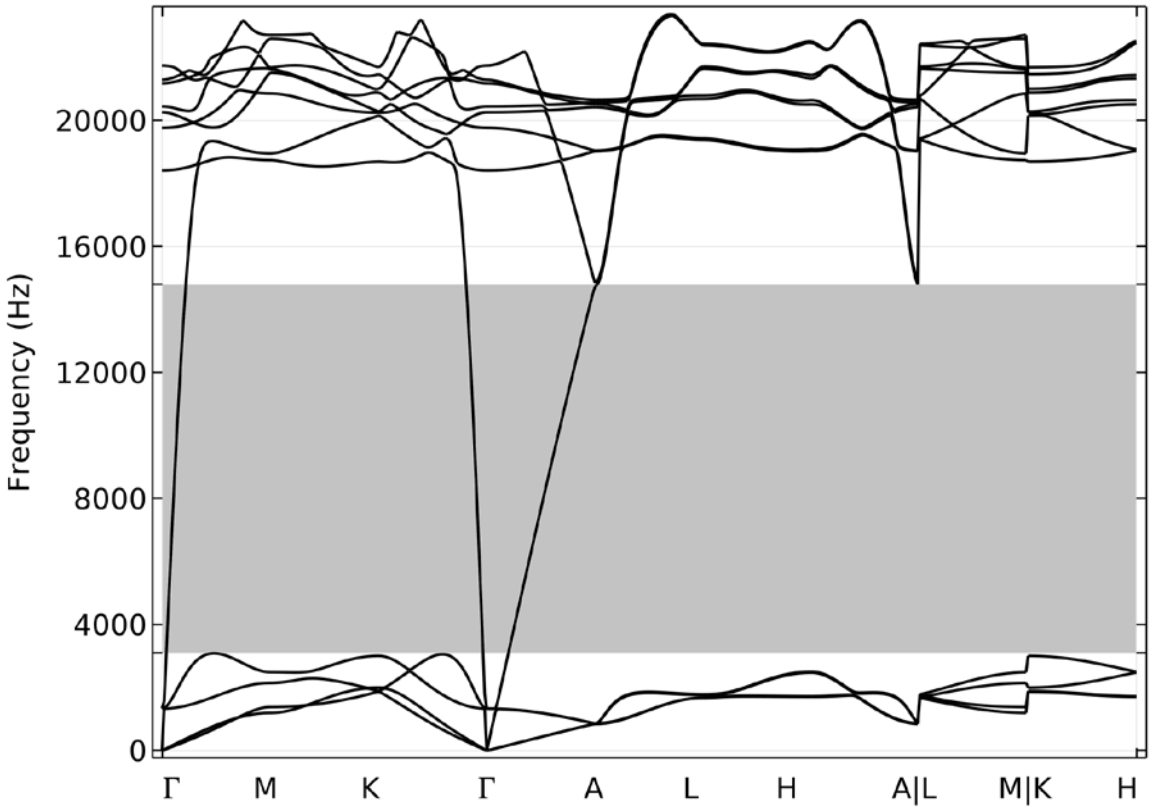

Figure 7.14 Dispersion relations of the primitive cell when h=0.372h_c (D=0.07l, d=0.01l)

The case when h=0 is special, as the primitive cell in Figure 7.15 shows. The three double-cones that connect to the vertical double cone are on a plane.

The dispersion relations for the Brillouin zone of the primitive cell of Figure 7.15 are calculated with COMSOL Multiphysics finite element software along all the edges of the irreducible zone. The results are shown in Figure 7.16. No frequency band with pure compressional modes exists, meaning that the material is not pentamode.

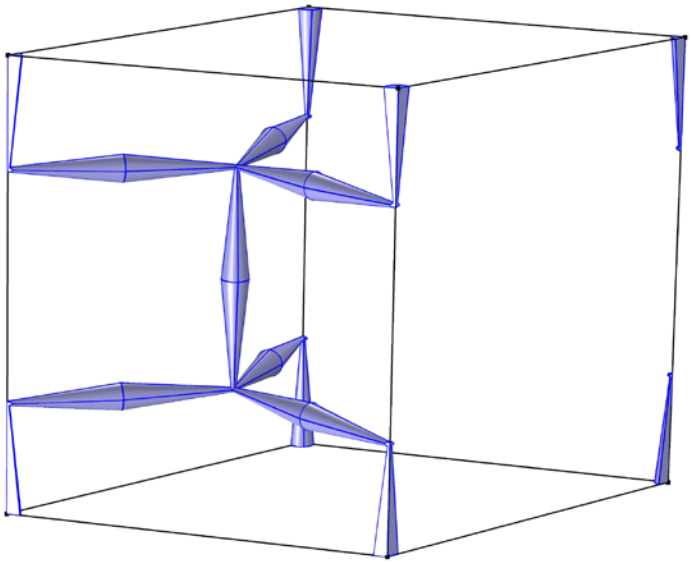

Figure 7.15 Primitive cell composed of double-cone structure when h=0 (D=0.07l, d=0.01l)

Besides the parameter h, the dimensions of the double-cones also affect the frequency band of pentamode materials. The dispersion relations for a larger D and d when h=h_c are shown in Figure 7.17 and Figure 7.18. Different characteristics result even though h=h_c for all the cases.

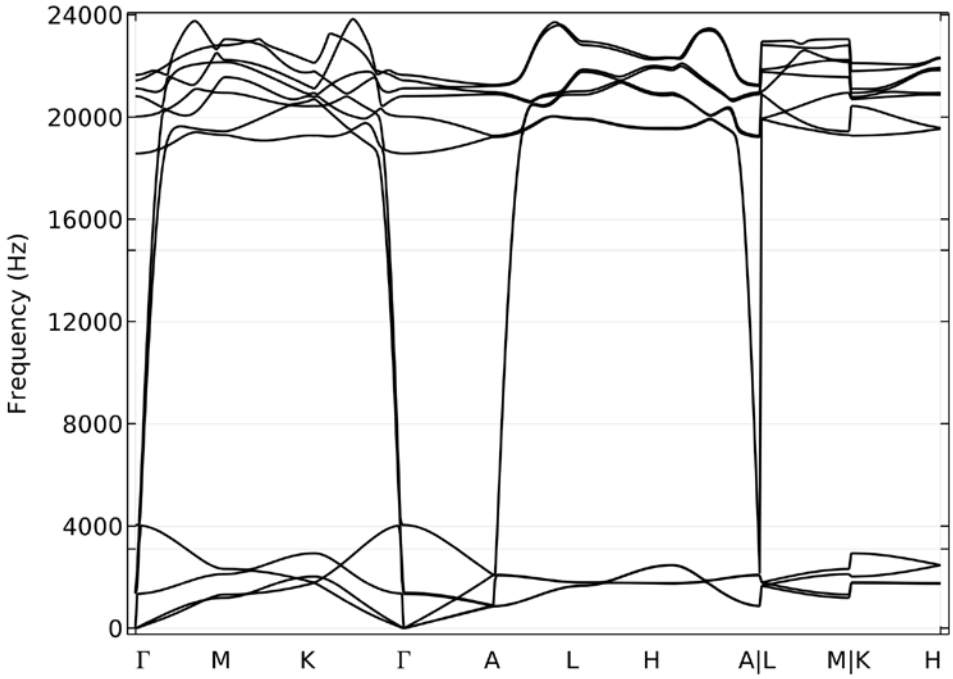

Figure 7.16 Dispersion relations of the primitive cell when h=0 (D=0.07l, d=0.01l)

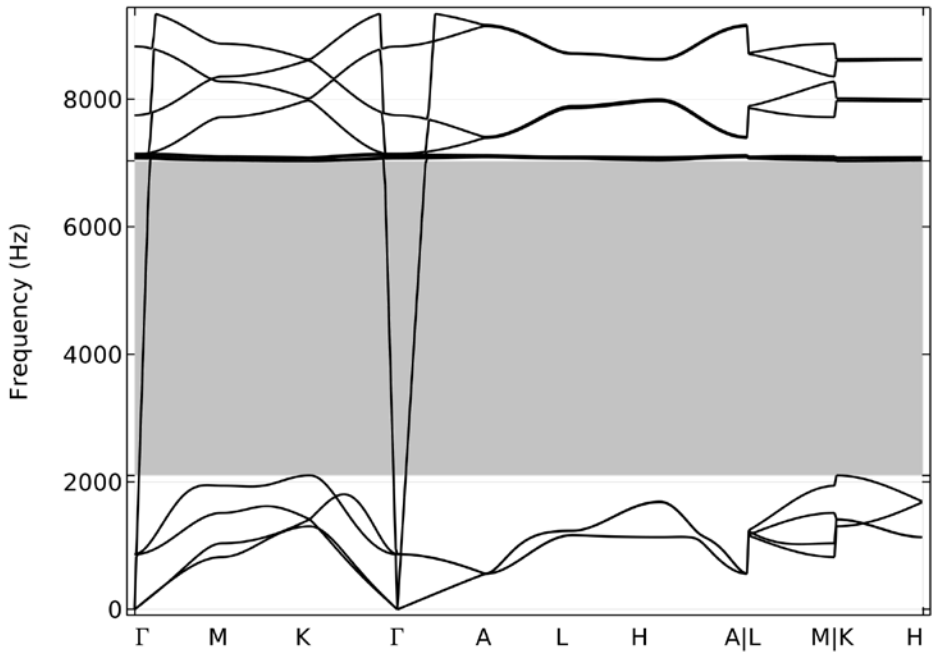

Figure 7.17 Dispersion relations of the primitive cell when D=0.2l (h=h_c, d=0.01l)

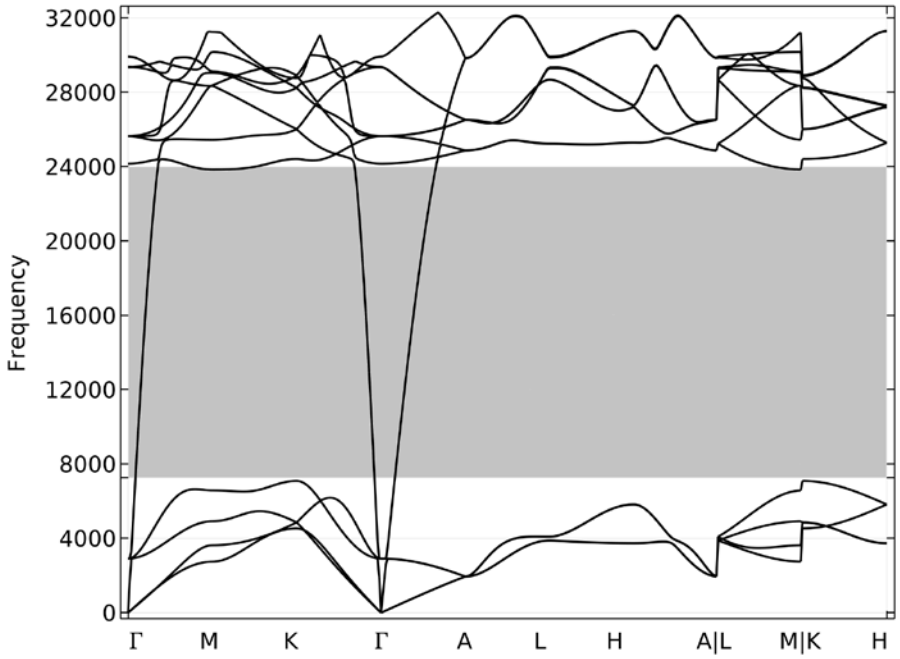

Figure 7.18 Dispersion relations of the primitive cell when d=0.02l (h=h_c, D=0.07l)

For most hexagonal unit cells, there are frequency band gaps for shear modes where only compressional modes exist. The structures are pentamode materials at these frequency bands. The dimensions of the unit cell affect the pentamode frequency ranges and can be used to tailor the material to a particular frequency band.

7.4 VARIATION OF THE PROPERTIES ON THE GEOMETRIC PARAMETERS OF THE DOUBLE-CONE STRUCTURE

The angles between any two double-cones of the four connected together are the same when h=h_c. If all the double-cones are the same, the properties are supposed to be isotropic.

The dispersion branches of the primitive cell in Figure 7.5 along *x*- and *z*- directions are calculated with COMSOL Multiphysics finite element software. The result is shown in Figure 7.19. At relatively low frequencies, the phase velocity ($v_p=\omega/k$) and group velocity ($v_g=d\omega/dk$) are equal (no dispersion). The velocities of the compressional waves along the two directions (the slopes of the two diagonal lines centered about a wavenumber of zero) are calculated to be the same.

The velocities along all the directions in the *xy*-plane are shown in Figure 7.20. The velocity of compressional wave is constant with θ, the angle in the *xy* plane. The velocities along all the directions in the *xz*-plane are shown in Figure 7.21. The velocity of the compressional wave is also constant with ϕ, the angle in the *xz* plane. Therefore, the velocity of the cell is isotropic when $h=h_c$.

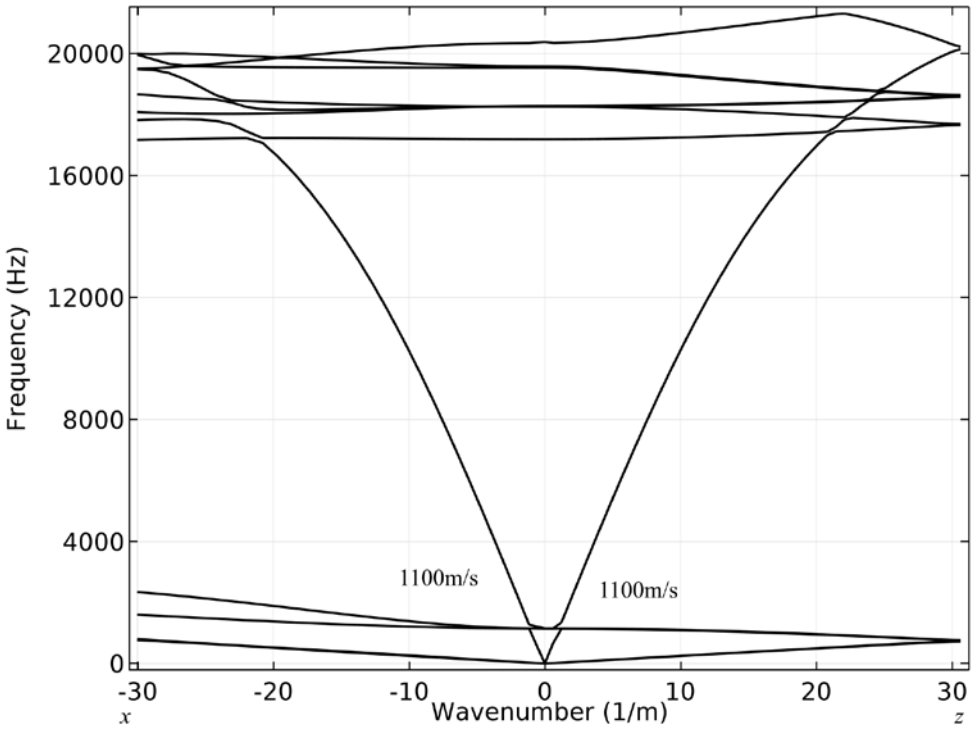

Figure 7.19 Dispersion branches along *x* and *z* directions when $h=h_c$ (D=0.07l, d=0.01l)

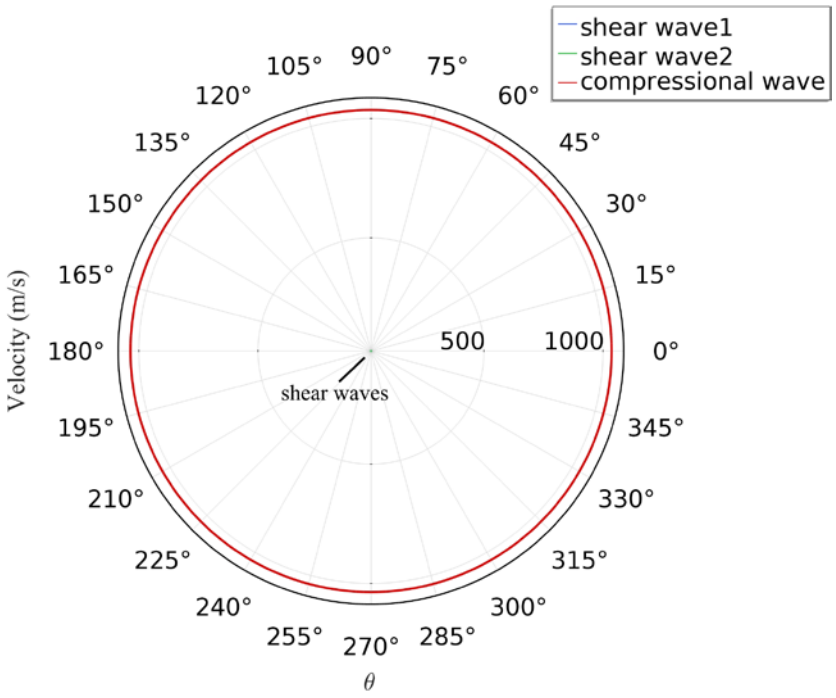

Figure 7.20 Velocities with θ in xy plane when $h=h_c$ (D=0.07l, d=0.01l)

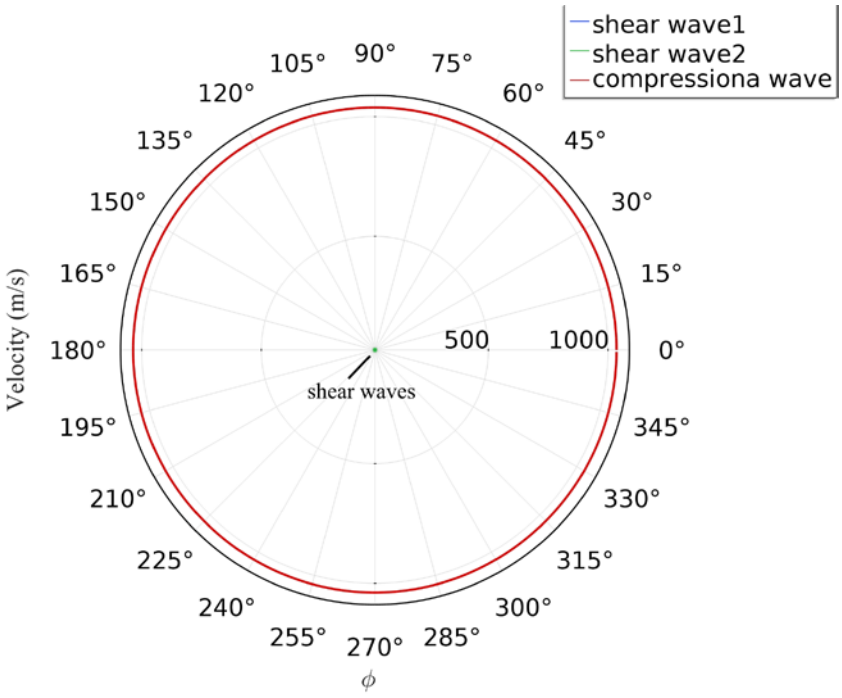

Figure 7.21 Velocities with ϕ in xz plane when $h=h_c$ (D=0.07l, d=0.01l)

The structure of the double-cone is shown in Figure 7.3. It is discussed that the parameter of the DCS (*d* and *D*) affects the dispersion relations of the primitive cell. As will be shown, they also affect the effective velocities of the cell.

The variation of the velocities of the cell with *d* is shown in Figure 7.22. The velocity of the cell is isotropic. The compressional wave velocities of the cell increase with the diameter of the thin-end when the diameter of the thick-end is held D=0.07l, so as the shear wave velocities. This intuitively makes sense, because the structure is becoming stiffer.

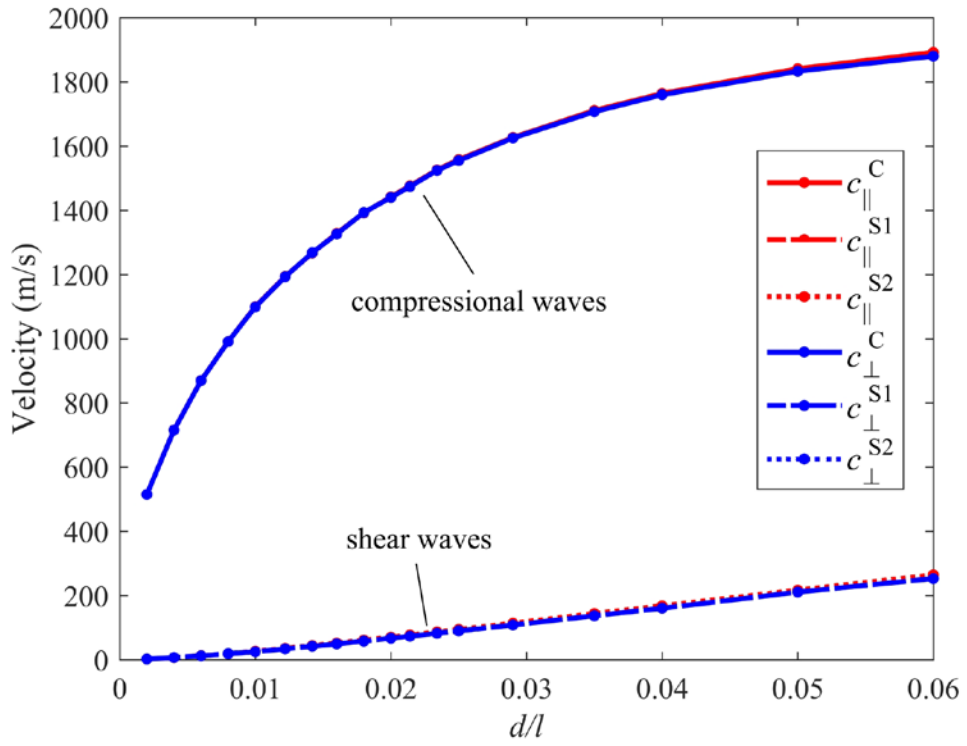

Figure 7.22 The effect of the thin-end radius of the double-cone structure on the properties (h=h_c, D=0.07l)

The variation of the velocities of the cell with the diameter of the thick-end is shown in Figure 7.23. The velocity of the cell is isotropic. The compressional wave velocities of the cell decrease with the diameter of the thick-end when the diameter of the thin-end is held d=0.01l,

while the shear wave velocities change little. A drop in sound speed is expected because of the gain in mass with higher D.

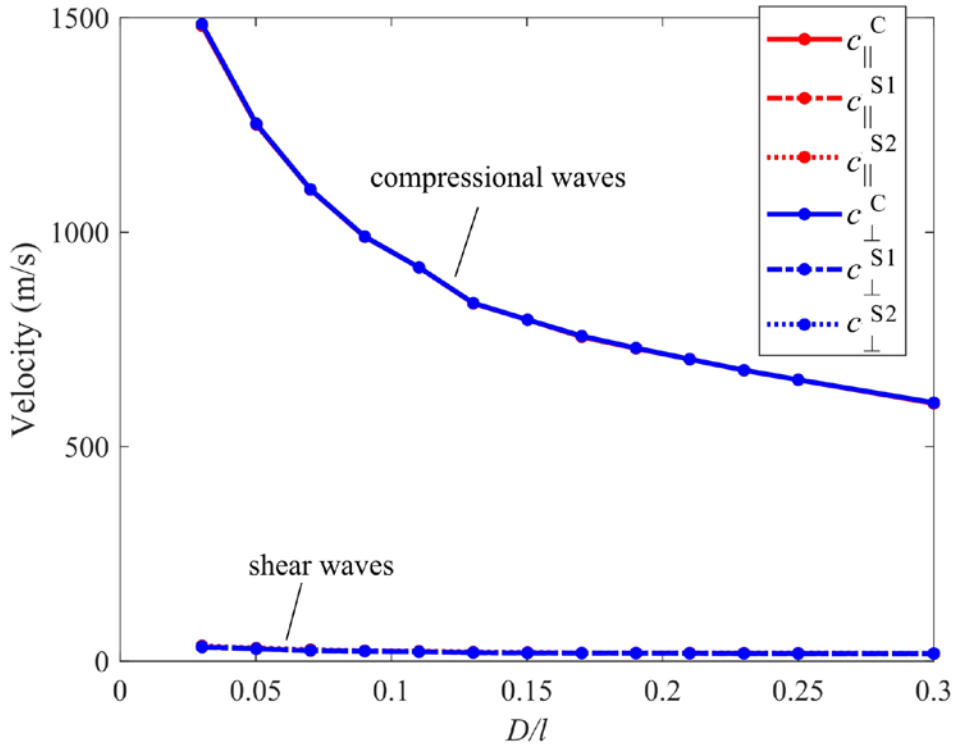

Figure 7.23 The effect of the middle radius of the double-cone structure on the properties ($h=h_c$, $d=0.01l$)

The aforementioned analysis is for the unit cell with $h=h_c$. The velocity is isotropic. It is anisotropic when $h\neq h_c$. The effects of anisotropy will be studied in the next chapter. When $h\neq h_c$, the same trends are observed with the change of the diameters of the thin-end and the thick-end.

7.5 WAYS TO INTRODUCE ANISOTROPY INTO HEXAGONAL CELLS

When $h\neq h_c$, anisotropy is introduced. Either larger or smaller h leads to anisotropic velocities. The taller primitive cell with $k=4.16k_c$ was shown in Figure 7.11. The dispersion branches of the

primitive cell along *x*- and *z*- directions are calculated with COMSOL Multiphysics finite element software. The result is shown in Figure 7.24. The velocities of sound along the two directions are quite different, as evidenced by the slopes of the compressional waves. The velocity in the *z* direction (2,370 m/s) is almost an order of magnitude larger than that in the *x* direction (250 m/s).

The velocities along all the directions in the *xy*-plane are shown in Figure 7.25. The velocity of compressional wave is constant with θ. Thus, the velocity is isotropic in the *xy*-plane. The velocities along all the directions in the *xz*-plane are shown in Figure 7.26. The velocity of compressional wave changes dramatically with ϕ. Therefore, when $h>h_c$, the velocity of the cell is anisotropic and $v_z>v_x$.

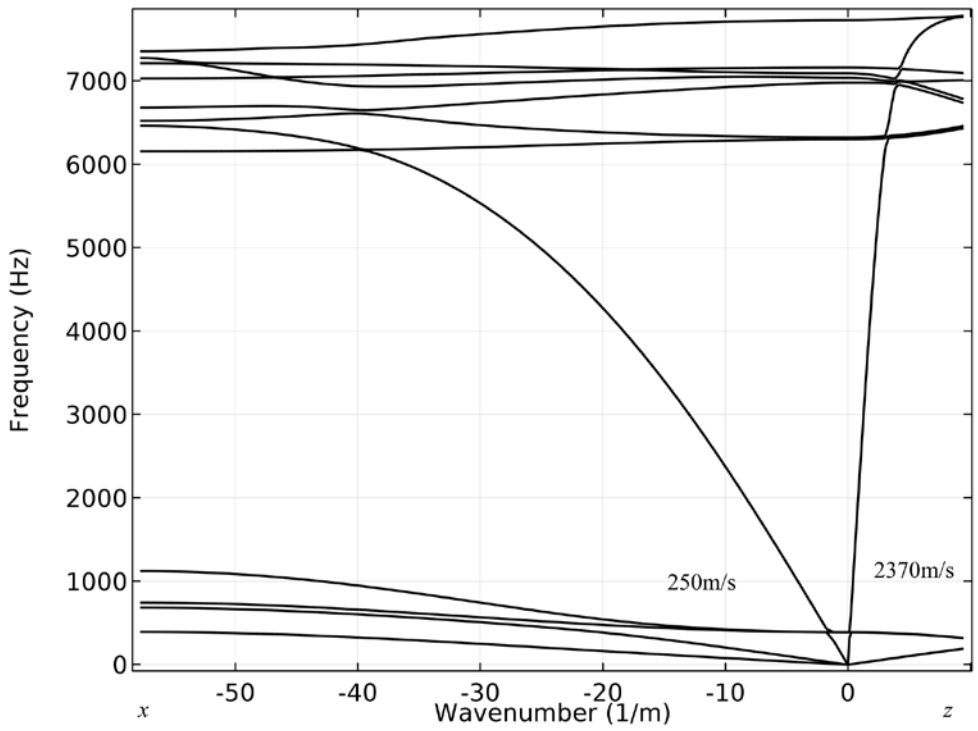

Figure 7.24 Dispersion branches along *x* and *z* directions when $h=4.16h_c$ ($D=0.07l$, $d=0.01l$)

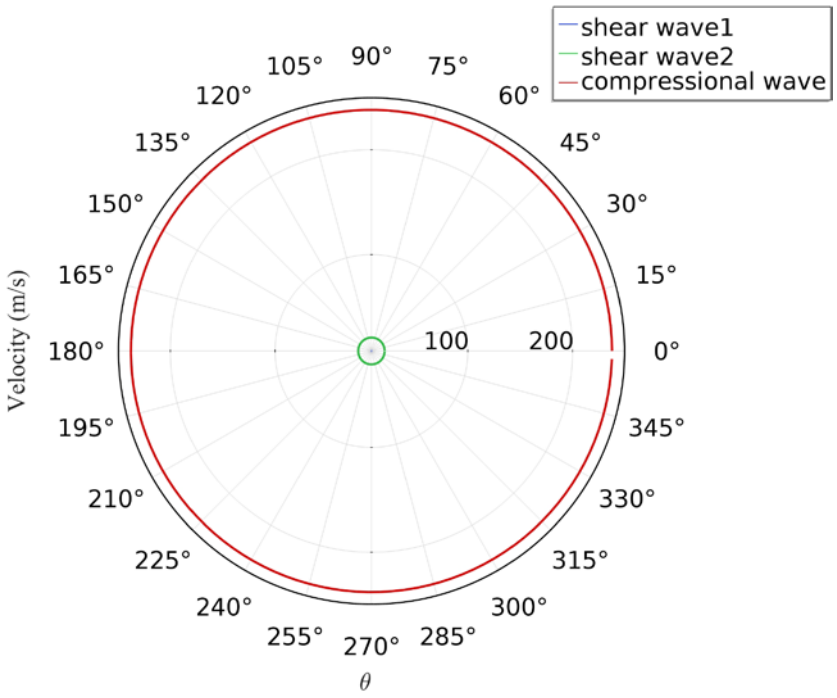

Figure 7.25 The velocities along the direction of θ when h=4.16h_c (D=0.07l, d=0.01l)

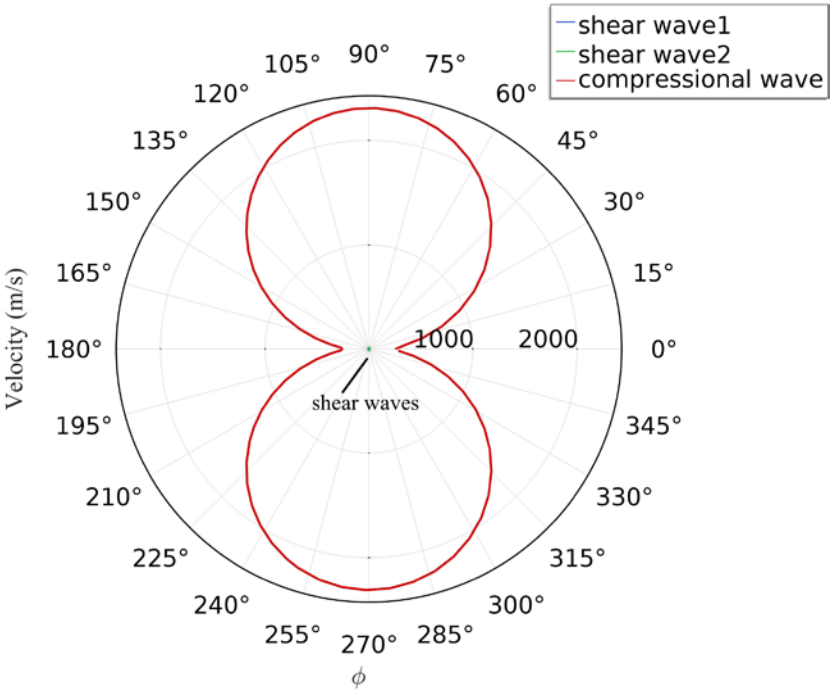

Figure 7.26 The velocities along the direction of ϕ when h=4.16h_c (D=0.07l, d=0.01l)

The shorter primitive cell with h=0.372h_c is shown in Figure 7.13. The dispersion branches of this primitive cell with h=0.372h_c along x- and z- directions are calculated with COMSOL Multiphysics finite element software. The result is shown in Figure 7.27. The velocities along the two directions are different, as expected. The velocity in the x direction (1,350 m/s) is much larger than that in the z direction (410 m/s).

The velocities along all the direction in the xy-plane are shown in Figure 7.28. The velocity of the compressional wave is constant with θ, and thus, the velocity is isotropic in the xy-plane. The velocities along all the directions in the xz-plane are shown in Figure 7.29. The velocity of the compressional wave changes dramatically with ϕ. Therefore, when $0<h<h_c$, the velocity of the cell is anisotropic and $v_z<v_x$.

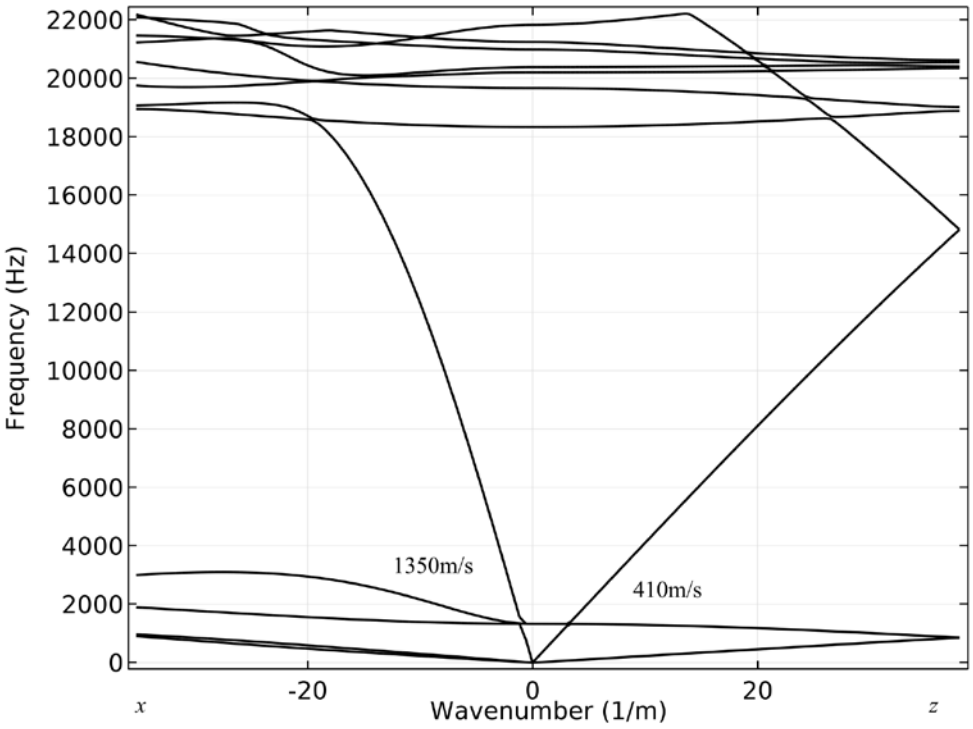

Figure 7.27 Dispersion branches in x and z directions h=0.372h_c (D=0.07l, d=0.01l)

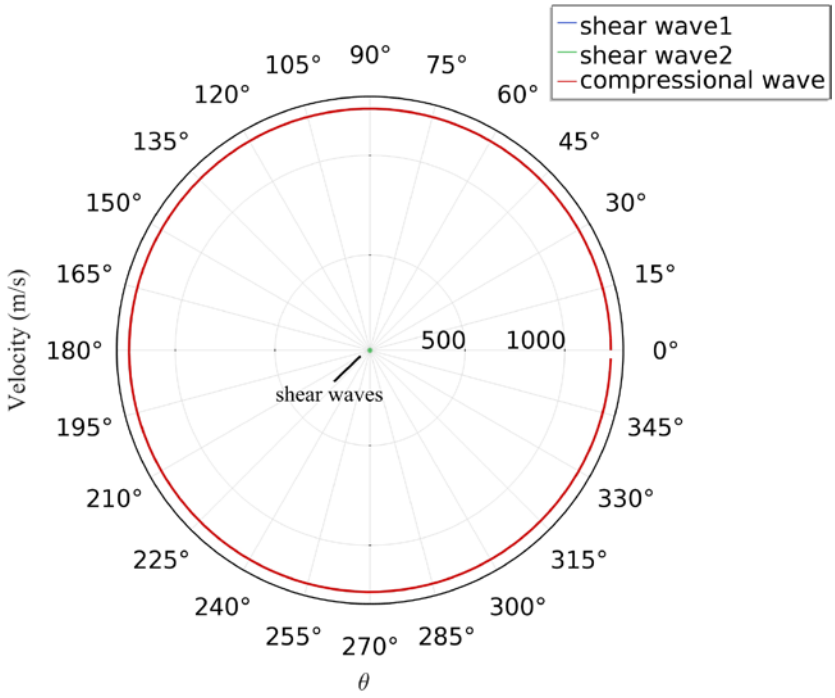

Figure 7.28 The velocities along the direction of θ when h=0.372h_c (D=0.07l, d=0.01l)

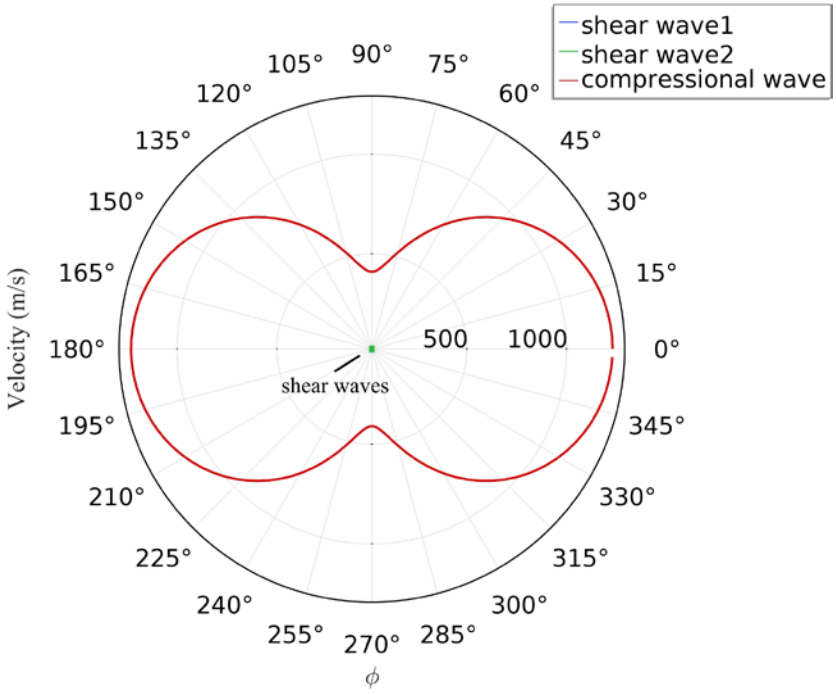

Figure 7.29 The velocities along the direction of ϕ when h=0.372h_c (D=0.07l, d=0.01l)

The compressional wave velocity is isotropic in the *xy*-plane for all the three cells. Since the parameter *h* shows the movement of the connection point in the vertical direction, the three non-vertical double-cones out of the four connected at one point are equivalent. It is reasonable that the velocity is isotropic in the *xy*-plane. Therefore, the two directions (|| and⊥) can be used to characterize the velocities of the cells.

The compressional wave velocities in the two directions vary with *h*, as shown in Figure 7.30. The compressional wave velocity in the horizontal direction decreases with the increase of *h*, while the compressional wave velocity in the vertical direction increases with the increase of *h*. The two velocities agree when $h=h_c$. As analyzed previously, the structure is isotropic when $h=h_c$. When $0<h<h_c$, the velocity in the horizontal direction is larger and When $h>h_c$, the velocity in vertical direction is larger.

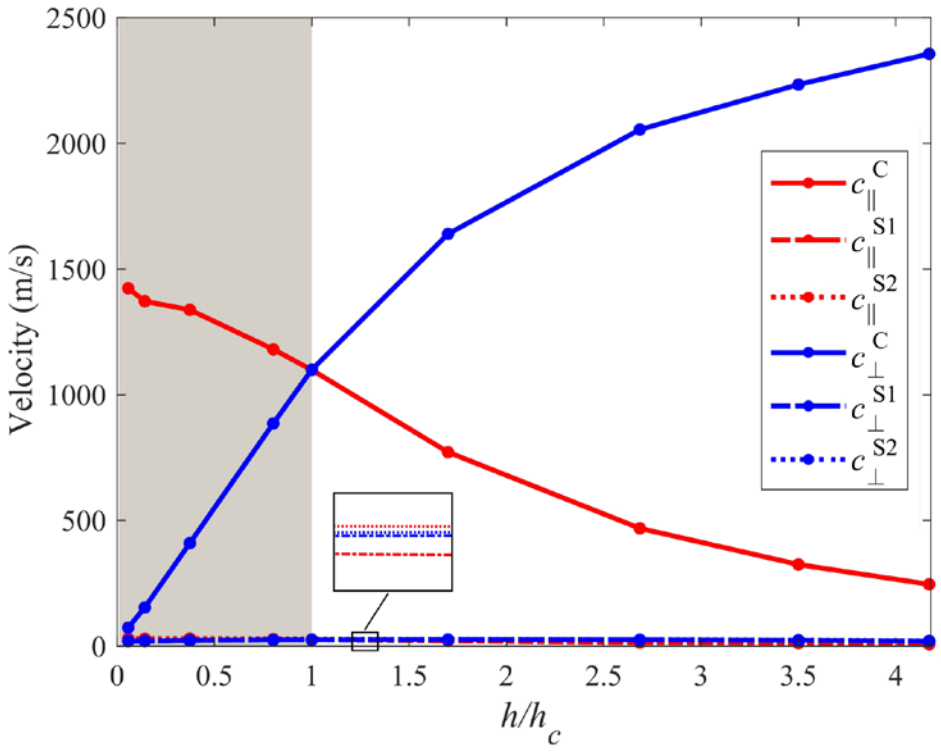

Figure 7.30 The variation of compressional velocities with *h* (*D*=0.07*l*, *d*=0.01*l*)

Another way to realize anisotropy is to change the uniformity of the double-cones used to construct the primitive cell. If a different velocity in the *z* direction from the *xy*-plane is required, the dimensions of the double-cone in the vertical direction are critical. The primitive cell with different double-cones is shown in Figure 7.31. The diameters of the double-cones in the vertical direction are different from the others.

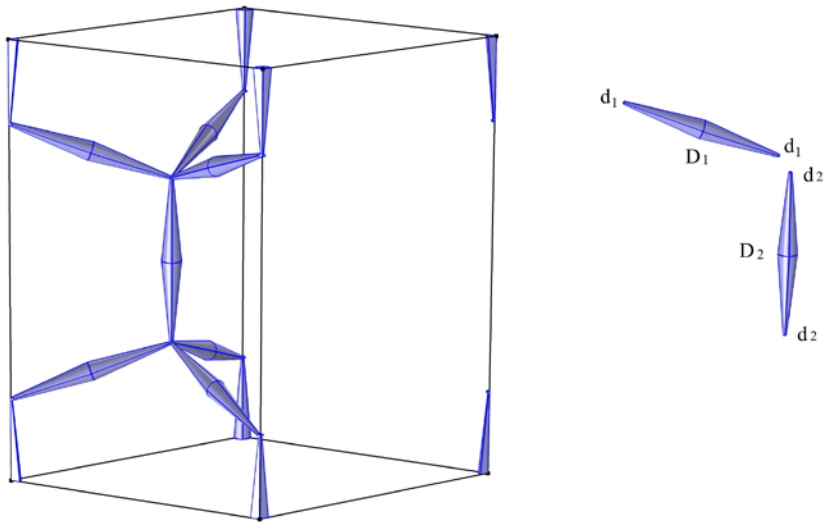

Figure 7.31 The primitive cell with different double-cones

The change of the uniformity of the double-cones introduces anisotropy. When d_1= 0.1l, D_1=D_2=0.5l and h=h_c, the variation of compressional wave velocities with d_2 is shown in Figure 7.32. The compressional wave velocity in the horizontal direction changes modestly while the compressional wave velocity in the vertical direction changes dramatically. When h=0.543h_c, the variation of the compressional wave velocities with d_2 is shown in Figure 7.33. It is similar to the case of h=h_c. The velocity in vertical direction increases dramatically with the increase of d_2. When d_2=1.9d_1, the two compressional wave velocities are almost the same. Thus, the change of d_2 can cause anisotropy.

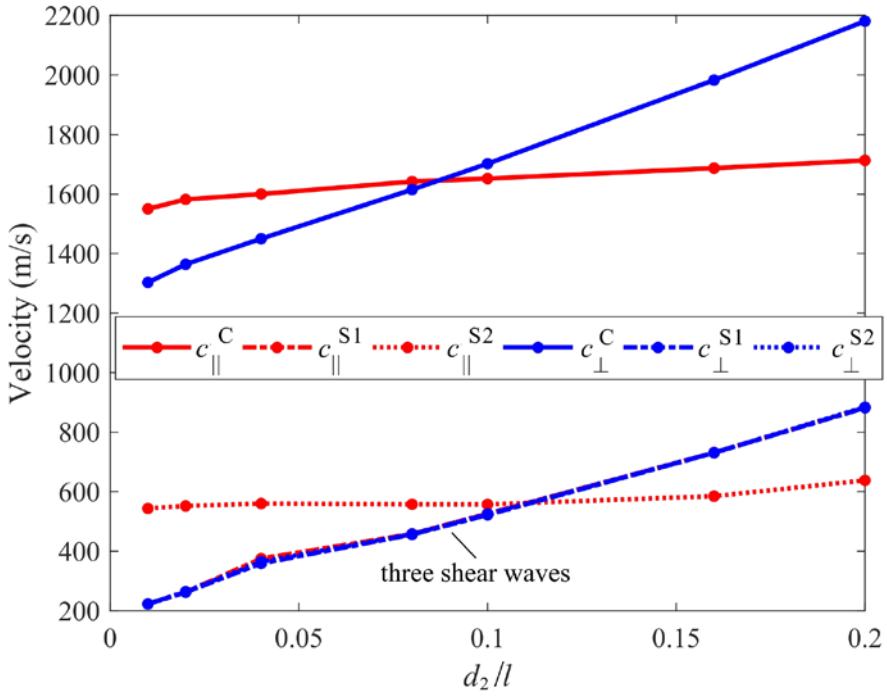

Figure 7.32 The variation of compressional velocities with d_2 (d_1= 0.1l, D=0.5l, h=h_c)

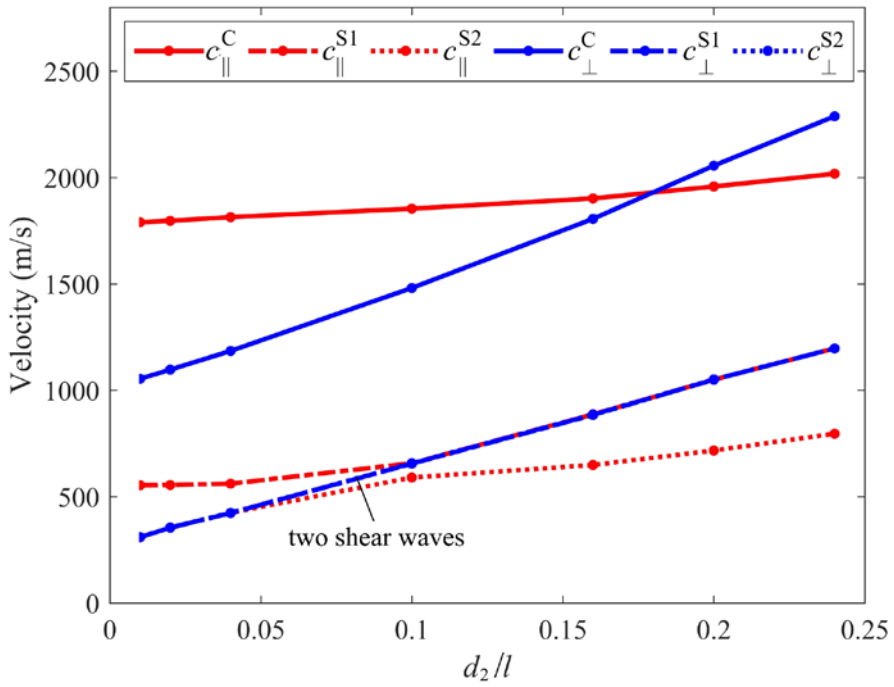

Figure 7.33 The variation of compressional velocities with d_2 (d_1= 0.1l, D=0.5l, h=0.543h_c)

Besides d_2, D_2 can vary, too. When d_1=d_2= 0.04l, D_1=0.5l, and h=h_c, the variation of the compressional wave velocities with D_2 is shown in Figure 7.34. From the figure, anisotropy can also be derived by changing D_2 when h=h_c. But the effect of D_2 on the anisotropy is not as significant.

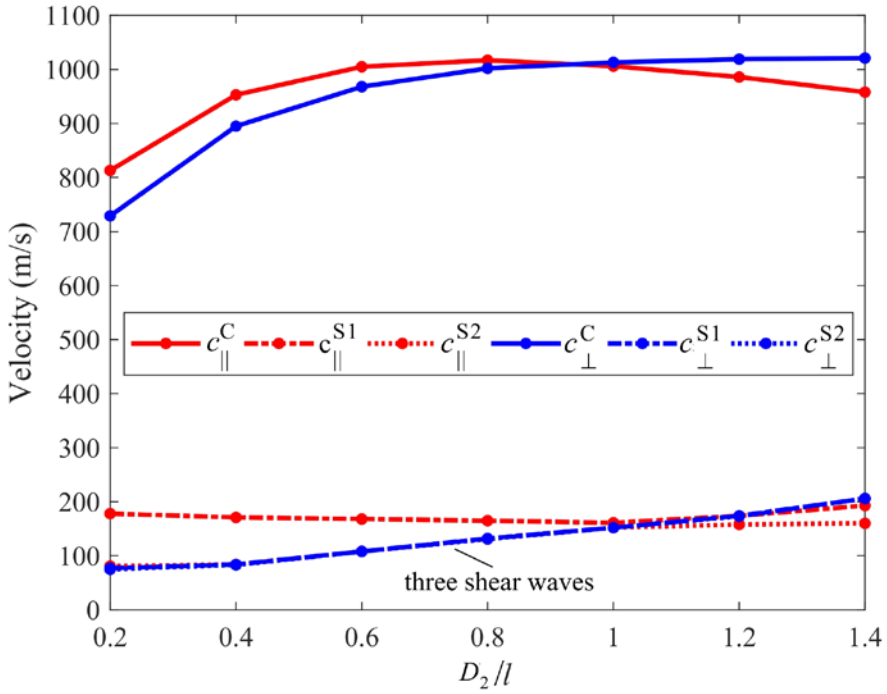

Figure 7.34 The variation of compressional velocities with D_2 (d_1=d_2= 0.04l, D_1=0.5l, h=h_c)

Both h and the change of the uniformity of the double-cones in the cell can be used to derive anisotropy. The two ways for deriving anisotropy can be combined together to get a higher anisotropy. As discussed in Section 7.3, the frequency bands of the pentamode materials vary with the changes of the primitive cells. Sometimes, shear waves cannot be avoided if very high anisotropy is required.

7.6 DESIGN OF PRIMITIVE CELLS FOR SPHERICAL PENTAMODE CLOAKS

Pentamode materials can be used to build pentamode cloaks. A spherical cloak can be composed of layers of pentamode materials with hexagonal unit cells approximately.

Properties of a spherical pentamode cloak can be determined using Equations (2.25) and (2.26). The properties of the cloaks depend on the transformation from the physical space to the virtual space. Letting the interior and exterior radii of the physical space are a and b, while the interior and exterior radii of the virtual space are δ and b. One special transformation (Gokhale, Cipolla, & Norris, 2012) is

$$f(r)=\sqrt[3]{\frac{b^3-\delta^3}{b^3-a^3}r^3-\frac{a^3-\delta^3}{b^3-a^3}b^3}\,. \tag{7.3}$$

The density of the cloak derived with the transformation of Equation (7.3) is

$$\frac{\rho}{\rho_b}=\frac{b^3-\delta^3}{b^3-a^3}. \tag{7.4}$$

It is constant for the whole cloak. The velocities of the cloak are

$$\begin{aligned}\frac{c_r}{c_b}&=\frac{b^3-a^3}{b^3-\delta^3}\frac{f^2}{r^2},\\ \frac{c_t}{c_b}&=\frac{r}{f}.\end{aligned} \tag{7.5}$$

When b=2a and δ=0.05a, and the background material outside the cloak is water, the required velocities are shown as curves in Figure 7.35.

The required density of the cloak in water is 1143kg/m^{-3}. For pentamode materials, the density is isotropic and simply equals the mass over the volume. Each unit cell is built with steel DCSs in vacuo. The dimensions of the primitive cells can be adjusted to approximate the

properties for each layer, as shown in Table 7.1. The compressional wave velocities of each primitive cell are also shown in Figure 7.35.

Table 7.1 Dimensions and properties of the primitive cell in each layer

	d_1/l	D_1/l	d_2/l	D_2/l	k/k_c	$c_{\parallel}$ (m/s)	$c_{\perp}$ (m/s)
1	0.038	0.1772	0.038	0.1772	0.845	1510	1294
2	0.0379	0.1767	0.0379	0.1767	0.834	1526	1292
3	0.0375	0.1769	0.0375	0.1769	0.824	1523	1274
4	0.0375	0.1758	0.0375	0.1758	0.780	1540	1222
5	0.0375	0.1750	0.0375	0.1750	0.745	1577	1209
6	0.039	0.1726	0.039	0.1726	0.684	1625	1156
7	0.0388	0.1702	0.0388	0.1702	0.589	1675	1063
8	0.039	0.1672	0.039	0.1672	0.484	1722	953
9	0.044	0.156	0.044	0.156	0.193	1937	806
10	0.047	0.1727	0.002	0.07	0.0569	2217	528
11	0.061	0.1663	0.0052	0.018	0.0136	2574	317

It can be seen from the figure that the pentamode materials with hexagonal unit cells have the potential of building acoustic cloaks. The sound speed in each layer (denoted by asterisks) well matches the required properties for cloaking (solid lines). There are some caveats. Shear modes are introduced because the diameters of the thin-ends are not zero. It is unneglectable when the diameters of the thin-end are relatively large. However, some of the diameters are

required to be large for high anisotropy. Another question is that the unit cell is made of DCSs in vacuo, which will require isolation from the background medium.

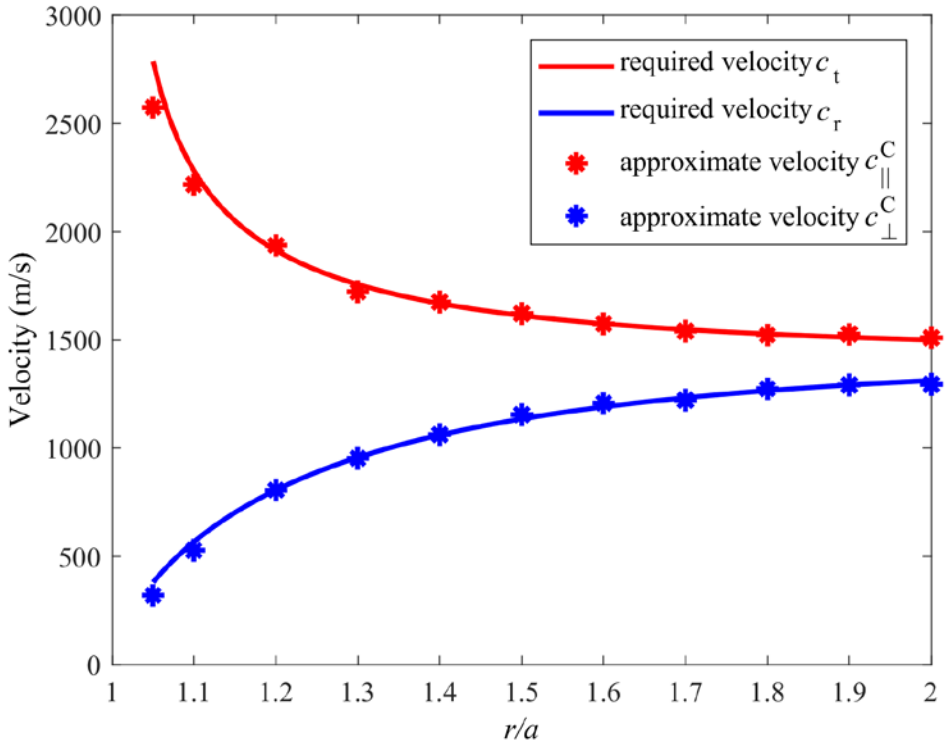

Figure 7.35 Compressional wave velocities of the layered pentamode cloak

8.0 CONCLUSION AND FUTURE WORK

This dissertation was concerned with the design of acoustic cloaks, which can make a space acoustically invisible. Much of the past efforts have focused on designing cloaks that have specific shapes (e.g. annular, square, and diamond shaped). The work presented, helped to extend this knowledge base. Both inertial cloaks and pentamode cloaks are studied. Inertial acoustic cloaks are those with anisotropic density and isotropic bulk modulus. Pentamode acoustic cloaks have anisotropic stiffness and isotropic density. Transformation acoustics was used to derive material properties for those cloaks. Additionally, a method of constructing a spherical pentamode material was presented, opening the door for 3D pentamode cloaks to be designed.

The specific contributions of this work are as follows.

1. A method of designing 2D cloaks with any arbitrary shape was presented. The structure is first divided into sections, which removed the transverse dependence on the properties. The resulting properties are anisotropic and inhomogeneous and realized with layered structures.
2. Next, a method of designing 2D cloaks of arbitrary shape with homogeneous properties was presented. A multi-transform approach was presented, which removes both the radial and transverse dependence on material properties. Anisotropy permits the material to act as a cloak.

3. A method of dividing any arbitrarily shaped 2D cloak into triangles and then transforming corresponding triangles from virtual space to physical space was presented. As with the method from item 2., the material properties are again homogeneous within each triangular part.
4. The methods in item 2. and 3. were extended to 3D by discretizing the cloak into tetrahedral parts. As with the 2D case, the properties of each part are homogeneous and any arbitrary shape can be realized, or at least approximated by tetrahedral parts.
5. Finally, a method of creating 3D cloaks using pentamode materials was devised. The structure is based upon double-cone structures, which are prevalent in pentamode structures. Although designing an actual cloak out of this material is quite complex and a topic of further study, it was shown that wide bandwidth bandgaps exist with pentamode behavior. A hexagonal unit cell was proposed in lieu of the standard face-centered-cubic cell that has been used in the past.

These methods are expanded in more detail below.

Two dimensional inertial acoustic cloaks can have arbitrary shapes. An area with a hollow space inside can be used for theses cloaks that hide objects inside. In general, transformation acoustics produces properties that are anisotropic and inhomogeneous. For circular cloaks, the properties at the same radius are the same, which can be approximated with concentric layers. For cloaks with arbitrary shapes, as presented in this thesis, the properties are more complicated. The properties are functions of both r and θ. It is different from the circular cloaks. But the cloaks can be divided into small sections. The boundaries of the sections can be replaced with linear segments. The properties can be derived for the sections. Within each

section, θ is small enough to be treated as constant. The properties on the centerline of each section are used to approximate the properties of the total section. The density tensor of each section has off-diagonal elements, but it can be transformed to principal directions, where the density tensor is diagonal. Then layered structures can be used to build the cloaks along principal directions. The properties of each layer are homogeneous and isotropic. But the sections can be different for an arbitrary cloak, thus the properties for each section are different. Even within one section, the properties of the layers are varying layer by layer.

To make it easier, two dimensional arbitrarily shaped acoustic cloaks composed of homogeneous parts are proposed. First, the cloak is divided into annular, pie-shaped sections. The sections do not need to be small. The boundaries of each section are also approximated with linear segments. Then, two-step transformation from the virtual space to the physical space is used within each section to derive the properties. The section is stretched in one direction first, and then stretched in another direction. After the two steps, each section is composed of two parts with homogeneous properties. The density tensor of each part can also be transformed to principal directions, and layered structures are used to build each part. Since the properties within each part are homogeneous, only two different materials are needed for each part. For a regular polygonal cloak, each section is equivalent. Then, only four materials are needed for a cloak. Some parameters affect the properties of each section. For a section from a regular polygonal cloak, two parameters are analyzed: the angle of the section and the side lengths of the virtual space corresponding to the cloaked space. The two parameters affect the properties of the cloaks significantly. It is easier for the cloak to be built when the section is smaller and the side lengths are larger. The side lengths of the virtual space corresponding to the cloaked area are the equivalent scattering cross section. As the side lengths become larger, cloaking performance

degrades. A balance can be obtained between the cloaking performance and the availability of building the cloak.

A general transformation method which maps a triangular virtual space to a triangular physical space is proposed for 2D cloaks. The properties of the triangular part are homogeneous. Thus, the cloaks can be divided into arbitrary triangular patterns, and virtual space is divided into similar patterns. Then, the virtual space is mapped to the physical space by corresponding triangles. The exterior boundary of the virtual space is the same with that of the cloak to satisfy the boundary matching. The division of the cloaks affects the properties of the parts significantly.

It is similar for arbitrarily shaped three-dimensional cloaks. If it is mapped from virtual space to physical space along radial directions, the properties are complicated. A three-dimensional acoustic cloak can also be divided into sections. A three-step transformation method which stretches or compresses the virtual space in one direction in each step leads to three parts with homogeneous properties. More generally, a transformation method that maps a tetrahedron in virtual space to a tetrahedron in physical space leads to homogeneous properties. Thus, a cloak can be composed of arbitrary homogenous parts. Two models are designed and numerically simulated. They have non-singular properties and good cloaking performance. The dependence of the required properties on the parameters is analyzed. It is easier to build the cloak when the size of the section is smaller or the virtual space corresponding to the cloaked space in physical space is larger, but at the cost of degraded cloaking performance. A balance is required for the cloaks between fabrication ability and cloaking performance.

The abovementioned cloaks are inertial cloaks. Pentamode materials can also be used to design cloaks. The previous pentamode model is face-centered-cubic unit cells. However, it is impossible to build a spherical cloak with these unit cells. The polyhedra with hexagonal

surfaces and six square surfaces are alternatives. A hexagonal cell composed of double-cone structures is proposed. Hollow spheres can be approximated with the unit cells. The dispersion relations of the primitive cells with different parameters are calculated. Compared with face-centered-cubic model, there is a similar frequency band where no shear modes exist. The compressional wave velocities of the cells can be varied by changing the geometries in the unit cell. High anisotropy of the compressional wave velocities can also be obtained by changing the structure of the unit cell. The cells for a spherical pentamode cloak are explored at last.

Future work could focus on a full simulation of a pentamode cloak using hexagonal unit cells and actually building and testing cloaks designed with the methods presented. A spherical pentamode cloak can be designed by layers of the hexagonal unit cells connected together. The dimensions of the unit cells at different layers are adjusted according to the required properties at the radius. Full simulations of the pentamode cloak using hexagonal unit cells can be conducted with Finite Element software. The properties of the layers in the inertial cloaks presented in the work are set with calculated values. More work can be done to adjust the properties of the cloaks to those of the natural materials. Simulations for inertial cloaks built with layers of natural materials can be conducted after the models are developed. If acoustic cloaks can be made of natural materials and have a good cloaking performance in simulation, the models can be fabricated and tested.

BIBLIOGRAPHY

Bi, Y., Jia, H., Lu, W., Ji, P., & Yang, J. (2017). Design and demonstration of an underwater acoustic carpet cloak. *Scientic Reports, 7*(1), 705.

Bi, Y., Jia, H., Sun, Z., Yang, Y., Zhao, H., & Yang, J. (2018). Experimental demonstration of three-dimensional broadband underwater acoustic carpet cloak. *Applied Physics Letters, 112*(22), 223502.

Boisvert, J. E., Scandrett, C. L., & Howarth, T. R. (2016). Scattering reduction of an acoustically hard cylinder covered with layered pentamode metamaterials. *The Journal of the Acoustical Society of America, 130*(4), 3404-3411.

Cai, C., Wang, Z., Li, Q., Xu, Z., & Tian, X. (2015). Pentamode metamaterials with asymmetric double-cone elements. *Journal of Physics D: Applied Physics , 48*(17), 175103.

Cessna, J. B., & Bewley, T. R. (2009). Honeycomb-structured computational interconnects and their scalable extension to spherical domains. *Proceedings of the 11th international workshop on System level interconnect prediction.* San Francisco.

Chen, H. (2009). Transformation optics in orthogonal coordinates. *Journal of Optics A: Pure and Applied Optics, 11*(7), 075102.

Chen, H., & Chan, C. T. (2007). Acoustic cloaking in three dimensions using acoustic metamaterials. *Applied physics letters, 91*(18), 183518.

Chen, H., & Chan, C. T. (2010). Acoustic cloaking and transformation acoustics. *Journal of Physics D: Applied Physics, 43*(11), 113001.

Chen, H., Liang, Z., Yao, P., Jiang, X., Ma, H., & Chan, C. T. (2007). Extending the bandwidth of electromagnetic cloaks. *Physical Review B, 76*(24), 241104.

Chen, H., Yang, T., Luo, X., & Ma, H. (2008). impedance matched reduced acoustic cloaking with realizable mass and its layered design. *Chinese Physics Letters, 25*(10), 3696.

Chen, X., Fu, Y., & Yuan, N. (2009). Invisible cloak design with controlled constitutive parameters and arbitrary shaped boundaries through Helmholtz's equation. *Optics express, 17*(5), 3581-3586.

Chen, Y., Liu, X., & Hu, G. (2015). Latticed pentamode acoustic cloak. *Scientific reports, 5*, 15745.

Cheng, Y., & Liu, X. J. (2009). Three dimensional multilayered acoustic cloak with homogeneous isotropic materials. *Applied Physics A: Materials Science & Processing, 94*(1), 25-30.

Cheng, Y., Yang, F., Xu, J. Y., & Liu, X. J. (2008). A multilayer structured acoustic cloak with homogeneous isotropic materials. *Applied Physics Letters, 92*(15), 151913.

Craster, R. V., & Guenneau, S. (2012). *Acoustic metamaterials: Negative refraction, imaging, lensing and cloaking*. Springer Science & Business Media.

Cummer, A., & Schurig, D. (2007). One path to acoustic cloaking. *New Journal of Physics, 9*(3), 45.

Cummer, S. A., Liu, R., & Cui, T. J. (2009). A rigorous and nonsingular two dimensional cloaking coordinate transformation. *Journal of Applied Physics, 105*, 056102.

Cummer, S. A., Popa, B. I., Schurig, D., Smith, D. R., Pendry, J., Rahm, M., et al. (2008). Scattering Theory Derivation of a 3D Acoustic Cloaking Shell. *Physical review letters, 100*(2), 024301.

Cummer, S., Popa, B., Schurig, D., Smith, D., & Pendry, J. (2006). Full-wave simulations of electromagnetic cloaking structures. *Physical Review E, 74*(3), 036621.

Fang, N., Xi, D., Xu, J., Ambati, M., Srituravanich, W., Sun, C., et al. (2006). Ultrasonic metamaterials with negative modulus. *Nature materials, 5*(6), 452.

García-Chocano, V. M., Sanchis, L., Díaz-Rubio, A., Martínez-Pastor, J., Cervera, F., Llopis-Pontiveros, R., et al. (2011). Acoustic cloak for airborne sound by inverse design. *Applied Physics Letters, 99*(7), 074102.

Garci´a-Salgado, R., Torrent, D., & S´anchez-Dehesa, J. (2012). Double-negative acoustic metamaterials based on quasi-two-dimensional fluid-like shells. *New Journal of Physics, 14*(10), 103052.

Gokhale, N. H., Cipolla, J. L., & Norris, A. N. (2012). Special transformations for pentamode acoustic cloaking. *The Journal of the Acoustical Society of America, 132*(4), 2932-2941.

Hu, J., Zhou, X., & Hu, G. (2009). A numerical method for designing acoustic cloak with arbitrary shapes. *Computational Materials Science, 46*(3), 708-712.

Huang, H., Sun, C., & Huang, G. (2009). On the negative effective mass density in acoustic metamaterials. *International Journal of Engineering Science, 47*(4), 610.

Jiang, W. X., Chin, J. Y., Li, Z., Cheng, Q., Liu, R., & Cui, T. J. (2008). Analytical design of conformally invisible cloaks for arbitrarily shaped objects. *Physical Review E, 77*(6), 066607.

Jo, C., Jeong, J., Kwon, B.-J., Park, K.-C., & Oh, I.-K. (2015). Omnidirectional two-dimensional acoustic cloak by axisymmetric cylindrical lattices. *Wave Motion, 54*, 157-169.

Kadic, M., Bückmann, T., Schittny, R., & Wegener, M. (2013). On anisotropic versions of three-dimensional pentamode metamaterials. *New Journal of Physics, 15*(2), 023029.

Kadic, M., Bückmann, T., Schittny, R., Gumbsch, P., & Wegener, M. (2014). Pentamode metamaterials with independently tailored bulk modulus and mass density. *Physical Review Applied, 2*(5), 054007.

Kadic, M., Bückmann, T., Stenger, N., Thiel, M., & Wegener, M. (2012). On the practicability of pentamode mechanical metamaterials. *Applied Physics Letters, 100*(19), 191901.

Kan, W., García-Chocano, V. M., Cervera, F., Liang, B., Zou, X.-y., Yin, L.-l., et al. (2015). Broadband Acoustic Cloaking within an Arbitrary Hard Cavity. *Physcial Review Applied, 3*(6), 064019.

Lai, Y., Chen, H., Zhang, Z. Q., & Chan, C. T. (2009). Complementary Media Invisibility Cloak that Cloaks Objects at a Distance Outside the Cloaking Shell. *Physical review letters, 102*(9), 093901.

Layman, C. N., Naify, C. J., Martin, T. P., Calvo, D. C., & Orris, G. J. (2013). Highly anisotropic elements for acoustic pentamode applications. *Physical review letters, 111*(2), 024302.

Li, C., & Li, F. (2008). Two-dimensional electromagnetic cloaks with arbitrary geometries. *Optics Express, 16*(17), 13414-13420.

Li, J., & Chan, C. (2004). Double-negative acoustic metamaterial. *Physical Review E, 70*(5), 055602.

Li, J., & Pendry, J. B. (2008). Hiding under the Carpet: A New Strategy for Cloaking. *physical Review Letters, 101*(20), 203901.

Li, Q., & Vipperman, J. S. (2014). Two-dimensional acoustic cloaks of arbitrary shape with layered structure based on transformation acoustics. *Applied Physics Letters, 105*(10), 101906.

Li, Q., & Vipperman, J. S. (2017). Two-dimensional arbitrarily shaped acoustic cloaks composed of homogeneous parts. *Journal of Applied Physics, 122*(14), 144902.

Li, Q., & Vipperman, J. S. (2018). Non-singular three-dimensional arbitrarily shaped acoustic cloaks composed of homogeneous parts. *Journal of Applied Physics, 124*(3), 035103.

Li, T., Huang, M., Yang, J., Lan, Y., & Sun, J. (2012). Homogeneous material constructed acoustic cloak based on coordinate transformation. *Journal of Vibration and Acoustics, 134*(5), 051016.

Li, W., Guan, J., Sun, Z., Wang, W., & Zhang, Q. (2009). A near-perfect invisibility cloak constructed with homogeneous materials. *Optics express, 17*(26), 23410-23416.

Martin, A., Kadic, M., Schittny, R., Bückmann, T., & Wegener, M. (2012). Phonon band structures of three-dimensional pentamode metamaterials. *Physical Review B, 86*(15), 155116.

Milton, G. W., & Cherkaev, A. V. (1995). Which elasticity tensors are realizable? *Journal of engineering materials and technology, 117*(4), 483.

Milton, G. W., Briane, M., & Willis, J. R. (2006). On cloaking for elasticity and physical equations with a transformation invariant form. *New Journal of Physics, 8*(10), 248.

Nicolet, A., Zolla, F., & Guenneau, S. (2008). Electromagnetic analysis of cylindrical cloaks of an arbitrary cross section. *Optics letters, 33*(14), 1584-1586.

Norris, A. N. (2008). Acoustic cloaking theory. *Proceedings of the Royal Society of London A: Mathematical, Physical and Engineering Sciences, 464*(2097), 2411-2434.

Pendry, J. B., & Li, J. (2008). An acoustic metafluid: realizing a broadband acoustic cloak. *New Journal of Physics, 10*(11), 115032.

Pendry, J. B., Schurig, D., & Smith, D. R. (2006). Controlling Electromagnetic Fields. *Science, 312*(5781), 1780-1782.

Popa, B. I., & Cummer, S. A. (2009). Design and characterization of broadband acoustic composite metamaterials. *Physical Review B, 80*(17), 174303.

Popa, B. I., & Cummer, S. A. (2011). Homogeneous and compact acoustic ground cloaks. *Physical Review B, 83*(22), 224304.

Popa, B., Zigoneanu, L., & Cummer, S. (2011). Experimental Acoustic Ground Cloak in Air. *Physical review letters, 106*(25), 253901.

Rajput, A., & Srivastava, K. V. (2014). Design of a two-dimensional metamaterial cloak with minimum scattering using a quadratic transformation function. *Journal of Applied Physics, 116*(12), 124501.

Sanchis, L., García-Chocano, V. M., Llopis-Pontiveros, R., Climente, A., Martínez-Pastor, J., Cervera, F., et al. (2013). Three-Dimensional Axisymmetric Cloak Based on the Cancellation of Acoustic Scattering from a Sphere. *Physical review letters, 110*(12), 124301.

Scandrett, C. L., Boisvert, J. E., & Howarth, T. R. (2010). Acoustic cloaking using layered pentamode materials. *The Journal of the Acoustical Society of America, 127*(5), 2856-2864.

Scandrett, C. L., Boisvert, J. E., & Howarth, T. R. (2011). Broadband optimization of a pentamode-layered spherical. *Wave Motion, 48*(6), 505-514.

Shen, H., Padoussis, M. P., JihongWen, Yu, D., Cai, L., & XisenWen. (2012). Acoustic cloak/anti-cloak device with realizable passive/active metamaterials. *Journal of Physics D: Applied Physics, 45*(28), 285401.

Sounas, D. L., Fleury, R., & Alù, A. (2015). Unidirectional Cloaking Based on Metasurfaces with Balanced Loss and Gain. *Physical Review Applied, 4*(1), 014005.

Torrent, D., & Sánchez-Dehesa, J. (2007). Acoustic metamaterials for new two-dimensional sonic devices. *New journal of physics, 9*(9), 323.

Torrent, D., & Sánchez-Dehesa, J. (2008). Acoustic cloaking in two dimensions:A feasible approach. *New Journal of Physics, 10*(6), 063015.

Urzhumov, Y., Ghezzo, F., Hunt, J., & Smith, D. R. (2010). Acoustic cloaking transformations from attainable material properties. *New Journal of Physics, 12*(7), 073014.

Wang, X., Qu, S., Wu, X., Wang, J., Xu, Z., & Ma, H. (2010). Broadband three-dimensional diamond-shaped invisible cloaks composed of tetrahedral homogeneous blocks. *Journal of Physics D: Applied Physics, 43*(30), 305501.

Wang, X., Qu, S., Xu, Z., Ma, H., Wang, J., Gu, C., et al. (2010). Three-dimensional invisible cloaks with arbitrary shapes based on partial differential equation. *Applied Mathematics and Computation, 216*(2), 426–430.

Wang, X.-P., Wan, L.-L., Chen, T.-N., Song, A.-L., & Wang, F. (2016). Broadband unidirectional acoustic cloak based on phase gradient metasurfaces with two flat acoustic lenses. *Journal of Applied physics, 120*(1), 014902.

Wu, Q., Zhang, K., Meng, F. Y., & Li, L. W. (2008). Material parameters characterization for arbitrary N-sided regular polygonal invisible cloak. *Journal of Physics D: Applied Physics, 42*(3), 035408.

Xiong, J., Chen, T., Wang, X., & Zhu, J. (2015). Design and assessment of an acoustic ground cloak with layered structure. *International Journal of Modern Physics B, 29*(27), 1550191.

Xu, T., Zhu, X. F., Liang, B., Li, Y., Zou, X. Y., & Cheng, J. C. (2012). Scattering reduction for an acoustic sensor using a multilayered shell pair of homogeneous isotropic single-negative media. *Applied Physics Letters, 101*(3), 033509.

Yang, J. J., Huang, M., Cai, G. H., Xie, R. S., & Yang, J. (2013). Design of Acoustic Metamaterial Devices Based on Inverse Method. *Journal of Vibration and Acoustics, 135*(5), 051024.

Yang, Y., Jing, L., Zheng, B., Hao, R., Yin, W., Li, E., et al. (2016). Full-Polarization 3D Metasurface Cloak with Preserved Amplitude and Phase. *Advanced Materials, 28*(32), 6866-6871.

Zhang, J., Luo, Y., Chen, H., & Wu, B. I. (2008). Cloak of arbitrary shape. *Journal of the Optical Society of America B, 25*(11), 1776-1779.

Zhang, S., Xia, C., & Fang, N. (2011). Broadband acoustic cloak for ultrasound waves. *Physical Review Letters, 106*(2), 024301.

Zhao, J., Chen, Z. N., Li, B., & Qiu, C. W. (2015). Acoustic cloaking by extraordinary sound transmission. *Journal of Applied Physics, 117*(21), 214507.

Zhu, J., Chen, T., Liang, Q., Xiaopeng Wang, Xiong, J., & Jiang, P. (2015). A unidirectional acoustic cloak for multilayered background media with homogeneous metamaterials. *Journal of Physics D: Applied Physics, 48*(30), 305502.

Zhu, R., Huang, G. L., & Hu, G. K. (2012). Effective dynamic properties and multi-resonant design of acoustic metamaterials. *Journal of Vibration and Acoustics, 134*(3), 031006.

Zhu, R., Zheng, B., Ma, C., Xu, J., Fang, N., & Chen, H. (2016). A broadband polygonal cloak for acoustic wave designed with linear coordinate transformation. *The Journal of the Acoustical Society of America, 140*(1), 95-101.

Zhu, W., Ding, C., & Zhao, X. (2010). A numerical method for designing acoustic cloak with homogeneous metamaterials. *Applied Physics Letters, 97*(13), 131902.

Zhu, X., Liang, B., Kan, W., Zou, X., & Cheng, J. (2011). Acoustic Cloaking by a Superlens with Single-Negative Materials. *Physical review letters, 106*(1), 014301.

Zhu, X., Ramezani, H., Shi, C., Zhu, J., & Zhang, X. (2014). PT-Symmetric Acoustics. *Physical Review X, 4*(3), 031042.

Zigoneanu, L., Popa, B. I., & Cummer, S. A. (2014). Three-dimensional broadband omnidirectional acoustic ground cloak. *Nature materials, 13*(4), 352-355.

Zigoneanu, L., Popa, B. I., Starr, A. F., & Cummer, S. A. (2011). Design and measurements of a broadband two-dimensional acoustic metamaterial with anisotropic effective mass density. *Journal of Applied Physics, 109*(5), 054906.